AD-A193 029

②

NAVAL POSTGRADUATE SCHOOL
Monterey, California

DISSERTATION

ANALYSIS OF GRAIN REFINEMENT AND SUPERPLASTICITY
IN ALUMINUM-MAGNESIUM ALLOYS

by

Ahmed Ahmed Abou-Salama

December 1987

Dissertation Advisor: Terry R. McNelley

REPORT DOCUMENTATION PAGE

1a REPORT SECURITY CLASSIFICATION UNCLASSIFIED		1b RESTRICTIVE MARKINGS			
2a SECURITY CLASSIFICATION AUTHORITY		3 DISTRIBUTION/AVAILABILITY OF REPORT Approved for public release; distribution is unlimited.			
2b DECLASSIFICATION/DOWNGRADING SCHEDULE					
4 PERFORMING ORGANIZATION REPORT NUMBER(S)		5 MONITORING ORGANIZATION REPORT NUMBER(S)			
6a NAME OF PERFORMING ORGANIZATION Naval Postgraduate School	6b OFFICE SYMBOL (If applicable) Code 62	7a NAME OF MONITORING ORGANIZATION Naval Postgraduate School			
6c ADDRESS (City, State, and ZIP Code) Monterey, California 93943-5000		7b ADDRESS (City, State, and ZIP Code) Monterey, California 93943-5000			
8a NAME OF FUNDING/SPONSORING ORGANIZATION	8b OFFICE SYMBOL (If applicable)	9 PROCUREMENT INSTRUMENT IDENTIFICATION NUMBER			
8c ADDRESS (City, State, and ZIP Code)		10 SOURCE OF FUNDING NUMBERS			
		PROGRAM ELEMENT NO	PROJECT NO	TASK NO.	WORK UNIT ACCESSION NO

11 TITLE (Include Security Classification)

ANALYSIS OF GRAIN REFINEMENT AND SUPERPLASTICITY IN ALUMINUM-MAGNESIUM ALLOYS

12 PERSONAL AUTHOR(S)
Abou-Salama, Ahmed Ahmed

13a TYPE OF REPORT Ph.D. Dissertation	13b TIME COVERED FROM ___ TO ___	14 DATE OF REPORT (Year, Month, Day) 1987 December	15 PAGE COUNT 167

16 SUPPLEMENTARY NOTATION

17 COSATI CODES			18 SUBJECT TERMS (Continue on reverse if necessary and identify by block number)
FIELD	GROUP	SUB GROUP	Superplasticity; Aluminum Magnesium Alloys; Thermomechanical Processing; Microstructural Evolution; Continuous Recrystallization; Microstructural Instability; Grain Growth

19 ABSTRACT (Continue on reverse if necessary and identify by block number)

Previous research had demonstrated superplastic behavior in aluminum-magnesium alloys of high magnesium content to result from deformation processing to an initially non-recrystallized condition. Analysis here of those data has demonstrated that such a result may be understood in terms of constitutive equations developed for fine-grained materials and that the constitutive equations are applicable to materials achieving grain boundary misorientations in the range of only 2° to 7° by a process of continuous recrystallization. The constitutive equations provide a basis for analysis of anomalous temperature dependence of the strength and of the activation energy for plastic deformation seen as well in this work. A study of the separate effects of processing variables has lead to a model for continuous recrystallization during deformation processing. This model considers recovery of dislocations to sub-boundaries to be the critical step in this process. Application of this model to development of advanced aluminum alloys for air frame structural applications will result in increased weight savings by such processing methods.

20 DISTRIBUTION/AVAILABILITY OF ABSTRACT ☒ UNCLASSIFIED/UNLIMITED ☐ SAME AS RPT ☐ DTIC USERS	21 ABSTRACT SECURITY CLASSIFICATION Unclassified	
22a NAME OF RESPONSIBLE INDIVIDUAL Prof. T. R. McNelley	22b TELEPHONE (Include Area Code) (408)646-2589	22c OFFICE SYMBOL Code 69Mc

DD FORM 1473, 84 MAR
83 APR edition may be used until exhausted
All other editions are obsolete
SECURITY CLASSIFICATION OF THIS PAGE
UNCLASSIFIED

i

Analysis of Grain Refinement and Superplasticity
in Aluminum-Magnesium Alloys

by

Ahmed Ahmed Abou-Salama
Brigadier General, Egyptian Air Force
B.Sc., Cairo University, 1962
M.Sc., Cairo University, 1976

Submitted in partial fulfillment of the
requirements for the degree of

DOCTOR OF PHILOSOPHY
IN MECHANICAL ENGINEERING

from the

NAVAL POSTGRADUATE SCHOOL

December 1987

Author: _____
Ahmed Ahmed Abou-Salama

Approved by:

John R. Neighbours
Professor of Physics

A. Jeffrey Perkins
Professor of Mechanical Engineering

David Salinas
Professor of Mechanical Engineering

Oleg D. Sherby
Professor of Materials Science
and Engineering
Stanford University

Terry R. McNelley
Professor of Mechanical Engineering
Dissertation Supervisor

Approved by:

Anthony J. Healey, Chairman
Department of Mechanical Engineering

Kneale T. Marshall, Acting Academic Dean

ABSTRACT

Previous research had demonstrated superplastic behavior in aluminum-magnesium alloys of high magnesium content to result from deformation processing to an initially non-recrystallized condition. Analysis here of those data has demonstrated that such a result may be understood in terms of constitutive equations developed for fine-grained materials and that the constitutive equations are applicable to materials achieving grain boundary misorientations in the range of only 2° to 7° by a process of continuous recrystallization. The constitutive equations provide a basis for analysis of anomalous temperature dependence of the strength and of the activation energy for plastic deformation seen as well in this work. A study of the separate effects of processing variables has lead to a model for continuous recrystallization during deformation processing. This model considers recovery of dislocations to sub-boundaries to be the critical step in this process. Application of this model to development of advanced aluminum alloys for air frame structural applications will result in increased weight savings by such processing methods.

Accesion For

NTIS CRA&I	☑
DTIC TAB	☐
Unannounced	☐
Justification	

A-1

3

TABLE OF CONTENTS

5

LIST OF TABLES

LIST OF FIGURES

11

12

13

14

16

17

DEDICATION

I dedicate this thesis to the great people of Egypt without whose sacrifices I would not have been able to accomplish this work.

19

ACKNOWLEDGMENTS

I. INTRODUCTION

A. HISTORICAL REVIEW OF SUPERPLASTICITY

Superplasticity is the ability of some metallic materials to deform to extremely large neck-free elongations under certain conditions of temperature and strain rate. The first report of the phenomenon appeared in 1912 (Bengough, 1912; Rosenhain and Ewen, 1912). Other early observations of superplasticity were made by Rosenhain (1920) in a cold rolled zinc-copper-aluminum ternary eutectic alloy, and by Haughton and Bingham (1920) who described viscous-like behavior in fine-grained metals. Sauveur (1924) noted that an iron bar twisted in temperature gradient exhibited regions of easy twisting at the transformation temperature. Pearson (1934), while studying mechanical properties of Sn-Pb and Bi-Sn alloys, reached relatively neck-free elongations of up to 2000% in a Bi-Sn eutectic alloy in creep testing.

Bochvar and Sviderskaya (1945) in the USSR introduced the term "superplastichnost" (literally ultra-high plasticity) to describe extreme elongations observed by them in dilatometric investigation of eutectoid Al-Zn alloys. Their term was subsequently adopted by other Russian workers and has generally been translated as "superplasticity." The most active early Soviet investigator of superplasticity is Presnyakov (1958, 1960). He and his co-workers studied Al-Zn, Al-Cu, Al-Si, Al-Ni, Al-Fe, Cu-Zn, and Cu-Ni alloys and have published several review articles. The effect is seen in either eutectic or eutectoid systems, but not in alloys with continuous solubility. The term "superplasticity" first appeared in English language literature in a paper by Lozinsky and Simeonova (1959).

Although Pearson (1934) demonstrated the attainment 2000% tensile elongation, this result was largely ignored for almost 30 years (Edington, et al., 1976). Interest was eventually stimulated by the first English language review by Underwood (1962) of the Russian work together with the work of Backofen and his coworkers in the U.S.A. (Avery, 1965, 1966; Holt, 1966; Backofen, 1968; Zehr, 1968). Up to that time, knowledge of superplasticity was limited. Certain

21

alloys, mainly eutectics, were known to exhibit extreme elongation when deformed at high temperature. The reason for this effect, the mechanism, its relation to microstructure, and the potential applications were all unknown. Since 1962, however, research on superplastic alloys and the development of their commercial applications has been extensive. In a span of eleven years (1962 – 1973) many of the unknowns became fairly well established (Alden, 1975):

- a large value of the strain rate sensitivity coefficient $m = \frac{\partial ln\sigma}{\partial ln\dot{\epsilon}} (m \stackrel{\sim}{>} 0.4)$ is an essential and unique characteristic superplasticity (Backofen, et al., 1964);

- mechanical properties depend strongly upon grain size and strain rate (Avery and Backofen, 1965; Alden, 1967);

- grain boundary sliding is an important deformation mechanism (Alden, 1967, 1969; Holt, 1968);

- the theory of diffusion-accommodated grain boundary sliding (Ashby and Verrall, 1973) to reconcile these observations.

Several reviews of superplasticity have appeared in recent years and a number of monographs have been published (Mukherjee, 1975; Gittus, 1975; Edington, 1976; Alden, 1977; Taplin, et al., 1979; Mukherjee, 1979; Wadsworth, et al., 1980; and Sherby, et al., 1981). Also, since the early 1980's, conferences and symposia on superplasticity and its applications have taken place annually. This reflects the growing understanding of the phenomenon and its applications in industry.

B. PRACTICAL IMPORTANCE AND APPLICATION OF SUPERPLASTICITY

Complex parts of intricate shapes can be produced in one piece by blow forming processes comparable to those employed in plastics processing. Complex and expensive tooling required in conventional metal forming operations may be replaced by simple one-piece tools; also, labor costs are reduced when components are made from superplastic materials. The first application of superplastic forming (SPF) in the aircraft industry came with titanium alloy Ti-6%Al-4%V (Weisert and Stacker, 1982; Williamson, 1982). Despite high material costs this alloy is employed due to its beneficial properties including high specific strength and relatively

22

good high temperature stability as well as high resistance to corrosion (Hammond, 1982; Wertz, et al., 1983).

The successful production implementation of SPF of titanium, the demands for weight saving in aircraft construction, and the high cost of Ti-alloys, have lead to interest in SPF aluminum (Lloyd and Moore, 1982; Hamilton, 1982). Supral, nominally Al-6% Cu-0.4% Zr, is the most widely employed SPF aluminum alloy industrially in the manufacture of secondary structural parts in the aircraft industry as well of components in the automobile industry (Grimes, et al., 1975). Supral alloys have been developed to correspond to the tensile strengths of several conventional alloys including the high-strength 7XXX-alloys.

Al-Li alloys (Wadsworth, 1983, 1984) are currently attracting much attention for application in the aerospace industries. The general interest in Al-Li alloys and SPF of them centers on the fact that Li is one of only two elements that significantly increase the elastic modulus and simultaneously decrease the density of Al; the other element is Be. For aerospace applications, improvements in specific modulus and specific strength directly lead to weight saving.

Finally, superplastic forming of nickel base alloys is used industrially in fabricating aircraft engine parts (Merrik, 1982; Giami, 1982). A single integrated component consisting of a disk with turbine blades has been produced. Superplastic forming of ultra-high carbon steels has also been introduced by Sherby and co-workers in recent years (Sherby, et al., 1975).

C. ALLOY DEVELOPMENT FOR SUPERPLASTICITY

Superplasticity is enhanced by a homogeneous and refined grain size which should remain stable during the deformation process (Alden, 1966; Griffith and Hammond, 1972; Kayadi, et al., 1979; Gifkins, 1976). At first, refined and stable grain structures were produced in eutectic or eutectoid alloys (Pearson, 1934; Lee, 1969; Ishikawa, et al., 1975). The structures were fine in the sense that the phases are intimately mixed and the dispersed phase is small in scale. In contrast to pure metals, such refined structures in these alloys may be grain size stable and the grains may resist coarsening during annealing or superplastic deformation. The

23

origin of this stability is the relative immobility of the interphase boundaries in the structure. Some of the superplastic eutectics are mixtures of terminal phases while others involve intermetallic compounds. Some examples of the former are Sn-Pb, Sn-Bi, Pb-Cd, Ag-Cu and Zr-Al, and of the latter Al-33%Cu, Cu-9.5%Al-4%Fe and Mg-33%Al (Alden, 1979).

Eutectoid superplastic alloys are relatively few in number. One important example is the extensively studied Zn-Al eutectoid (Presnyakov and Chervyakova, 1960; Backofen, et al., 1964; Holts, 1968; Ball and Hutchinson, 1969; Darekar and Chandhuri, 1970; Nuttall, 1972; Johnson, et al., 1972; Weiss, 1972; Young, et al., 1972; Kayali, 1972; Vaidia, et al., 1973; Ishikawa, et al., 1975; Naziri, et al., 1975; Sherby et al., 1975; Yarovchuk, et al., 1976; Kaibyshev, 1978; Motohashi and Shibata, 1980, 1982; Portnoy, et al., 1981; Senkov and Myshlyaev, 1986). The other is the Fe-C eutectoid which has been investigated by Marder (1969), Yoder and Weiss (1970), Young, et al., (1972), Kayali (1972), and Sherby, et al., (1975). If the eutectic or eutectoid alloys are subjected to the appropriate thermomechanical treatments, a fine phase size can be produced, which is stable at elevated temperature for the separate phases inhibit growth in each other (Johnson, 1970; Davies, et al., 1970).

While such alloys may show superplastic properties at high temperature, they often contain large volume fractions of brittle phases which make the alloy brittle at room temperature, thus limiting practical applications. It was thought at the beginning that microstructures sufficiently fine to sustain the mechanisms of superplastic deformation could be attained only in such alloys. If the grain size of a nominally single-phase alloy remains fairly fine during the superplastic deformation process, due to the presence of a small amount of stable, uniformly dispersed and fine second phase particles that stabilize the structure and remain undissolved, then a nominally single phase alloy could behave superplastically when deformed under suitable conditions (Cline and Alden, 1967; Ujiye, 1969; Matsuki, et al., 1976). Ideally such alloys are single phase at an initial temperature of hot working and undergo precipitation either immediately after the working or during working at progressively lower temperatures. Materials of this type are Sn-5% Bi, Pb-5%

Cd, Ni-Fe-Cr alloys, dilute Zn-Al alloys, probably Ti alloys and ally, the wrought Al-alloys.

D. DEVELOPMENT OF THEORY AND MECHANISM OF SUPERPLASTICITY

Backofen, Turner and Avery (1964) first noted that the basis of superplastic flow is to be found in the strain rate sensitivity m of flow stress. Avery and Backofen (1965) demonstrated the dependence of strain rate on grain size in superplastic flow. Alden (1967) and Holt (1968) introduced the importance of grain boundary sliding as a deformation mechanism in superplastic flow. Ashby and Verrall (1973) put forward a widely recognized theory involving diffusion accommodated flow based on a model in which grains were rearranged through a neighbor switching process. They view superplasticity in terms of a transition between diffusion-accommodated flow at low strain rates and dislocation creep at high strain rates. Most of the mechanisms proposed for superplastic flow rely on the fact that the grain boundary sliding is the dominant mechanism in SPD (Holt and Backofen, 1966; Stowell, et al., 1969; Lee, 1969; Ball and Hutchinson, 1969; Johnson, 1970; Davies, et al., 1970; Mukherjee, 1971; Matsuki, et al., 1976). For this sliding to occur continuously on all boundaries and for grain compatibility to be maintained, at least one accommodation process should exist (Holt and Backofen, 1966; Davies, et al., 1970; Mukherjee, 1971; Kashyap and Mukherjee, 1985).

Several models have been suggested. Ball and Hutchinson (1969) proposed a model based on dislocation pile-up within the grains. They proposed that groups of grains slide as a unit. Mukherjee (1971) proposed a similar model but assumed that the grains slide individually rather than in groups. Gifkins (1976) proposed a model, the physical basis of which puts emphasis on the role played by grain boundary dislocations. He introduced the mantle and core concept. The mantle is envisioned as a region near the grain boundary in which sliding and the accommodation processes take place while the core is the non-deforming interior region. Arieli and Mukherjee (1980) proposed a model in which they assume that the strain is achieved mainly by three-dimensional grain rearrangement which proceeds by interface sliding accompanied by grain migration and grain rotation and

25

accommodated by individual dislocations climbing in a narrow region near the boundary and being annihilated into the boundary.

Nix (1984) considers slip within the grains to provide the torque for grain rotation: this rotation is a central feature of superplasticity. Recently, Sherby and co-workers (1982) proposed phenomenological equations to describe superplastic flow in fine-grain materials based on the core and mantle theory proposed by Gifkins. They introduced the effective diffusivity concept to superplasticity to describe the temperature dependence of superplastic flow. They concluded that grain boundary sliding and migration, accommodated by slip processes at regions adjoining the grain boundaries, constitute the most likely mechanism of deformation during superplastic flow of fine grain size materials.

E. MICROSTRUCTURAL PREREQUISITES FOR SUPERPLASTICITY

The first metallurgical requirement for superplasticity is a fine, equiaxed grain structure. The reported dependences of strain rate on grain size can be grouped into those showing inverse second power ($\dot{\epsilon} \propto d^{-2}$) and those showing inverse third power ($\dot{\epsilon} \propto d^{-3}$) (Sherby and Wadsworth, 1982). Because superplastic deformation involves considerable holding time of ultra-fine grained structures at high temperature, it is expected that grain growth will take place. The growth usually occurs at an enhanced rate during deformation. The m value decreases with the increase in grain size, which in turn lessens the superplastic behavior of the material (Edington, et al., 1976). Decreasing the grain size increases and moves to higher strain rates the maximum value of m. In order to retard grain growth, the presence of a second phase is required. Inhibition of the grain growth is improved if the quantity of the second phase is increased, provided the size of the second phase remains fine and its distribution remains uniform. Also, the second phase must be able to deform with the matrix to avoid stress concentration and early fracture.

The second structural prerequisite concerns the nature of the grain boundary. The grain boundaries should be of high-angle character (Sherby and Wadsworth, 1982) because low-angle boundaries are not able to slide. The low-angle grain

boundaries can be changed in some cases to high-angle ones either by a static discontinuous recrystallization process prior to before SPD or through a continuous recrystallization process in the early stages of superplastic deformation (Wadsworth, et al., 1980; Sherby et al., 1981).

F. DEVELOPMENT OF SUPERPLASTICITY IN Al-ALLOYS

The development of superplasticity in various Al alloys including Al-Cu (Holt and Backofen, 1966), Al-Zn (Ball and Hutchinson, 1969), Al-Ca (Piatti, et al., 1976), Al-Ga (Marya and Wyon, 1976; Weill and Wyon, 1979), Al-Pd, Al-Si, and Al-Mg-Si (Otsuka, et al., 1974) has been reviewed recently (Wadsworth, et al., 1984). Early investigations of superplasticity in alloys in which aluminum was the major component were mainly limited to those of eutectic or near eutectic composition such as Al-33%Cu and none of these alloys possesses attractive service properties. An investigation of a hypoeutectric Al-17% Cu alloy was introduced with the objectives of developing a material which exhibits a superplasticity at elevated temperatures and reasonable strength and ductility at room temperatures (Cahoon, 1975). Probably the first alloy to be used in commercial forming operations was based on the Zn-22%Al eutectoid alloys which possess remarkable superplastic properties (Grimes, et al., 1975).

Grimes, et al. (1976), developed a high level of superplasticity in an Al-6%Cu-0.5%Zr alloy that also has ambient temperature properties typical of a normal, medium-strength aluminum alloy. This alloy differs from most superplastic alloys in that only a relatively small proportion of the alloying additions are not present in solid solution during superplastic deformation. It has been shown that by introducing a dispersion of very fine but stable Al_3Zr particles it is possible to produce material in which the grain size is also extremely stable at elevated temperature. This can be achieved with a volume fraction of second phase particles which can be less than 0.6% (Grimes, et al., 1975).

Matsuki, et al. (1973, 1976, 1977), have reported that Al-Zn-Mg alloys, containing zirconium and prepared by severe cold working and recrystallization to give an equiaxed fine grain structure, can behave superplastically when deformed

under suitable conditions. They reported that an Al-6%Mg alloy containing Zr, Cr and Mn was also found to deform superplastically when produced in a heavily cold-rolled and recrystallized condition.

Recent work by Wert, et al. (1981, 1982), has indicated that grain refinement in commercial high strength, 7000 series, Al-Zn-Mg-Cu alloys is possible through special thermomechanical processing. An attractive feature of this type of treatment is that conventional commercial alloys can be thermomechanically processed to a sufficiently fine grain size that they became superplastic.

Two general approaches have been used with aluminum alloys to obtain the fine, stable structure that is required for superplasticity. The first approach is that used by Wert, et al. (1981 1982) and Paton, et al. (1982), on developing superplasticity in the 7XXX series high strength Al-alloys. Their approach involves precipitation of an intermetallic phase followed by cold working to provide stored strain energy. Fine grains are produced by nucleation and migration of boundaries upon subsequent heating. The fine grain sizes that are produced are prevented from growing by the presence of a fine scale Cr-rich dispersoid. The second approach, used by Watts, et al. (1976), utilizes Zr in amounts ranging from about 0.3 to 0.5 weight percent to maintain very fine grain sizes through fine scale precipitation of Al_3Zr. Superplasticity was observed after thermomechanical treatments leading to continuous recrystallization, a process of transforming an initially deformed structure to a recrystallized condition in the absence of high-angle boundary migration.

G. OUTLINE AND CONTRIBUTIONS OF THIS THESIS

The Al-Mg alloys of interest in this research are part of an alloy system which has been extensively studied. Thus the high temperature creep characteristics of Al-Mg alloys as an example of Class I solid solution alloy behavior are introduced. Models, mechanisms and phenomenological equations of superplasticity are then discussed along with current understanding of phenomena involved in microstructural evolution.

Subsequently, a model based on interaction of a dislocation creep processes and superplastic deformation by grain boundary sliding, as described by Sherby and

28

Wadsworth (1982), is presented to describe behavior of these thermomechanically processed (TMPed) Al-Mg alloys. Later chapters consider effects of TMP variables, leading to a new model to describe microstructural evolution during TMP. Finally, application to other Al-base alloys, where lower temperature superplasticity of interest, is considered.

II. HIGH TEMPERATURE DEFORMATION AND MICROSTRUCTURAL EVOLUTION IN Al AND Al-Mg ALLOYS

A. CONSTITUTIVE EQUATIONS FOR CREEP AND SUPERPLASTICITY

1. Classification of High Temperature Creep

Deformation of metals at elevated temperatures is often assumed to follow a power law relation of the form $\dot{\epsilon} \propto \sigma^n$ where $\dot{\epsilon}$ is the creep (or strain) rate, σ is the stress and $n = 1/m$ is the stress exponent. Two general classes may be distinguished by the value of the stress exponent. Class I (alloy type, or class A) is found to exhibit a stress exponent of 3. Class II (metal type, or class M) behaves like pure metals with $n = 5$. Creep of many pure metals follows class II behavior, while creep behavior of alloys falls into one of these two classes (Sherby and Burke, 1967; Bird et al., 1969; Cannon and Sherby, 1970; Murty et al., 1972; Mohammed and Langdon, 1974; Murty, 1974). The steady state creep behavior of Al-Mg alloys is recognized as a typical example of class I. The substructure formed during creep consists of a uniform distribution of dislocations with little evidence of well defined subgrains. On the other hand, in class II a regular array of subgrains is formed. The first attempt to predict the class of creep behavior in solid solution alloys was made by Cannon and Sherby (1970). They concluded that class II will be found in alloys with large elastic modulus, whereas class I is favored when the atom misfit ratio, and thus the dislocation solute interaction, is large.

2. Creep of Pure Al

Creep of polycrystalline pure metals in general and of pure Al in particular has been thoroughly studied by many investigators (Servi and Grant, 1951; Harper and Dorn, 1957; Barrett et al., 1972; Mohamed et al., 1973; Luthy, et al., 1980; Mohamed and Ginter, 1982). It is often proposed that the steady state creep rate $\dot{\epsilon}_s$, can be described by the following relation:

$$\dot{\epsilon}_s = K \left(\frac{D_{eff}}{b^2} \right) \left(\frac{\sigma}{E} \right)^5 \qquad (2.1)$$

where K is a constant approximately equal to 10^{11} for high stacking fault energy metals, D_{eff} is the effective diffusion coefficient, b is the Burgers vector, σ is the applied stress, and E is the dynamic unrelaxed average Young's modulus. Equation (2.1) describes the creep rate in the power law region. Sherby et al., (1977, 1979) used Garofalo's (1963) expression to describe the data in both the power law and power law breakdown regions, i.e., at intermediate and high stresses. Equation (2.1) becomes

$$\dot{\epsilon}_s = \frac{K}{\alpha^5} \left(\frac{D_{eff}}{b^2} \right) \left(\sinh \left(\alpha \frac{\sigma}{E} \right) \right)^5 \tag{2.2}$$

where for aluminum $K = 2 \times 10^{12}$, b is Burger's vector (2.8×10^{-10} m), and $\alpha = 2600$ (it is the value of $\left(\frac{\sigma}{E} \right)^{-1}$ at the start of power law breakdown). It was shown (Wu and Sherby, 1984) that the predicted curve using Equation (2.2) coincides with experimental data over 21 orders of magnitude of diffusion compensated strain rate ($\dot{\epsilon}/D_{eff}$) and three orders of magnitude of modulus compensated stress σ/E. Equation (2.2) is valid for coarse grained, polycrystalline, high stacking fault energy materials. It has also been demonstrated that the steady state creep rate of pure polycrystalline face centered cubic metals is related to the stacking fault energy by the relation

$$\dot{\epsilon}_s \propto \gamma^3 \tag{2.3}$$

where γ is the stacking fault energy. Thus the effect of stacking fault energy can be expressed (Sherby and Burke, 1968, Mohamed and Langdon, 1974) as

$$K = \bar{K} \left(\frac{\gamma}{Eb} \right)^3 \tag{2.4}$$

where $\bar{K}$ is a material constant. Incorporating the stacking fault energy term in Equation (2.2) yields

$$\dot{\epsilon}_s = \frac{\bar{K} \left(\gamma/Eb \right)^3}{\alpha^5} \left(\frac{D_{eff}}{b^2} \right) \left(\sinh \left(\alpha \frac{\sigma}{E} \right) \right)^5 \tag{2.5}$$

Addition of alloying elements to pure metal decreases the stacking fault energy, thus decreasing the steady state creep rate, either directly by increasing the distance between partial dislocation or through the development of fine subgrains in low

31

stacking fault energy material (Sherby and Burke, 1967). The dashed line in Figure 2.1 represents creep of pure Al and was calculated using Equation (2.5) and the data of Wu and Sherby (1984).

3. Creep of Class I Solid Solution Alloys

A Cottrell atmosphere forms preferentially around edge dislocations when the difference in size between the solute atom and the solvent atom is large. In the presence of a solute atmosphere, an additional stress is required for glide motion of the dislocations. The extra stress is called the dragging stress. As the disiocations attempt to move in response to an applied stress, the solutes may also move diffusively and are pulled along by the dislocations. Weertman (1960) derived an equation for the steady state creep rate $\dot\epsilon_g$ for such a glide controlled process, which may be written as

$$\dot\epsilon_g = \frac{\pi(1-\nu)(2(1+\nu))^2 E}{6A}\left(\frac{\sigma}{E}\right)^3 \tag{2.6}$$

where $\dot\epsilon_g$ is the glide-controlled creep rate, ν is Poisson's ratio, and A is a constant which depends on the details of the solute-dislocation interaction which can be evaluated from the details of this interaction. There are two approaches to calculate the value of A.

The first is based on the Cottrell and Jaswon (1949) model. For their model, A was calculated by Weertman (1960) to be equal to

$$A = \frac{e^2 c b^5 G^2}{kT\tilde{D}} \tag{2.7}$$

where e is the atom misfit parameter or the fractional size difference between the solute and solvent atom, c is the solute concentration, G is the shear modulus $(C = E/2(1+\nu))$, k is Boltzmann's constant, T is the absolute temperature and $\tilde{D}$ is the chemical interdiffusity. The parameter e is the linear derivative of the size factor (King 1966).

$$e = \left(\frac{\Omega_B}{\Omega_A}\right)^{\frac{1}{3}} - 1 \tag{2.8}$$

32
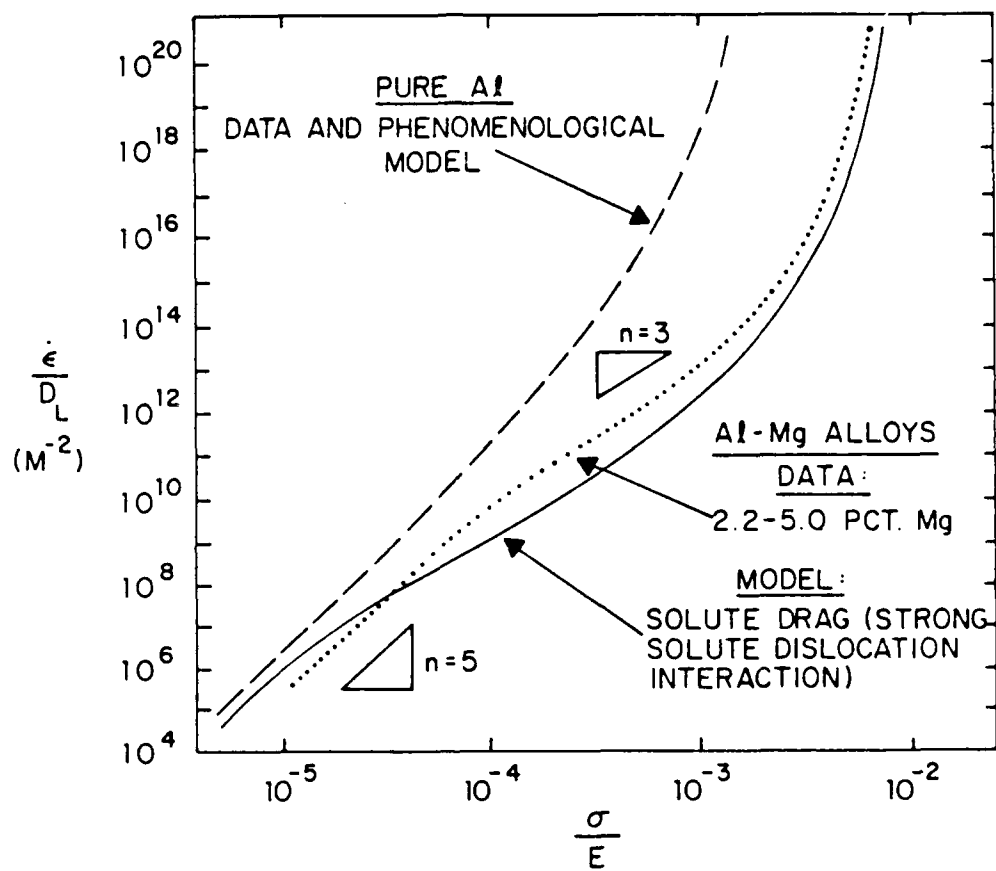
Figure 2.1. Diffusion-compensated strain rate versus modulus-compensated stress for pure Al and Al-Mg solid solution alloys containing from 2.2–5.0 percent Mg. The behavior the modified Friedel model is also illustrated. The transitions from stress exponent n=5 to n=3 to power law breakdown are shown for the solid solution.

33

where Ω_B is the effective atomic volume of the solute and Ω_A is the atomic volume of A in pure A. For binary solid solutions, $\tilde{D}$ is given by the Darken (1949) expression for binary solutions

$$\tilde{D} = (X_A D_B + X_B D_A)\left(1 + \frac{\partial \ell n \gamma_A}{\partial \ell n X_A}\right) \tag{2.9}$$

where X_A and X_B are the atomic fractions of A and B atoms, D_A and D_B are the tracer diffusivities of the A and B atoms in the AB alloy, and γ_A is the activity coefficient of the A species. $\tilde{D}$ may be approximated by using the tracer diffusivity data (Mohamed and Langdon, 1974).

The second approach developed by Friedel (1964) and subsequently elaborated by Bird et al. (1969) considers A to be independent of the solute concentration and the solute-solvent size difference. Friedel (1964) assumes a strong dislocation-solute interaction resulting in a short range interaction of solutes with the dislocations and essentially saturation of dislocations with solutes for ordinary solute concentrations. Using this model, A is given by

$$A = \frac{2kT}{b\tilde{D}} \tag{2.10}$$

Substituting the value of A given in Equation (2.4) or (2.7) into the general Equation for glide-controlled creep (Equation (2.3)), gives for Cottrell-Jaswon (1949) analysis:

$$\dot{\epsilon}_g = \frac{8\pi(1-\nu)(1+\nu)^4}{3} \frac{kT\tilde{D}}{Ee^2cb^5}\left(\frac{\sigma}{E}\right)^3 \tag{2.11}$$

and for the Friedel model

$$\dot{\epsilon}_g = \frac{\pi(1-\nu)(2(1+\nu))^3 Eb\tilde{D}}{12kT}\left(\frac{\sigma}{E}\right)^3 \tag{2.12}$$

Equation (2.11) shows an inverse dependence of creep rate on solute concentration and the square of the atomic misfit e, while equation (2.12) shows that the creep rate is concentration independent.

Mohamed and Langdon (1974) analyzed glide controlled creep based on the concentration dependent Cottrell and Jaswon model. According to Mohamed and

Langdon (1974), addition of Mg to Al decreases the creep rate and thus strengthens the material. Increasing the Mg concentration should be expected to lead to an increase in the stress and result in a concentration dependent behavior such as that of Equation (2.11). More recent analysis by Oliver and Nix (1982) on the effect of Mg content on the creep behavior of Al-Mg solid solutions has shown that the data for alloys containing from 2.2-5.0%Mg fall on a common curve. A similar analysis by Northwood (1984) on the data for material containing 1.7-3% Mg has been found to fit the same curve. As will be seen later in the next chapter, data for high Mg, alloys containing up to 10.2% Mg fall on the same curve as the data for lower Mg content alloys. This suggests that the creep resistance of Al-Mg solid solution alloys is concentration independent above 1.7% Mg. As suggested by McNelley (1987), the addition of smaller amounts of solute of small size difference may result in glide creep governed by Equation (2.10) in which the creep rate is concentration dependent. When the solute concentration is increased, dislocations become solute saturated and the addition of more solute has little further effect on the dislocation motion and therefore does not lead to further decrease in creep rate. Equation (2.11) underestimates the creep rate. Equation (2.12), based on the Friedel model, describes the creep behavior more accurately.

The Al-Mg solid solutions exhibit power law breakdown at $\frac{\sigma}{E} \cong 10^{-3}$ (Oliver and Nix, 1982). Following Garofalo's (1963) approach and as Wu and Sherby (1984) have done, a hyperbolic sine law is suggested to describe the creep in both the power law and power law breakdown region. This is done by replacing the term

$$\left[\frac{\sigma}{E}\right]^3 \quad \text{with} \quad \left[\frac{1}{\alpha_g^3}\right] \left[\sinh\left(\alpha_g \frac{\sigma}{E}\right)\right]^3 .$$

Equation (2.12) becomes

$$\dot{\epsilon}_g = \frac{\pi(1-\nu)2(1+\nu)^2 E b \tilde{D}}{12\alpha_g^3 kT} \left[\sinh\left(\alpha_g \frac{\sigma}{E}\right)\right]^3 \tag{2.13}$$

or

$$\frac{\dot{\epsilon}_g}{\tilde{D}} = \frac{K_g}{\alpha_g^3} \left[\sinh\left(\alpha_g \frac{\sigma}{E}\right)\right]^3 \tag{2.14}$$

35

where α_g is the value of $\left(\frac{\sigma}{E}\right)^{-1}$ at the onset of power law breakdown and K_g is a concentration independent factor describing the retarding force exerted upon dislocations by solutes that saturate the dislocation.

4. Transitions in Creep Behavior of Al-Mg Solid Solution

Dislocations move by sequential glide and climb processes. The total creep rate will be determined by the slower process for sequential glide and climb

$$\frac{1}{\dot{\epsilon}_t} = \frac{1}{\dot{\epsilon}_c} + \frac{1}{\dot{\epsilon}_g} \tag{2.15}$$

where $\dot{\epsilon}_t$ is the total creep rate, $\dot{\epsilon}_c$ is the climb-controlled creep rate given by Equation (2.2) or (2.5) and $\dot{\epsilon}_g$ is the glide controlled creep rate. Rearranging,

$$\dot{\epsilon}_t = \frac{\dot{\epsilon}_c \dot{\epsilon}_g}{\dot{\epsilon}_c + \dot{\epsilon}_g} \tag{2.16}$$

For pure metals $\dot{\epsilon}_c << \dot{\epsilon}_g$ and thus $\dot{\epsilon}_t \approx \dot{\epsilon}_c$. For alloying additions having a strong interaction with dislocations, $\dot{\epsilon}_g$ will decrease due to the solute dislocation interaction. Thus when $\dot{\epsilon}_g = \dot{\epsilon}_c$ a transition from climb-controlled to glide-controlled creep takes place. Al-Mg alloys exhibit such a transition in behavior in the form of change in the stress exponent. The creep behavior of the alloy changes from that of the alloy class to that of the metal class as the applied stress is reduced below a certain critical value; the data for Al-Mg exhibit this transition at $\frac{\sigma}{E} \simeq 10^{-4}$.

Figure 2.1 has three curves. The dashed curve describes the creep behavior of coarse grained pure Al as given by Wu and Sherby (1984). The dotted curve describes the creep behavior for Al-Mg solid solutions containing from 1.7–5% Mg. As we will see later the data up to 10% Mg fits the same curve. The solid curve is the predicted curve using the Friedel model for a concentration- independent creep rate, modified by the hyperbolic sine relation for the stress dependence. This latter model is assumed to act in series with the climb-controlled relation given by Equation (2.5). Applying Equation (2.15) gives the result seen in the lower part of Figure 2.1 where a transition in stress exponent from n=3 to 5 is seen as $\frac{\sigma}{E}$ decreases.

36

5. Models for the Mechanisms of Superplasticity

Some of the more general features of models for superplastic deformation were introduced in Chapter I. Here, more detailed discussion of these models, leading to introduction of constitutive equations for superplastic flow, is given. Ball and Hutchinson (1969) proposed a model in which dislocations pile-up within the grains (Figure 2.2). They considered that groups of grains slide as a unit until unfavorably oriented grains obstruct the sliding process. The stress concentration is relaxed by dislocation motion in the blocking grains. These dislocations pile-up against the opposite grain-boundary until the back stress prevents further activation of the source and stops sliding. The leading dislocation in the pile-up climbs into and along the grain boundaries and is eventually annihilated.

Mukherjee (1971) proposed a similar model in which the grains slide individually (Figure 2.3). Dislocations, generated by ledges and protrusions in the grain boundaries, traverse the grains and pile-up at opposite grain boundaries. The rate of sliding is then controlled by the rate of climb of the leading dislocations into annihilation sites at grain boundaries. Mukherjee (1975) proposed a modified version of his original model in which the grain boundary sliding is rate controlled by dislocation motion in the grain boundary by a combined climb-glide process.

Gifkins (1976) proposed a model which places emphasis on the role played by grain boundary dislocations (Figure 2.4). In this model, grain boundary dislocations (GBD's) move to give grain boundary sliding and then pile-up at triple edges. Under the stress concentration they dissociate into lattice dislocations in the sliding grains and then glide and climb in a mantle along the adjacent grain boundaries where their motion results in grain rotation. They are annihilated or recombine to form new GBD's. The mantle is a region near the grain boundary in which the accommodation processes take place and surrounds a core not involved in the accommodation processes, but which must also deform (Figure 2.5).

Arieli and Mukherjee (1980) proposed a model in which they consider that the strain is achieved by three dimensional grain rearrangement which proceeds by interface sliding followed by grain rotation. Accommodation is by climbing of individual dislocations into a narrow region near the boundary where they are

37
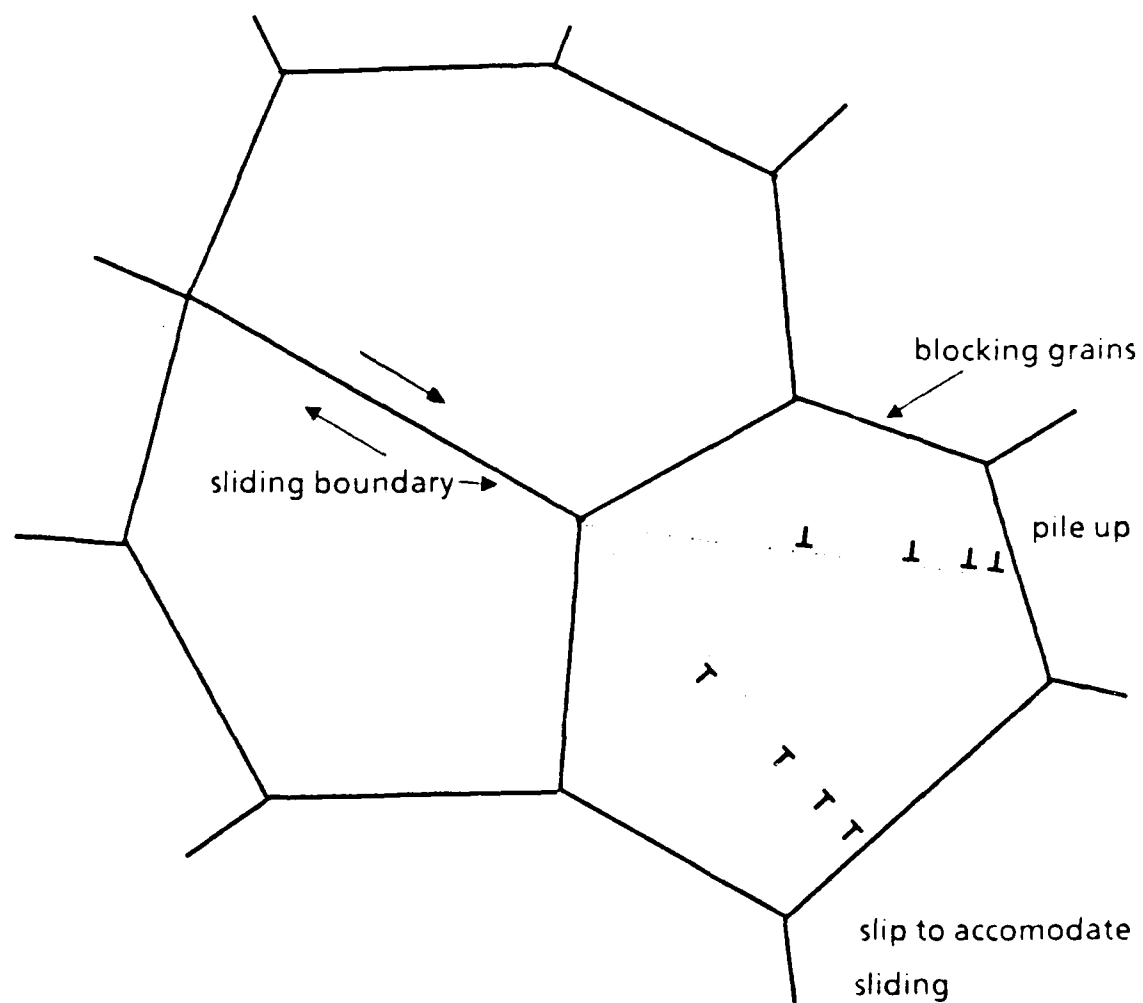
Figure 2.2 Slip accommodation of grain boundary sliding. Dislocations pile up within the blocking grains and climb of the leading dislocations in these pileups controls the sliding process. The grains slide in groups (adapted from Ball and Hutchinson, 1969).

annihilated. The individual dislocations, when climbing the short distance to the boundary, create new dislocations by the Bardeen-Herring mechanism. The stress concentrations created by the dislocations climbing into the boundary are relaxed by grain boundary diffusion. The dislocation activity in the narrow region near the boundary is the major accommodation mechanism for sliding. Because of the different sliding rates at different boundaries the grains rotate.

Some of the proposed models consider that accommodation is by dislocation motion within the grains (Matsuki, et al., 1976 and Nix, 1984). Slip within the grains must occur to provide torque necessary for grain rotation, a central feature of superplasticity. Other authors see that the accommodation process is by slip occurring both within the grains and in the vicinity of the grain boundaries. According to other models (Gifkins, 1976; Ruano and Sherby, 1982; Arieli and Mukherjee, 1980) the accommodation is by slip processes in the mantle. Shin, et al. (1987), through transmission electron microscopy studies, show dislocation activity near some grain boundaries. This too is consistent with the view that superplastic deformation is controlled by grain boundary sliding accommodated by slip processes in the mantle region.

6. Phenomenological Equations for Superplastic Flow

Slip, diffusional flow and grain boundary sliding are three principal processes of plastic flow (Ruano, et al., 1981, 1985, Shin, et al., 1987). These mechanisms are independent and the fastest is rate controlling. Creep equations discussed earlier may be written in an alternate form

$$\dot{\epsilon} = A' \left(\frac{b}{d} \right)^p \left(\frac{\sigma}{E} \right)^n \exp - \frac{Q_C}{RT} \qquad (2.17)$$

where $\dot{\epsilon}$ is the creep rate, A', n, and p are constants depending on the deformation mechanisms, σ is the creep stress, E is the dynamic unrelaxed average Young's modulus, d is the grain size, b is the Burger's vector, R is the gas constant, T is the absolute temperature and Q_C is the activation energy for the creep mechanism. For slip, p is usually 0; n is either 3, 4, 5 or 7, and Q_C is equal to the activation energy for solute diffusion, Q_s, the activation energy for lattice diffusion, Q_L, or the activation energy for pipe diffusion, Q_p. Some of these processes were considered

39
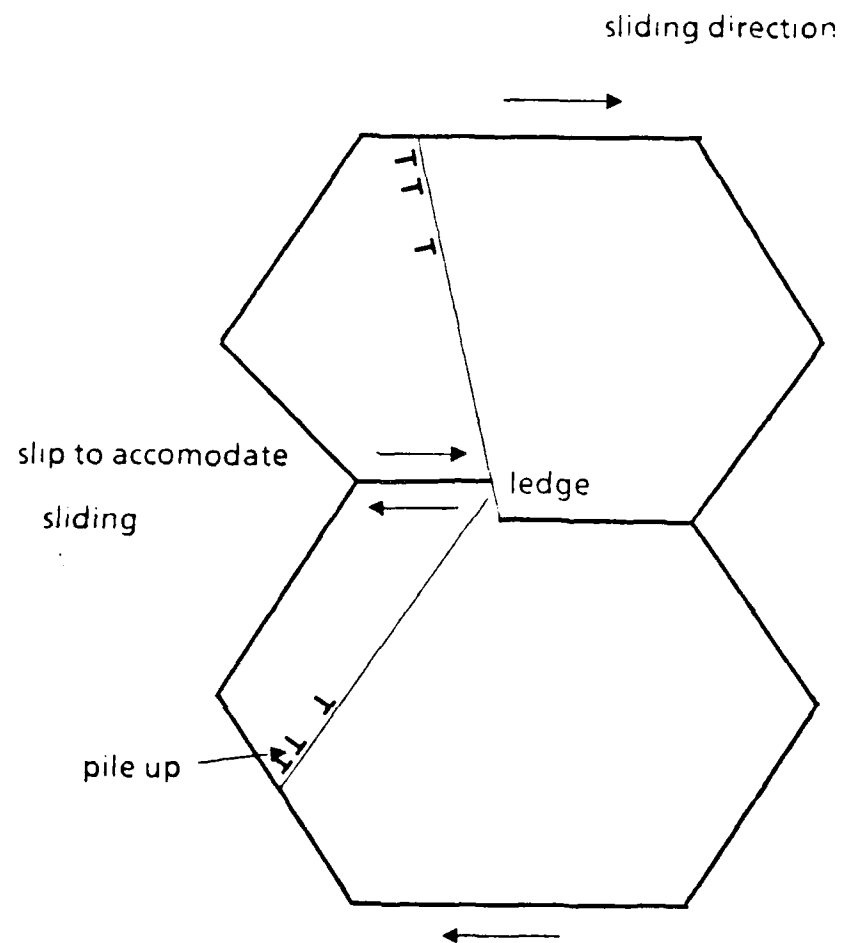
Figure 2.3. Slip accommodation of grain boundary sliding. Dislocations are emitted from ledges and pile up within the sliding grains. The grains slide individually (adapted from Mukherjee, 1969).

40
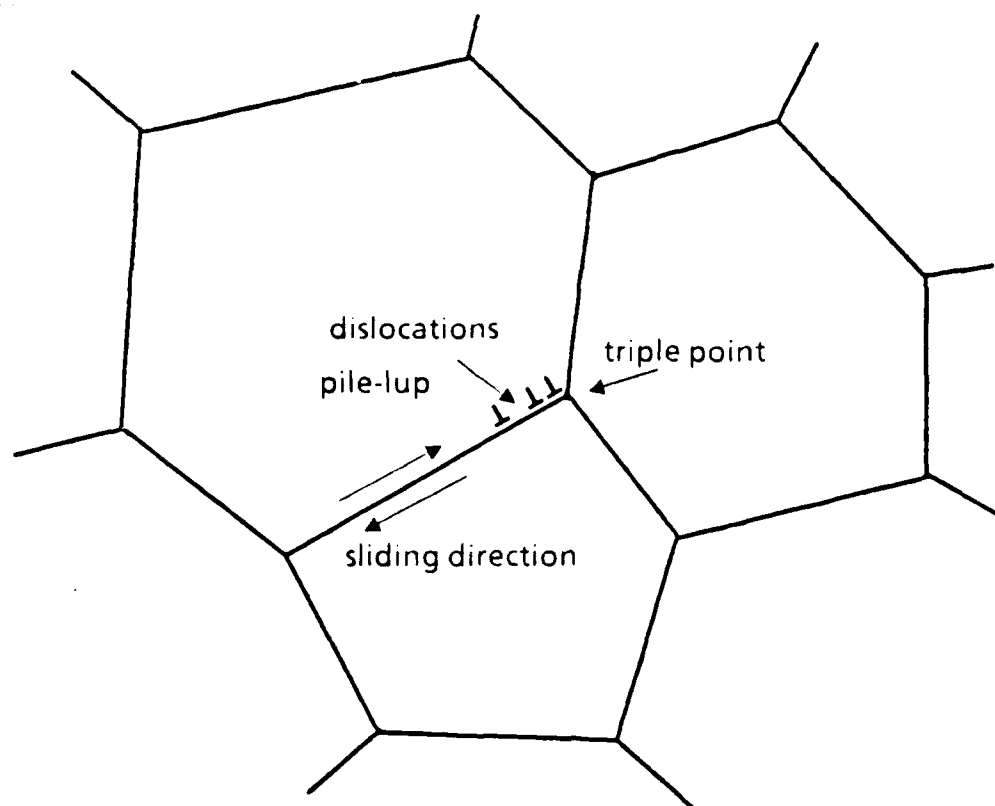
Figure 2.4. Grain boundary sliding accommodated by slip. Grain boundary dislocations pile up at boundary triple points and then dissociate into lattice dislocations in the sliding grains, and undergo climb in the mantle. The accommodation process is by moving of dislocations in the mantle (adapted from Gifkins, 1976).

41

mantle : accommodation
processes, boundary
slidng

core
slip processes
subgrain formation

a
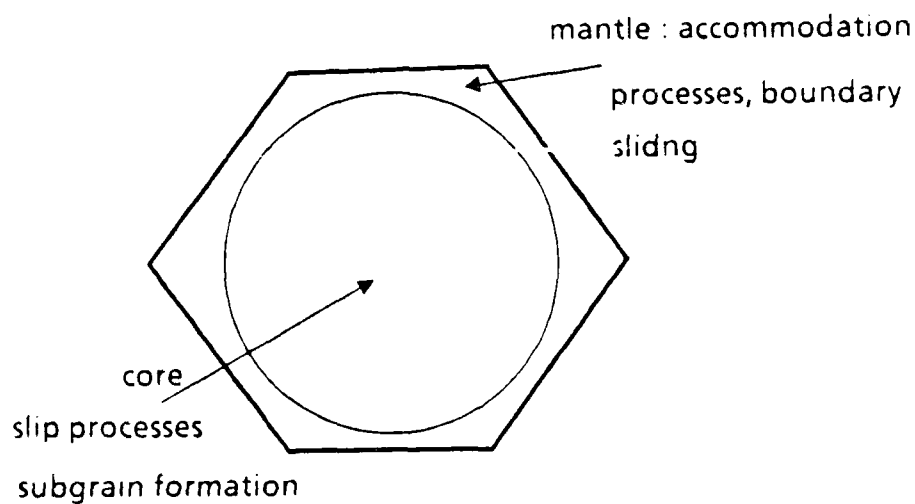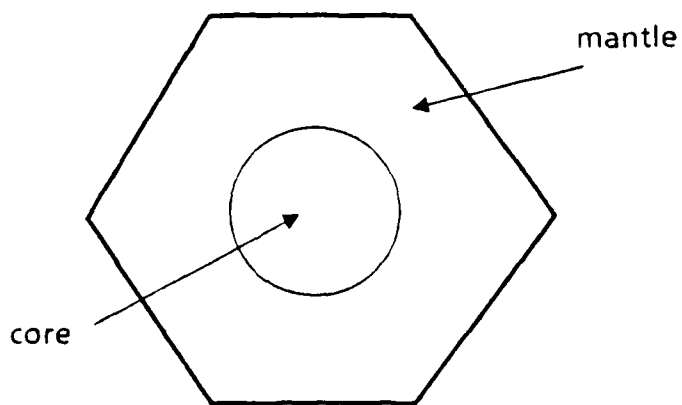
mantle

core

b

Figure 2.5. Core and mantle regions of a grain. At high strain rates and low temperatures, core processes dominate (a) while the mantle processes dominate deformation behavior at low strain rates and high temperature (b) (adapted from Gifkins, 1976).

42

earlier in Section IIA. For diffusional flow, $n = 1$; with $p = 2$, $Q_C = Q_L$; and with $p = 3$, $Q_C = Q_{gb}$. For grain boundary sliding, $n = 2$; with $p = 2$, $Q_C = Q_L$; with $p = 3$, $Q_C = Q_{gb}$, where Q_{gb} is the activation energy for grain boundary diffusion.

Sherby and Wadsworth (1982) propose that superplastic flow by grain boundary sliding may be described by a constitutive equation of the form

$$\dot{\epsilon}_{spf} = A'' \frac{D^*_{eff}}{d^2} \left(\frac{\sigma}{E}\right)^2 \tag{2.18}$$

where $\dot{\epsilon}_{spf}$ is the strain rate during superplastic deformation, A'' is a material constant containing the b^2 term, D^*_{eff} is the modified effective diffusion coefficient, d is the grain size, σ is the flow stress, and E is the elastic modulus. The modified effective diffusion coefficient D^*_{eff} is given by

$$D^*_{eff} = g_L D_L + C g_{gb} D_{gb} \tag{2.19}$$

where D_L is the lattice diffusion coefficient, C is a constant which is equal to 0.01 for superplastic deformation, g_L is the fraction of atoms associated with lattice diffusion, g_{gb} is the fraction of atoms associated with grain boundary diffusion ($g_{gb} \approx \frac{\pi \delta}{d}$ where δ is the thickness of the grain boundary layer which is usually taken as 2b, where b is the Burger's vector) and D_{gb} is the grain boundary diffusion coefficient. Because

$$g_{gb} = \frac{\pi \delta}{d} << 1, g_L \simeq 1 \text{ and}$$

Equation (2.19) can be written as

$$D^*_{eff} = D_L + \frac{C \pi \delta}{d} D_{gb} \tag{2.20}$$

D^*_{eff} is the weighed average of the lattice diffusion coefficient and grain boundary diffusion coefficient, and the weighting factor $\frac{C \pi \delta}{d}$ is essentially the fraction of atoms associated with the grain boundary layer. The coefficient $C \simeq 0.01$ was introduced to reflect the observation that grain boundaries are not as effective as high diffusivity paths as usually anticipated in the definition of D_{eff} (with $C = 1.0$). Equation (2.20) implies that superplastic flow is controlled by lattice diffusion when $D_L >> \left(\frac{C \pi \delta}{d}\right) D_{gb}$; under such conditions the deformation rate is proportional to

43

the inverse square of the grain size, i.e., $\dot{\epsilon}_{spf} \propto d^{-2}$. Conversely at lower temperatures and with a fine grain size where $\left(\frac{C\pi\delta}{d}\right) D_{gb} >> D_L$, grain boundary diffusion controls the superplastic flow and deformation rate is proportional to the inverse cube of the grain size $\dot{\epsilon}_{spf} \propto d^{-3}$.

At sufficiently low temperature the high diffusivity paths around dislocations can also act as short circuits effectively speeding the overall diffusion process. An effective diffusion coefficient $D_{L,eff}$ was developed by Hart (1957) to describe the additive contribution of lattice and dislocation pipe diffusion to the overall diffusion process in grain interiors. In essence, this term modifies the lattice diffusivity D_L in Equation (2.20). This $D_{L,eff}$ can be expressed by

$$D_{L,eff} = f_L D_L + f_p D_p \tag{2.21}$$

where f_L is the fraction of atoms associated with lattice diffusion ($f_L \simeq 1.0$) f_p is the fraction of atoms sites in the high diffusivity dislocation pipes and D_p is the dislocation pipe diffusion coefficient. The fraction f_p is a variable with the dislocation density:

$$f_p = \frac{n}{N}\rho \tag{2.22}$$

where n is the number of atoms at dislocation cores contributing to pipe diffusion, N is the number of atoms per (meter)^2 ($N = \frac{1}{b^2} = 2.5\times10^{15}$) and ρ is the dislocation density. The dislocation density is related to stress through Taylor relation

$$\rho \cong \frac{10}{b^2}\left(\frac{\sigma}{E}\right)^2 . \tag{2.23}$$

Substituting for ρ in Equation (2.22) gives

$$f_p = \frac{n}{N}\left(\frac{10}{b^2}\right)\left(\frac{\sigma}{E}\right)^2 ;$$

assuming that about 10 atoms contributing to dislocation pipe diffusion at each lattice plane threaded by a dislocation, $f_p = 200\left(\frac{\sigma}{E}\right)^2$. This leads to

$$D_{L,eff} = D_L + D_p\left[200\left(\frac{\sigma}{E}\right)^2\right] \text{ and}$$

$$\dot{\epsilon}_{spf} = \frac{A''}{d^2}\left[D_L + 200D_p\left(\frac{\sigma}{E}\right)^2 + \frac{C\pi\delta}{d}D_{gb}\right]\left(\frac{\sigma}{E}\right)^2 \tag{2.24}$$

44

At low $\frac{\sigma}{E}$ the term $200 D_p \left(\frac{\sigma}{E}\right)^2 << D_L$ and can be neglected. Under this low stress condition (at a higher temperature) and for coarser grain material Equation (2.24) simplifies to

$$\dot{\epsilon}_{spf} = A'' \frac{D_L}{d^2} \left(\frac{\sigma}{E}\right)^2 \tag{2.25}$$

and $Q_C = Q_L$; also, a σ/d^2 dependence of the strain rate is predicted. For finer grain structures at somewhat lower T, where $\frac{C\pi\delta}{d} D_{gb} >> D_L$,

$$\dot{\epsilon}_{spf} = A \frac{C\pi\delta D_{gb}}{d^3} \left(\frac{\sigma}{E}\right)^2 \tag{2.26}$$

and $Q_C = Q_{gb}$ with a σ^2/d^3 dependence of the strain rate. At high stresses, the term $D_p f_p$ may dominate D_{eff}. Then the term $200 D_p \left(\frac{\sigma}{E}\right)^2 >> D_L$ and

$$\dot{\epsilon}_{spf} = A \frac{D_p}{d^2} \left(\frac{\sigma}{E}\right)^4 ; \tag{2.27}$$

now, $Q_c \simeq Q_p$. Equations (2.25)–(2.27) predict a stress exponent of 2 at lower stress and a stress exponent of 4 at high stress.

B. RECRYSTALLIZATION MODES AND MICROSTRUCTURAL EVOLUTION

Dislocations are generated when a metal is plastically deformed. The dislocation density increases very rapidly due to the interaction of mobile dislocations with each other and with dislocations already present. Subsequent recovery may take place through two processes, annihilation and polygonization.

1. Annihilation

Annihilation of excess dislocations occurs by coming together of dislocation segments of opposite sign (that is, negative edge dislocations with positive edge dislocations, and left hand screw dislocations with right hand screw dislocations) (Reed-Hill, 1973). In this process both slip and climb mechanisms are involved.

2. Polygonization

The excess edge dislocations form arrays that constitute low-angle grain boundaries. When edge dislocations of the same sign accumulate on the same slip plane, their strain fields are additive. If the same dislocations are stacked one

45

above the other on parallel slip planes, the strain fields of the adjacent dislocations partially cancel each other. These low-angle boundaries are called subboundaries and the crystals that they separate subgrains. An edge dislocation moves by slip on its slip planes or climbs in a direction perpendicular to its slip plane. Both kinds of motion are required in polygonization. At low temperatures edge dislocations cannot climb. Because dislocation climb depends on the movement of vacancies, the rate of polygonization increases rapidly with temperature. Slip also becomes easier at high temperatures. Thus the higher the temperature the more complete is the polygonization process. The next step in substructure evolution is coalescence of these low-angle boundaries where two or more subboundaries combine to form a single boundary. The angle of rotation of the subgrain across the boundary grows in this process if the density of dislocations in the boundaries increases.

a. Dynamic Recovery

When these processes take place during plastic deformation, the metal is said to undergo dynamic polygonization or recovery (McQueen, 1968, 1977; McQueen, et al., 1967, 1973; McQueen and Jonas, 1975). Dynamic recovery occurs more readily as temperature is increased again because the mobility of the dislocations increases. Dynamic recovery occurs most easily in metals of high stacking fault energy. The primary mechanism involved in dynamic recovery is the cross slip.

b. Static Recovery

In static recovery, the movement of the dislocations into cell walls occurs as a result of the interaction stresses between the dislocations themselves. In dynamic recovery, the applied stress causing the deformation is added to the stresses acting between the dislocations. As a result, dynamic recovery effects may extend to lower temperatures (McQueen, 1977, 1968; McQueen, et al., 1967, 1973; McQueen and Jonas, 1975).

3. Recrystallization

In recrystallization, a new set of grains is formed. New crystals are nucleated at points of high stored strain energy in the lattice (Doherty, 1978). A number of models for the mechanisms of recrystallizations have been proposed. According

46

to Cahn (1950) and Beck (1949), polygonization may produce a subgrain capable of growing out into the surrounding polygonized matrix. Another mechanism proposed by Li (1962, 1966) involves the concept of subgrain coalescence or the combination of subgrains to form a strain free region large enough in size to grow.

The formation and motion of a high angle boundary of sufficient mobilities to act as a reaction front and sweep through surrounding material is termed discontinuous recrystallization. It is a nucleation and growth process. Alternatively, formation of subboundaries, by either or both of dynamic or static recovery processes, such that boundary misorientation increases to moderately large values, is termed in-situ or continuous recrystallization

4. Discontinuous Recrystallization

When a mobile grain-boundary is present, it is subjected to a number of forces. The sum of these forces $\sum F$ together with the grain-boundary mobility m determine the growth rate v of the recrystallization front (Figure 2.6):

$$v = m \sum F. \qquad (2.28)$$

Such a boundary could either be one formed within the original microstructure, or one which has been formed by a nucleation process involving subgrain rearrangement. The necessary condition for discontinuous recrystallization, i.e. for migration of a recrystallization front (Haessner, 1978; Koster; Hornbogen and Koster, 1978), is

$$F_n + F_c > F_p + F_s \qquad (2.29)$$

where F_n is the driving force associated with the elimination of dislocations and/or subgrain boundaries, F_c is the driving force due to discontinuous precipitation of particles within the advancing boundary, or for the transformation of metastable particles into stable ones, F_s is the retarding force due to segregation of foreign atoms from the solid solution into the reaction front, and F_p is the retarding force exerted on the migrating boundary by stable precipitated particles. If this condition is not satisfied, the reaction front does not move and discontinuous recrystallization will not occur.

47
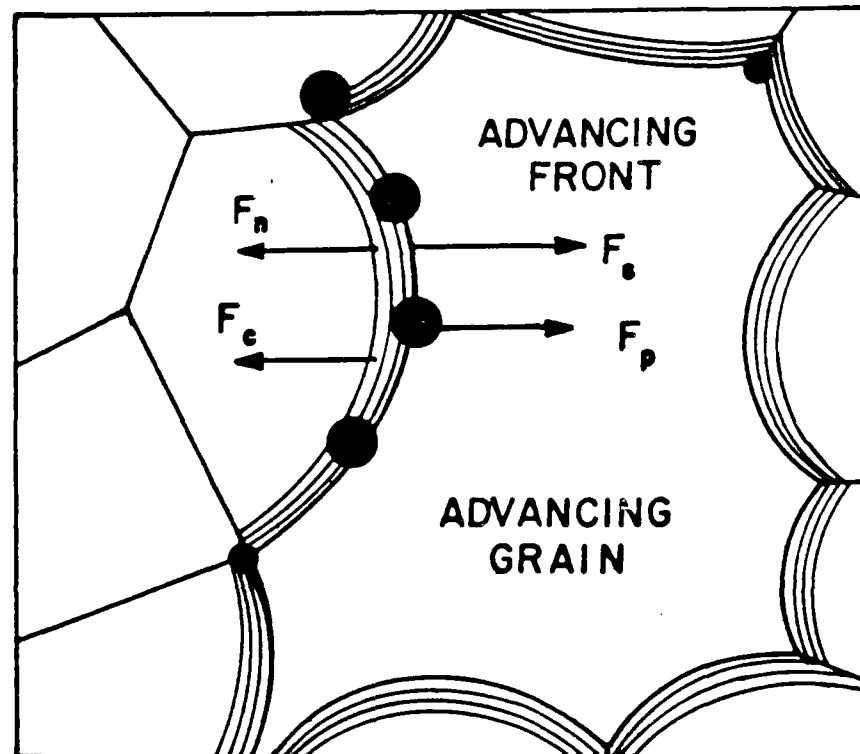
Figure 2.6. Schematic diagram of discontinuous recrystallization. F_n and F_c are driving forces for recrystallization while F_s and F_p are the retarding forces. For discontinuous recrystallization to take place and the reaction front to be able to grow the driving forces should exceed the retarding force, $F_n + F_c > F_s + F_p$ (adapted from Haessner, 1978).

48

5. Continuous Recrystallization

If it is assumed that no grain boundaries are present or that existing grain boundaries are held by preferential precipitation, i.e. Equation (2.29) is not satisfied, no recrystallization by the formation and migration of a reaction front can occur. It is still possible to form essentially strain free regions, i.e. new grains, by the continuous recrystallization process. For example, when a particle located at a dislocation node dissolves, these dislocations can migrate more easily than those still pinned by particles. A subgrain boundary thus can be annealed out by Y-node motion or rotation of a subgrain as illustrated schematically in Figure 2.7 (Hornbogen and Koster, 1978; Haessner, 1978). The defect-free areas and the angles between them increase, leading to a gradual increase in sub-grain size and an increase in the misorientation between subgrains. Growth can proceed when the dislocation networks assume the character of grain boundaries even though the condition for discontinuous recrystallization may still be unfulfilled. This process leads, without any migration of recrystallization fronts, to a grain structure differing from the discontinuously recrystallized structure only in the distribution of grain size and particles and in the texture. Continuous recrystallization by subgrain growth leads to retention of rolling texture, while recrystallization by motion of high angle boundary leads to a change in texture.

6. Competition Between Continuous and Discontinuous Recrystallization Modes.

Depending upon the supersaturation, the amount of work, the density and distribution of dislocations, segregation of solute atoms, the presence of particles associated with dislocations, and temperature a binary alloy can recrystallize either continuously or discontinuously. Figure 2.8 summarizes the influence of concentration on the recrystallization behavior of deformed, supersaturated Al-Mg alloys. In region I, the α-phase solid solution, normal recrystallization takes place without precipitation. Crossing the solubility line into the two phase $(\alpha + \beta)$ field, recrystallization with subsequent precipitation is expected in region II. In region III, the precipitation and recrystallization processes exert a mutual influence; in this region, discontinuous recrystallization with concurrent precipitation exists. In stage

49

IV only continuous recrystallization occurs. In the thermomechanically processed Al-Mg alloys, zones II and III likely are very small and extend to near the solvus line. For the Al-10%Mg-0.1%Zr and for Al-10%Mg-0.52%Mn alloys studied, the continuous recrystallization zone apparently extends above 300°C.

According to Wert, et al. (1985), to obtain continuous recrystallization the comparatively rapid discontinuous recrystallization reaction must be suppressed. This requires drag on the boundary sufficient to prevent discontinuous recrystallization. Particle dispersions can provide this necessary drag force, suggesting that continuous recrystallization may be observed in alloys containing high densities of small particles. According to Tweed, et al. (1984), the drag pressure on low angle ' boundaries is lower than that on high angle boundaries for a given value of $\frac{f}{r}$, where f is the volume fraction of particles and r their size. This allows the low angle boundaries to migrate while high angle boundary motion is suppressed. The continuous recrystallization is thus encouraged by the presence of fine scale zirconium containing precipitates, by the presence of a high Mg content in solution, i.e. by high supersaturation (Ahlborn, 1969; Grimes 1975; 1976; Gardner and Grimes 1979; Wert, et al., 1985; Nes, 1985; Nes, et al., 1985). In Chapter VII, the competition between the two modes will be discussed in conjunction with the microstructure evolution during the rolling process.

7. Models for Microstructures Evolution During SPD.

Superplastic Zr-bearing aluminum alloys may also recrystallize by a continuous reaction during the initial stage of hot deformation. (Watts, et al., 1976; Ives, 1978, 1979; Bricknell, 1979). Nes measured the change in subgrain size and misorientation with strain (Nes, 1979) and found that during the initial 50% strain both the grain size and misorientation are more than doubled. Nes proposed two models for this rapid strain induced subgrain growth and the rapid increase in misorientation (Nes, 1985); these are described in a subsequent section.

8. Application of the Two Modes for Grain Refinement in Al Alloy

Currently, there are two recrystallization processes for grain refinement in Al alloys being utilized industrially. These are described below (Wadsworth, 1984; Wert, 1985).

50
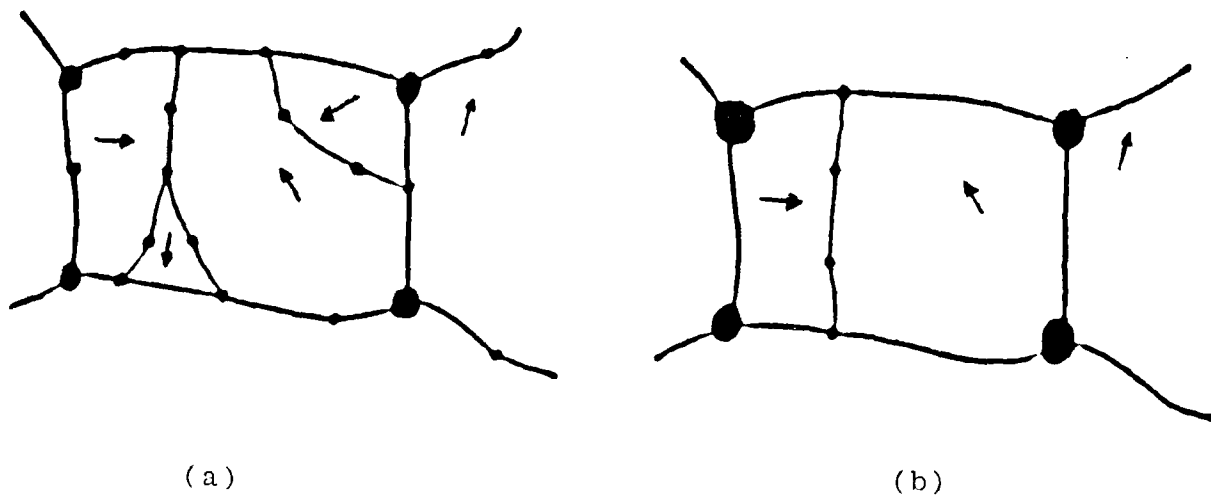
Figure 2.7. Subgrain growth by coalescence. In (a) the subgrains are pinned by particles. In (b) after dissolution of the smallest particles a subgrain can anneal out of Y-node motion or by subgrain rotation (after Hornbogen, 1978).

51
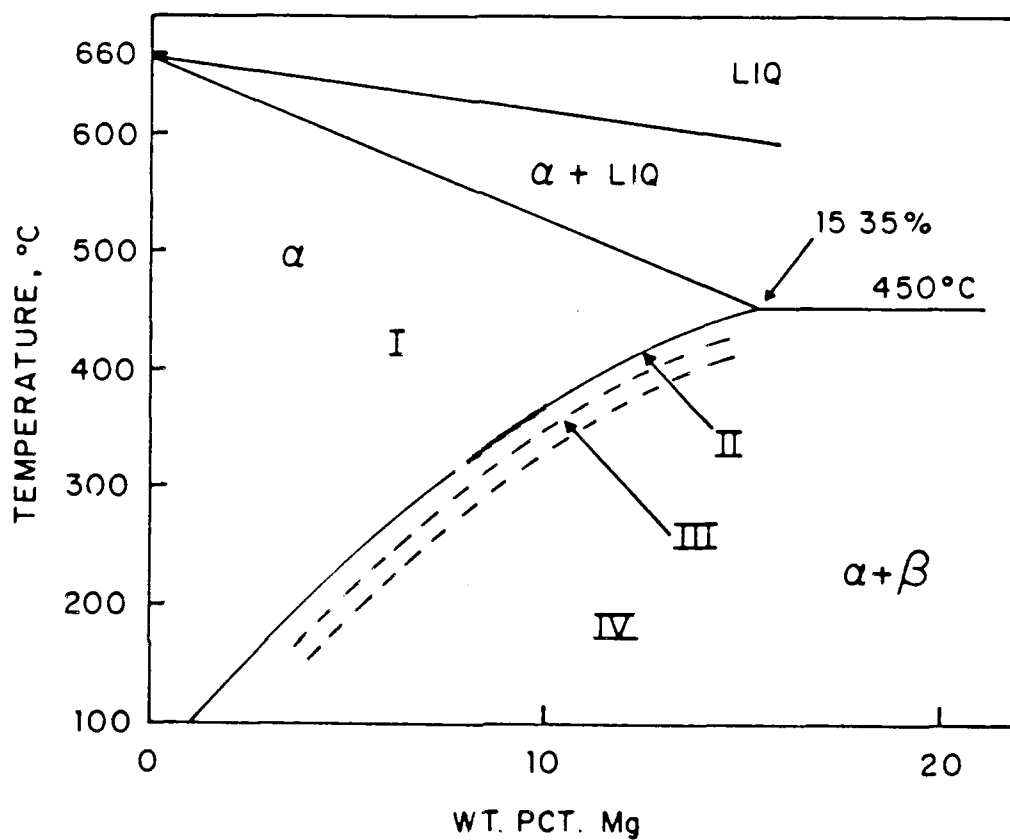
Figure 2.8. Influence of concentration on the recrystallization behavior of deformed supersaturated solid solutions. In zone I, normal recrystallization occurs with no precipitation; in zone II, recrystallization takes place with subsequent precipitation; during zone III, discontinuous recrystallization occurs with simultaneous precipitation; and in zone IV, continuous recrystallization is the dominant transformation mode. In Al-Mg Zones II and III are narrow and Zone IV extends to high temperatures. (adapted from Haessner, 1978).

a. Thermomechanical Processing (TMP) Using the Discontinuous Recrystallization Mode

TMP's using the discontinuous recrystallization mode are used for alloys which have dispersoid distribution giving low drag on boundaries (Wert, 1985). Discontinuous recrystallization is therefore rapid. Concurrent deformation at the recrystallization temperature is not required. Material designed for superplastic forming applications can be recrystallized and evaluated before superplastic deformation.

b. Thermomechanical Processing Using Continuous Recrystallization for Grain Size Control

This requires alloy compositions having dispersoid distributions giving high drag pressure (Wert, 1985). Continuous recrystallization requires either prolonged annealing or concurrent deformation at elevated temperature. Suppression of discontinuous recrystallization is sensitive to variations in alloy and process parameters. Materials designed for superplastic forming applications are generally supplied in the as-rolled condition and the superplastic properties depend strongly on the initial stages of deformation for each component. Thermomechanical processing for discontinuous recrystallization cannot produce grain size as fine as those that can be achieved through a properly controlled continuous process.

C. GRAIN GROWTH IN SUPERPLASTIC DEFORMATION
1. Grain Growth Phenomenon During Superplastic Deformation

A number of investigators have reported that the kinetics of coarsening are enhanced by deformation, i.e. the grain size in the deformed specimens is larger than in specimens held for the same time at the deformation temperature (Alden, 1967; Backofen and Lee, 1967; Backofen and Zehr, 1968; Alden, 1968; Backofen et al., 1968; Stowell et al, 1969; Clark and Alden, 1973). Such microstructural coarsening is of great importance because superplasticity can occur only in sufficiently fine-grained structures. Coarsening of the microstructure causes "hardening" as the flow stress for a given strain rate increases. This hardening may bring superplasticity to an end as other mechanisms comes to dominate the flow. Strain

hardening is more pronounced at low strain rates. The actual shape of the true-stress true-strain curve is actually affected by two considerations: (1) deformation induced grain coarsening that produced a hardening, and (2) the presence of a large number of cavities also causing a softening effect.

The concurrent grain growth and associated hardening usually lead to a decrease in strain rate sensitivity coefficient (m). Typical tensile data obtained at constant strain rate shows a continuous load rise at the slower strain rates and load drop at the higher strain rates as seen in Figure 2.9. Most investigators attribute the strain hardening to the grain growth; the softening, some authors attribute to cavitation while others to the onset of dynamic recrystallization. Jonas (1982) has stated that the flow softer 's process was identified with the break-up of an extruded microstructure into approximately equiaxed grains. In other studies the grain size remained virtually unchanged and the dislocation density was found to increase, both in the matrix and at the grain boundaries with increasing strain level. The increased dislocation density is then judged responsible for the strain hardening of the material.

2. Models for Grain Growth During Superplastic Deformation

a. Clark and Alden Model

Clark and Alden (1973) have proposed a model which was based on deformation-enhanced grain boundary mobility. The suggested mechanism for enhanced growth has as its basis the production of excess vacancies in the grain boundary region, leading to increased boundary mobility. Deformation in the high strain-rate sensitivity region is accompanied by large amounts of grain boundary sliding and grain rotation. Because of the importance of grain boundary sliding and grain rotation in superplasticity, the possibility exists for grain coalescence to occur during deformation. The amount of sliding and grain rotation, and hence the number of coalescence reactions, should increase continually during straining. Consequently the amount of grain size enhancement should also increase with strain. They found that the percentage of the total strain due to the grain boundary sliding reaches a maximum at a strain rate of maximum m. Thus for a given amount of strain, the amount of grain rotation and the grain size enhancement should reach

54
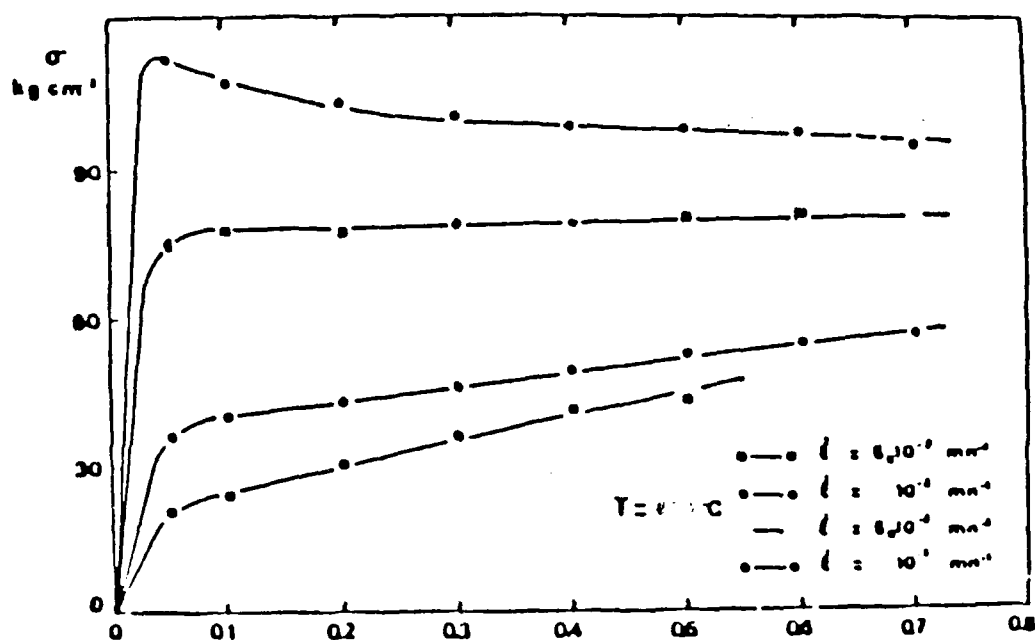
Figure 2.9. True stress versus true strain at various strain rates for a 60/40 brass deformed at 600° C. These data illustrate the strain hardening due to grain growth at lower strain rate and the softening due to the evolution of an equiaxed structure at the higher strain rates (after Suery and Baudelet, 1978).

a maximum in the superplastic region. They assumed that grain boundary sliding does produce an excess of vacancies in the grain boundary region and describe a simple model for mobility enhancement based on this assumption.

b. Holm Model

The Holm, et al., (1977) model is based on the assumption that this enhancement can be explained by particle coalescence during grain neighboring switching. The neighbor switching mechanism proposed by Ashby and Verrall (1973) also provides for the possibility of particle agglomeration during flow.

c. Nes Model

Nes (1985) studied grain growth during superplastic flow and proposed two models, one based on geometric particle coarsening and the other based on strain induced particle reversion. According to the latter model, as a result of thermomechanical treatment prior to hot forming a subgrain structure is established. Hot deformation then forces the sub-boundaries to migrate and this migration in turn causes the stabilizing Al_3Zr fine particles to go partially back into solution. A consequence of this straining-induced reversion is a rapid subgrain growth.

After some time, homogeneous precipitation of Al_3Zr is observed. The volume fraction of the small Al_3Zr particles is observed to decrease with increasing strain as the Zr is being redistributed from the small particles toward larger, more stable particles. At a critical strain of about 0.5, all the small Al_3Zr particles were dissolved and the grain structure was then stabilized by the coarser particles which were assumed to remain stable. This model thus accounts for both the grain growth in the initial stage of deformation and the stagnation of grain growth at larger strain.

d. Suery and Baudelet Analysis

Suery and Baudelet (1978) studied the effect of grain growth various constitutive equations for superplastic deformation. These analyses considered that the grain growth occurs with strain at any given strain rate. This influence is expressed by the parameter $f_{\dot{\epsilon},T} = \left(\frac{\delta \log d}{\delta \log \epsilon} \right)_{\dot{\epsilon},T}$. At any given strain, the growth tends to be greater for the lower strain rates. This can be expressed by a term of

the form $g_{\epsilon,T} = \left(\frac{\delta \log d}{\delta \log \dot{\epsilon}}\right)_{\epsilon,T}$. Also, grain growth is a function of temperature. The influence of temperature is included by $h_{\dot{\epsilon},\epsilon} = \left(\frac{\delta \log d}{\delta \frac{1}{T}}\right)_{\dot{\epsilon},\epsilon}$.

Their analysis of superplastic deformation shows that the structure tends to evolve toward an equiaxed state and to undergo grain growth with straining. They calculated relationships among deformation parameters such as m and Q as affected by grain growth. They show, for instance, that an apparent strain rate sensitivity of the stress m which does not take into account grain growth, is lower than $\bar{m}$, the true rate sensitivity coefficient and tends toward $\bar{m}$ when $\dot{\epsilon}$ in the superplastic region increases:

$$m = \bar{m}\left(1 + \bar{a}g_{\dot{\epsilon}T}\right) \tag{2.30}$$

where $\bar{m}$ is the value of the strain rate sensitivity coefficient when grain growth is taken into account ($\bar{m} = 1/2 = 0.5$ in Equation (2.25)) and $\bar{a}$ is the exponent on grain size (e.g. 2.0 in Equation (2.25)). Similarly, the activation energy Q is given by

$$mQ = \bar{m}\left(\bar{Q} + \bar{a}h_{\epsilon,\dot{\epsilon}}\right)$$

or

$$Q = \frac{\bar{Q} + \bar{a}h_{\epsilon,\dot{\epsilon}}}{1 + \bar{a}g_{\epsilon,T}} \tag{2.31}$$

where $\bar{Q}$ is the activation energy for the underlying diffusional process ($\bar{Q} = Q_L$ in Equation (2.25)). Equation (2.31) implies that grain growth with increasing temperature will decrease the apparent activation energy.

D. ASSESSMENT AND REVIEW OF THE PREVIOUS WORK AT THE NAVAL POSTGRADUATE SCHOOL

McNelley and Garg (1984) showed that highly refined subgrain structures can be produced in high Mg, Al-Mg alloys utilizing a thermomechanical process (TMP) to attain the microstructural refinement. The essential features of the TMP used were: solution treatment above the Mg-solvus; upset forging above the solvus; quenching through the solvus; reheating to a temperature below the solvus, 300°C,

and warm rolling to a large strain, $\epsilon > 2.0$. Processing under such conditions resulted in concurrent precipitation of a homogeneous, refined and uniform dispersion of about 0.5 μm intermetallic $\beta(Al_8Mg_5)$ in a solid solution matrix composed of elongated grains also containing 0.5–1.0μm size subgrains. This structure may be further refined and stabilized by the addition of dispersoid forming elements such as Mn or Zr. The structure obtained by the TMP would not be expected to exhibit a superplastic response, as such non-recrystallized microstructures would not be expected to sustain grain boundary sliding.

However, superplastic elongations up to 600% were recorded at 300°C and at strain rate of 2–5 $\times 10^{-3}s^{-1}$, an order of magnitude faster than typically reported for wrought Al alloys (Lee and McNelley, 1987). Since the usual microstructural prerequisites were not realized and nucleation and growth of new grains were not observed, it was proposed that a continuous recrystallization mechanism would account for the results (McNelley, Lee and Mills, 1986; Lee, McNelley and Stengel, 1986). This mechanism was judged responsible for transformation of the microstructure from the as-rolled, heavily deformed structure to a fine structure capable of sustaining grain boundary sliding. Hales and McNelley (1987) measured the boundary misorientations in Al-10%Mg-0.1%Zr in various processing conditions. They showed that the high initial dislocation density in as-rolled material rapidly transformed into a well defined structure containing boundaries. After 10 minutes annealing boundaries with misorientations of 1–5°were observed, increasing to 2–7°with further annealing. During superplastic deformation misorientation increased to 20–30°. They also concluded that boundaries of this moderate angle can sustain grain boundary sliding. They concluded that continuous recrystallization is the mechanism responsible for converting a high dislocation density structure into a fine grained structure. When the temperature dependence of the flow stress was studied, the as-rolled material exhibited an anomalous behavior in the form of an increase in stress when the temperature is increased. This behavior extended from 325°C to 350°C. This temperature is below the solvus for the β phase. Initially annealed and recrystallized material did not show this anomalous behavior but exhibited a smoothly decreasing strength with temperature increase. At

58

temperatures below 325°C the as-rolled material is weaker than the recrystallized material while at high temperatures above 325°C the two materials are identical in strength. This behavior was interpreted in terms of structural/substructural coarsening in the as-rolled material prior to commencement of deformation, although microscopy to support this was not done.

E. APPROACH IN THIS RESEARCH

The initial part of this effort was devoted to a review of the literature and assessment of existing models of superplastic deformation. This resulted in the conclusion that the superplastic response documented by McNelley, Lee and Mills (1986), Lee, McNelley and Stengel (1986) and Lee and McNelley (1987) could be interpreted in terms of existing models for fine-grain superplasticity if a grain size of approximately 2.0μm had been achieved during TMP and in the early stages of deformation. It was this observation that lead to evaluation of the misorientation of boundaries in the warm- rolled Al-10%Mg-0.1%Zr material.

Subsequent work was directed at evaluation of the effects of changes in the TMP process parameters. Continuous recrystallization involves dislocation rearrangements leading to formation of boundaries. The dislocation density prior to rearrangement would be expected to have considerable influence on the resultant boundary structure, with higher initial dislocation density leading to greater subsequent boundary misorientation. This was anticipated to lead to enhancement of the subsequent superplastic response. A matrix of process parameters was established to assess this conclusion. The results of this portion of the experimental effort contradicted this assumption, and this lead to a new model for the process of continuous recrystallization during the processing of the material and subsequent heating and deformation. The final efforts in this research involved application of the models for behavior of the Al-Mg alloys to other aluminum-base alloys of interest for superplastic forming.

III. MATERIALS AND EXPERIMENTAL TECHNIQUES

A. MATERIALS

The materials used in this study were supplied by Alcoa Technical Center, Alcoa Center, Pennsylvania. The aluminum alloys contained either 8 or 10 wt.% Mg. The material was provided in the form of direct-chill cast ingots fabricated using 99.99% pure aluminum as the base metal. Commercially pure Mg was used for alloying. Zr or Mn were added from master alloys to form dispersoids. The composition of the alloys studied in this investigation is given below in Table III-1. The as-cast ingots were sectioned into billets with a cross section 31.8 mm (1.25 in) square and a length of 95.3 mm (3.75 in) to facilitate further processing.

TABLE III-1
ALLOY COMPOSITIONS (IN WT. PCT.) FOR THE Al-Mg ALLOYS OF THIS INVESTIGATION

Alloy	Mg	Zr	Mn	Si	Fe	Ti	Be	Al
1	9.89	0.09	–	0.02	0.02	0.01	0.0003	balance
2	10.2	–	0.52	0.01	0.03	0.01	0.0002	balance
3	8.05	0.13	–	0.01	0.02	0.01	0.0002	balance

B. THERMOMECHANICAL PROCESSING (TMP)

The TMP used is shown schematically in Figure 3.1. The first step is solution treatment at 440°C for 40 hours. This temperature is well above the solvus for these alloys ($\sim$ 380°C for 10% Mg), but still below the eutectic temperature ($\sim$ 451°C). Homogenization is completed by hot working via upset forging at 440°C, reheating for one hour, and then quenching in oil. Subsequently, the billets were heated for 30 minutes at the rolling temperature to achieve isothermal conditions prior to the first rolling pass. The rolling temperature was 300°C for most of

60
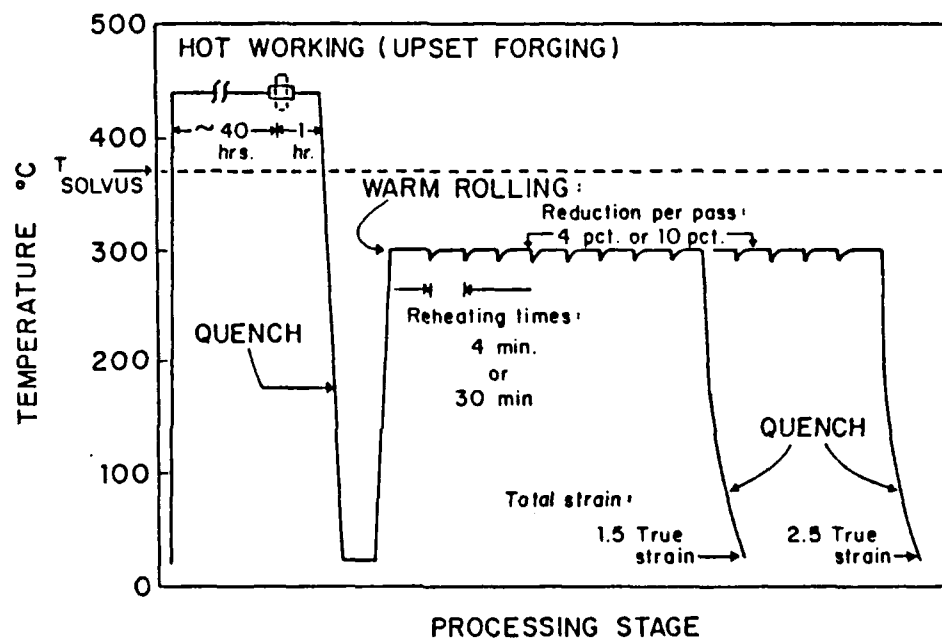
Figure 3.1. Schematic diagram of the thermomechanical processing (TMP) method.

the processing; two other temperatures utilized were 220°C and 380°C. In all cases, isothermal conditions were maintained by reheating between each rolling pass. Reduction was held constant, resulting in increased strain and strain rate as deformation was accumulated. For the rolling done at 300°C a variety of processing schemes were evaluated. These involve different combinations of reductions, reheating times and total strains and are summarized in Table III-2.

TABLE III-2
TMP VARIABLES FOR PROCESSING OF Al-Mg ALLOYS

	Reduction/Pass, mm	Reheating Time Between Passes, Min	Total Strain
TMP-I	1	4	1.5
TMP-II	2.5	4	1.5
TMP-III	1	4	2.5
TMP-IV	1	30	2.5
TMP-V	2.5	4	2.5
TMP-VI	2.5	30	2.5

In some cases, samples of processed material were reheated and annealed at the prior solution temperature to accomplish static recrystallization and produce a fully annealed condition. This was done by heating for 30 minutes at 440°C in a neutral salt bath for accurate control of the temperature.

C. TENSION TESTING

Mechanical testing was accomplished utilizing constant crosshead speed. An Instron electromechanical machine, Model TT-D, with a Marshall Model 2232 three-zone furnace for temperature control, was used to conduct the testing. The specimens were heated in the furnace for about 45 minutes before the start of testing to assure equilibration at the test temperature. The crosshead speeds used

in this research ranged from 0.05 mm/min (0.002 in/min) to 127 mm/min (5.0 in/min) corresponding to nominal strain rates varying from $6.67 \times 10^{-5} \ s^{-1}$ to $1.67 \times 10^{-1} s^{-1}$. Elongation was determined by measuring the marked gage section before and after testing and percent elongation was determined by measuring the distance between these gage marks and dividing by the initial length.

The Instron strip chart measured applied load (in lbs.) versus chart displacement. From the strip chart raw data points of load and chart displacement were taken after determination of an initial slope. All the data obtained were analyzed using a computer program and graphically presented using the Easyplot routine on an IBM 3033 computer.

D. MICROSCOPY

Both optical and transmission electron microscopy methods were employed during this research. The essential details are given below.

1. Optical Microscopy

After mounting, the specimens were wet ground in successive steps using silicon carbide abrasive sheets of 220, 320, 400 and 600 grit. During the grinding process adequate water was used to flush away abrasive particles. After each grinding step the specimens were thoroughly washed to prevent carrying over the abrasive particles from the coarser grades to the finer ones. After grinding the specimens were mechanically polished in two steps. The first step used $6\mu m$ diamond paste with a special extender as a lubricant. The second step used Magomet® (MgO) powder. Specimens were anodized using Barker's reagent (2.5 ml HBF_4 in 100 ml H_2O) at 0.2 A/dm^2 with a DC voltage of about 20 volts for 40–60 seconds and using Al for a cathode. The specimens were then examined by polarized light methods to reveal grain contrast. Optical microscopy was used primarily to study the instability of the structure and grain growth at temperatures near or above the Mg solvus, especially for the Al-10%Mg-0.1%Zr alloy.

63

2. Transmission Electron Microscopy

Transmission electron microscopy (TEM) studies were conducted on specimens in the as-rolled and in the annealed condition to study the evolution of microstructure and grain growth at temperature near the rolling temperature (300°C). TEM samples were selected from both grip and gage sections. Samples from grip sections were taken from specimens subjected to deformation at the highest strain rate used, $1.67 \times 10^{-1} s^{-1}$. This strain rate was chosen since average times to failure at this strain rate were only about 15 seconds. Thus the total time the sample is subjected to temperature is approximately 45 minutes, i.e., the time of heating before superplastic deformation. Other samples were taken from the deformed gage sections of specimens subjected to deformation at a strain rate $\dot{\epsilon} = 6.67 \times 10^{-3} s^{-1}$. This is approximately the strain rate of the highest ductility. The specimens were removed from the bulk material such that the foil normal was parallel to the sheet normal direction. Electrothinning was accomplished in a solution of 25% HNO_3 in methanol at -20° C and 15 volts DC. A JEOL JEM-100CX transmission electron microscope was used to examine the microstructure. The accelerating voltage used throughout this work was 120 KV.

3. Mean Linear Intercept

The mean linear intercept (MLI) method was used to measure the grain size according

$$d = 1.773 \bar{L} \tag{3.1}$$

where d is the grain size and $\bar{L}$ is the MLI determined from micrographs. For TEM samples, twelve photographs were taken for each specimen from four different locations and at three different tilting angles. This was done to assure imaging of all boundaries prior to evaluation of $\bar{L}$. In optical microscopy, three photographs representing three different areas were taken for each specimen. The number of intercepts were measured on ten different lines in each micrograph and the value of $\bar{L}$ was calculated according to the relation (Voort, 1984)

$$\bar{L} = \frac{1}{P_L}, \tag{3.2}$$

where, $P_L = \frac{P}{\frac{L_T}{M}}$, and P is the number of grain boundaries intersecting along the line. L_T is the total line length and M is the magnification.

IV. MODELING THE SUPERPLASTIC RESPONSE OF THERMOMECHANICALLY PROCESSED Al-Mg ALLOYS

A. THE STRAIN RATE AND TEMPERATURE DEPENDENCE OF DEFORMATION IN Al-10Mg-0.1Zr

The initial part of this investigation involved analysis of data originally reported by Hartmann (1985) and Alcamo (1985). These data were obtained on an alloy of nominal composition Al-10%Mg-0.1%Zr; the details of the composition are given in Table I, where it is the first listed.

The material was processed by TMP III. The details of the processing are listed in Table II. This involved rolling at 300°C, with four minutes reheating between passes and 1.0 mm reduction per pass, to a total strain of 2.5. This alloy, in this processing condition, was examined by Hales and McNelley (1987) and shown to exhibit continuous recrystallization to a grain size of approximately 1.9 μm upon heating to 300°C after completion of processing.

Mechanical property data were also reported by Hartmann (1985) on this material in an annealed, fully recrystallized condition. This condition was obtained by reheating the processed material to the original solution treatment temperature following the procedure outlined in Chapter III. The original solution treating temperature was 440°C and thus the Mg, precipitated during the rolling, was taken back into solution. This also resulted in recrystallization and grain growth to an approximate grain size of 35 μm.

The microstructures of these two conditions are shown by optical microscopy in Figure 4.1. The as-rolled condition appears unrecrystallized (Figure 4.1a) in comparison to that of the annealed and recrystallized condition (Figure 4.1b). Mechanical property data and activation energy data obtained by tension testing of these two conditions, for test temperatures ranging from 150°C to 425°C, are summarized in Figures 4.2 and 4.3. The warm rolled material clearly exhibits an anomalous temperature dependence of the flow stress in the temperature interval
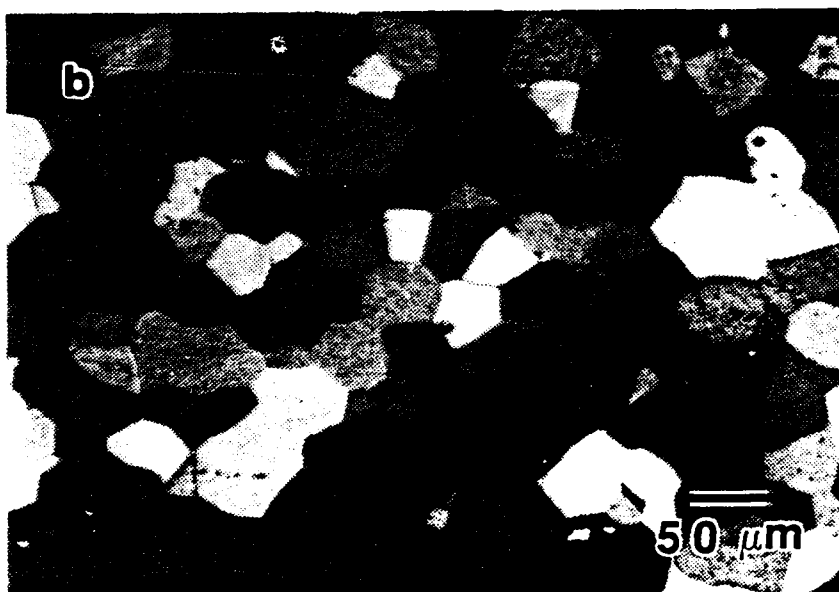
Figure 4.1. Optical micrographs cf an Al-10%Mg-0.1%Zr alloy. In (a), the material has been processed to the warm-rolled condition by TMP-III, while in (b) it has been reheated to 440°C after rolling to result in an annealed and recrystallized condition. Samples were etched in Barkers reagent and examined under polarized light.

66
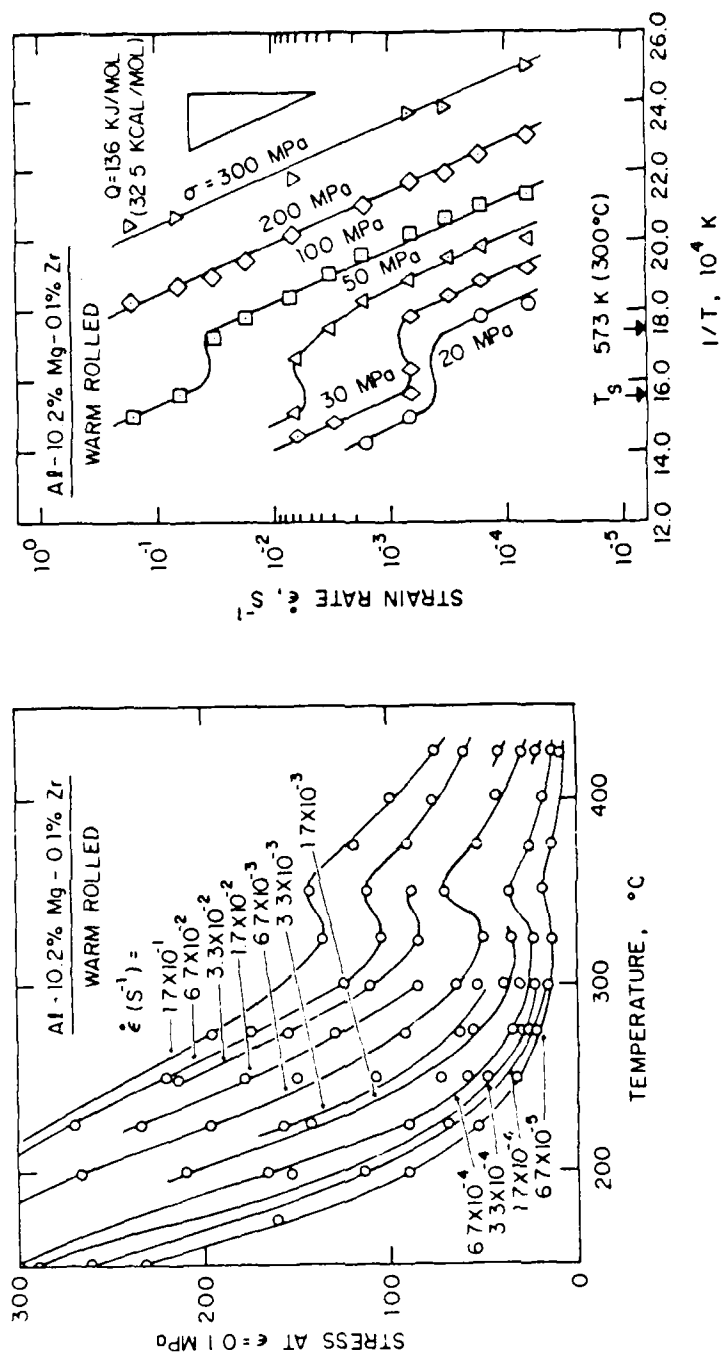
Figure 4.2. Flow stress versus temperature data (a) and activation energy data (b) for warm rolled Al-10%Mg-0.1%Zr alloy. The flow stress-temperature data exhibits an anomalous increase in strength between 325°C and 350°C; this is also seen in the activation energy data as a region of low and even negative values of Q.

67
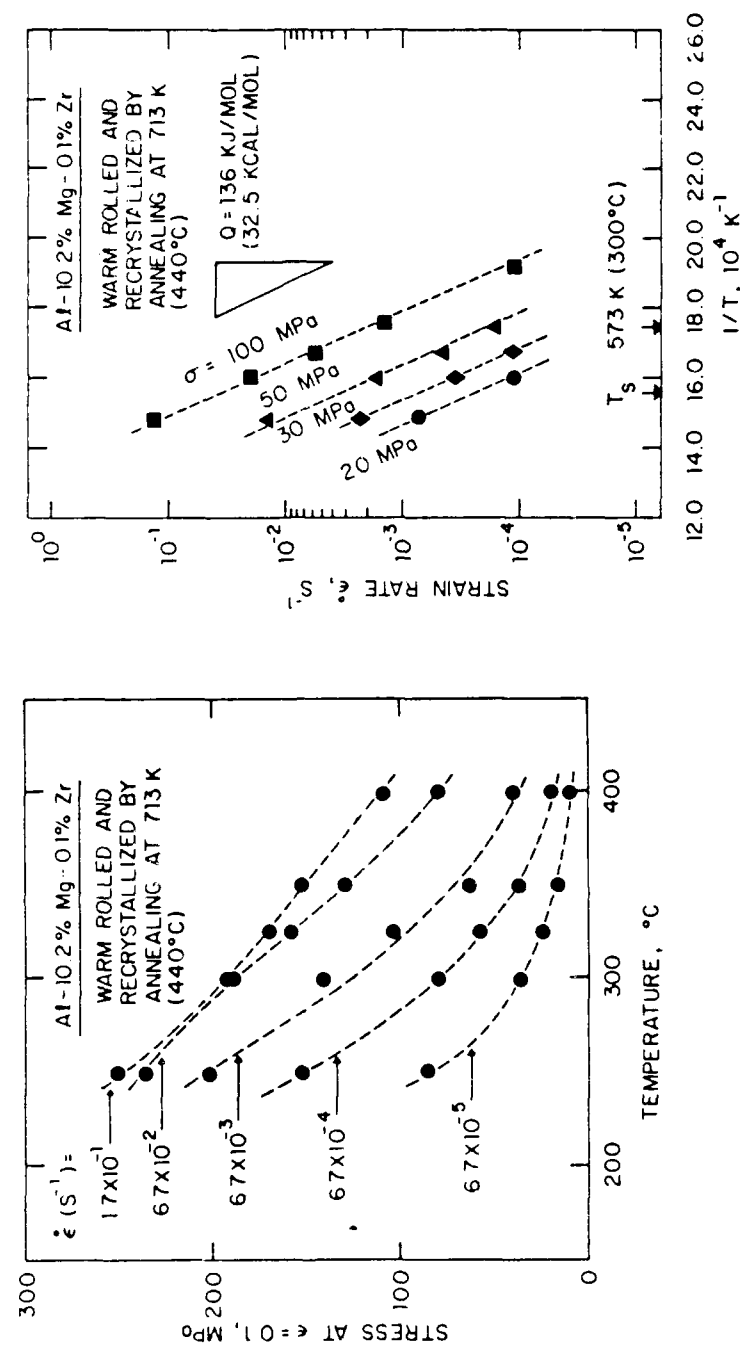
Figure 4.3. Flow stress versus temperature data (a) and activation energy data (b) for the annealed, recrystallized condition of the Al-10%Mg-0.1%Zr alloy. In this condition, the alloy exhibits normal softening with increased temperature and an activation energy similar to that for Mg-diffusion in Al.

68

from $325^\circ C$ to $350^\circ C$, where it is seen that the flow stress increases with increasing temperature (Figure 4.2a). This is apparent for all of the strain rates evaluated. The activation energy data were obtained by assuming an Arrhenius temperature dependence of the strain rate and applying the relation

$$Q_{obs,\sigma} = -R\frac{\partial \ell n \dot\epsilon}{\partial\left(\frac{1}{T}\right)}\bigg|_\sigma \tag{4.1}$$

where $Q_{obs,\sigma}$ is the observed activation energy at a stress σ, R is the gas constant, $\dot\epsilon$ is the strain rate and T the absolute temperature. The anomalous temperature dependence of the flow stress is reflected in a regime of decreased and even negative values for $Q_{obs,\sigma}$ in the same temperature interval, as seen in Figure 4.2b.

In contrast, the flow stress-temperature and activation energy data for the annealed and recrystallized condition exhibit normal behavior over this temperature range (Figure 4.3). The activation energy for the annealed and recrystallized condition has a value $Q_{obs,\sigma} \simeq 136\ KJ/mol$ for stresses from 20 to 100 MPa and temperatures from $250^\circ C$ to $425^\circ C$. This is the same value seen for the material in the warm rolled TMP-III condition either above or below the temperature interval $325^\circ C$ – $350^\circ C$. This is evident in Figure 4.4, a comparison of flow stress-temperature data (Figure 4.4a) and activation energy data (Figure 4.4b). Below this temperature interval, the warm rolled condition is weaker than the same material in the annealed and recrystallized state.

Mechanical property data from the $300^\circ C$ testing of these two conditions is shown in Figure 4.5. The warm rolled condition is seen to exhibit a sigmoidal stress vs. strain rate response and strain rate sensitivity coefficient $m = 0.45$ at a strain as small as 0.02 (bottom plot); the corresponding ductility versus strain rate data for this condition show peak ductility of $\sim 500\%$ elongation at a strain rate of $\dot\epsilon = 6.7 \times 10^{-3}\ s^{-1}$ (upper plot). This strain rate is that for peak ductility. The annealed condition is both higher in strength and less ductile than the warm rolled condition; the strain rate sensitivity coefficient m is about 0.3 at lower strain rate.

69

a value expected if the solute drag mechanism controls deformation (Weertman, 1957).

The microstructure of the warm rolled condition at the initiation of a stress-strain test at 300°C is shown in Figure 4.6a. This micrograph was obtained from the grip section of a sample pulled to failure at 1.67×10^{-1} s^{-1}; as noted in Chapter III, the test duration is very short and therefore the heating time is essentially the same as that just prior to testing. This structure is fine with a grain size of approximately 1.9μm (Lee and McNelley, 1987). Hales and McNelley (1987) analyzed this structure and demonstrated these boundaries to have misorientation of $2°-7°$, apparently sufficient to sustain fine-grain superplastic mechanisms. Figure 4.6b shows the structure from the gage section of a sample deformed superplastically to failure ($\sim$500 pct. elongation) at $300°$ C and a strain rate of $6.7 \times 10^{-3} s^{-1}$. The structure has coarsened to $d = 2.3\mu m$ and has remained equiaxed. Few dislocations are evident in grain interiors; misorientation data obtained by Hales and McNelley (1987) indicate that the boundaries evident in Figure 4.7b have misorientations of $20°$ to $30°$. These observations suggest the behavior of this material may be analyzed according to the phenomenological relations proposed by Sherby and Wadsworth (1982). The mechanical test data for the annealed and recrystallized condition suggests that its behavior may be interpreted in terms of the solute drag formulation developed by Weertman (1957).

B. ANALYSIS OF CONSTITUTIVE EQUATIONS

Equations (2.13) and (2.25)–(2.27) all may be rewritten to relate the diffusion compensated deformation rate $\dot{\epsilon}/D$ to the modulus compensated stress σ/E. Data is not available for the dynamic modulus of Al-10%Mg as a function of temperature; instead, modulus data (Köster, 1948) for pure Al was used. Also, the activation energy seen in both processing conditions is close to the self-diffusion activation energy for pure Al reported by Lundy and Murdock (1961) and so their data was used to calculate the lattice diffusion coefficient D_L:
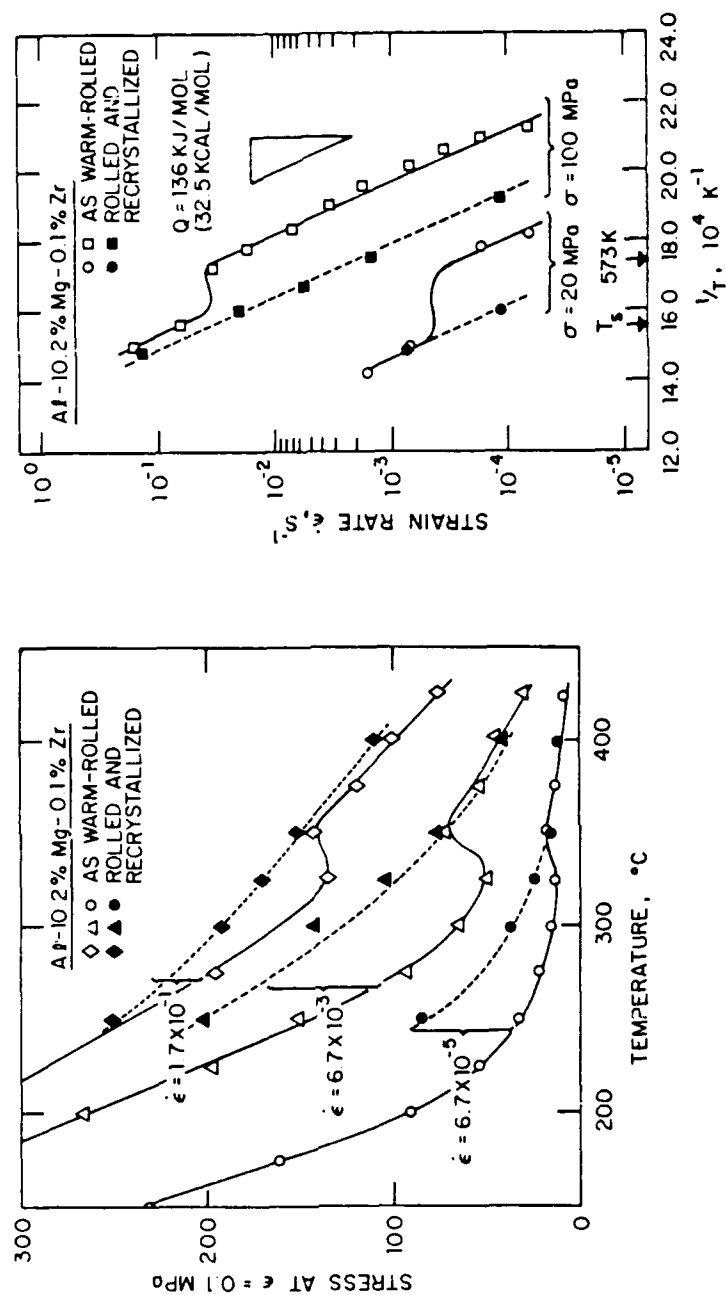
Figure 4.4. A comparison of the warm rolled and annealed conditions. The flow stress-temperature data (a) show the warm rolled condition to be weaker below 350°C while identical in behavior to the annealed condition above this temperature. The activation energy data (b) reveal similar values of Q above and below the region of anomalous behavior.

71
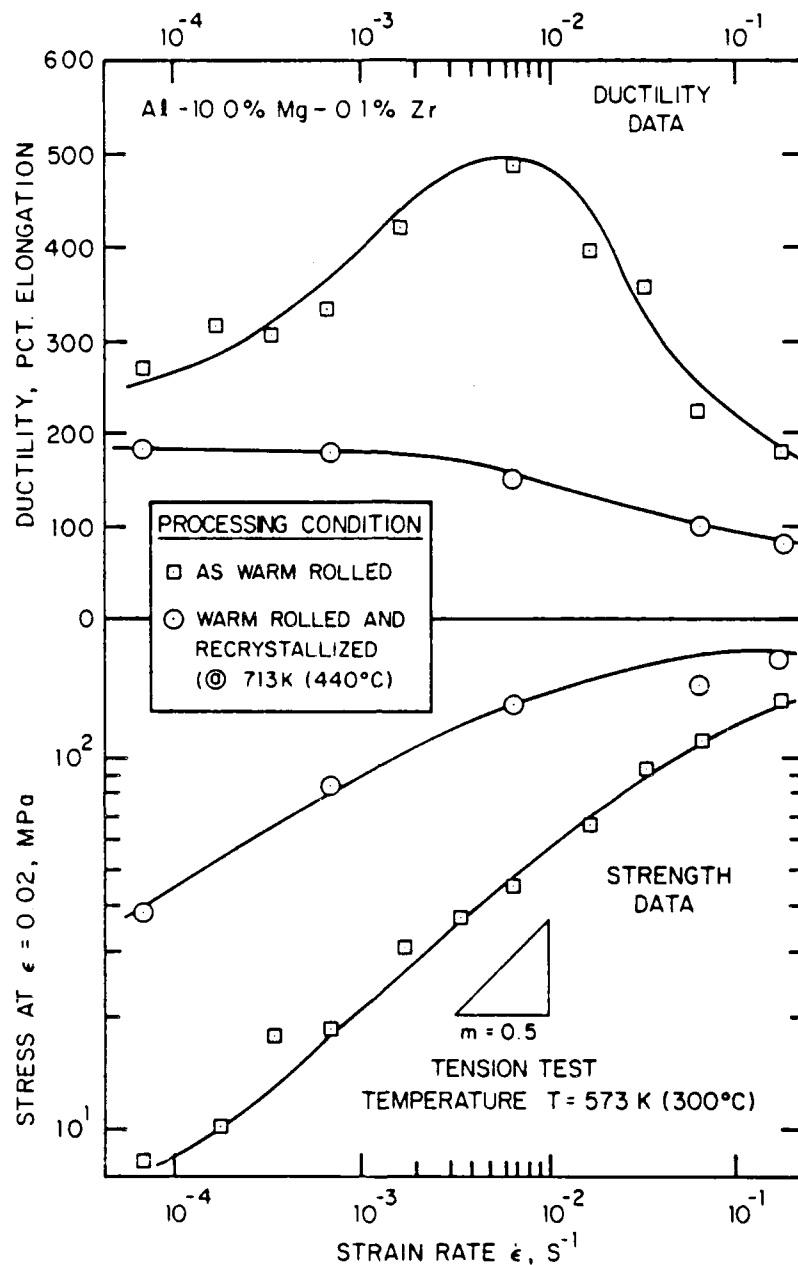
Figure 4.5. Mechanical test data comparing the warm rolled and the recrystallized conditions of the Al-10%Mg-0.1%Zr alloy during testing at 300°C. The warm rolled condition exhibits superplastic ductility in conjunction with $m \simeq 0.45$ while the annealed condition is much less ductile and has $m \simeq 0.3$ at lower strain rates.

$$D_L = 1.71 \exp(-140/RT) \tag{4.2}$$

where R is the gas constant in KJ/mol and T is the absolute temperature.

In Figure 4.7 the data of Figure 4.2 is replotted as strain rate versus modulus compensated stress for the Al-10%Mg-0.1%Zr material in the warm-rolled condition. Figure 4.8 illustrates the same analysis for the material in the recrystallized condition. Figures 4.9 and 4.10 give the strain rate versus modulus compensated stress for the Al-10%Mg-0.52%Mn material in the warm-rolled and recrystallized conditions, respectively; these plots are based on analysis of the data given by McNelley, Lee and Mills (1986) and Lee, McNelley and Stengel (1986).

The plots of Figures 4.7 – 4.10 reflect the more common data representation used in creep analysis. In Figures 4.7 and 4.9, for the warm rolled conditions, the anomalous temperature dependence previously described is still apparent. It is less pronounced, however, in the Mn containing material. Activation energies obtained from these data are slightly smaller numerically due to correction for the temperature dependence of Young's modulus E but otherwise exhibit the same trends seen in Figures 4.2 – 4.4.

Equation (4.2) was therefore used to calculate the diffusion- compensated strain rate for all of the data of Figures 4.7 – 4.10. Figure 4.11 is a plot of diffusion compensated strain rate $\frac{\dot{\epsilon}}{D_L}$ versus modulus compensated stress $\frac{\sigma}{E}$ for the warm rolled Al-10%Mg-0.1%Zr alloy. The data for the warm rolled material are superimposed on the data previously discussed (Chapter II) for pure Al and Al-Mg alloys containing 1.7 – 5.0 wt. pct. Mg. The data for test temperatures from 150°C to 250°C appear to fall on a single curve; this curve corresponds to the behavior of the Al-Mg solid solution alloys above $\dot{\epsilon}/D \approx 10^{16} m^{-2}$. Below this value of $\dot{\epsilon}/D$, the warm rolled condition of this alloy is weaker and exhibits a stress exponent n ($= 1/m$) approaching a value of 2.0.

For test temperatures from 275°C to 325°C, the data do not fall on a single curve. Rather a series of curves, one for each test temperature, appears necessary.

73

Figure 4.6. TEM micrographs in bright field showing the Al-10%Mg-0.1%Zr alloy in the TMP III condition for a test temperature of 300°C. The microstructure in the grip section (a) is seen to be slightly finer (grain size of 1.9μm) than that of the deformed gage section (b) (grain size of 2.3μm).

74

The material now appears stronger at each successive temperature than extrapolation of the data for the previous, lower temperature would suggest. Finally, as the test temperature reaches 350°C or higher, the data correspond very closely to those reported for the lower Mg alloys.

Figure 4.12 presents the data for the annealed and recrystallized condition of this same alloy. It is apparent that the behavior of the material now follows very closely that reported for lesser Mg content Al-Mg alloys over the entire range investigated. This suggests that the behavior of Al-Mg alloys, containing from 1.7 to 10 pct. Mg, follow a constitutive law having no Mg-concentration dependence. As discussed previously, this suggests interpretation of the behavior in terms of glide of solute-saturated dislocations as suggested by Friedel (1964), but with modification to the stress dependence to include a sinh law as originally suggested by Garofalo (1963). Finally, Figure 4.13 illustrates a superposition of the data of Figures 4.11 and 4.12. This superposition illustrates the same effect noted in Figure 4.4, but here in terms of diffusion compensated rate and modulus compensated stress.

The behavior of the warm rolled condition may be described in terms of the phenomenological relations developed by Sherby and Wadsworth (1982) and summarized as Equations (2.25), (2.26) and (2.27). Also, the behavior predicted by these relations will be assumed to act in an independent manner with dislocation glide controlled deformation as described by Equation (2.13), or the dotted curve on Figures 4.11 – 4.14.

The activation energy data presented in Figure 4.2 indicate a value of $Q_{obs,\sigma} = 136 \ KJ/mol$ for essentially all stresses and for temperatures below 300°C, although a lesser value is suggested by the data for $\sigma = 50MPa$ and $T \simeq 300°C$. The activation energy for lattice diffusion Q_L in Al was noted earlier to be 140 KJ/mol. In contrast, the activation energy for grain boundary diffusion $Q_{gb} \simeq 1/2Q_L$ and the activation energy for pipe diffusion $Q_p \simeq 2/3Q_L$. Thus, it is assumed that Equation (2.25) may be used to describe the superplastic regime of behavior for the warm rolled condition of this alloy.

The grain size seen at the initiation of stress-strain testing at 300°C was 1.9μm. As the continuously recrystallized grain size likely would vary with temperature, a

75
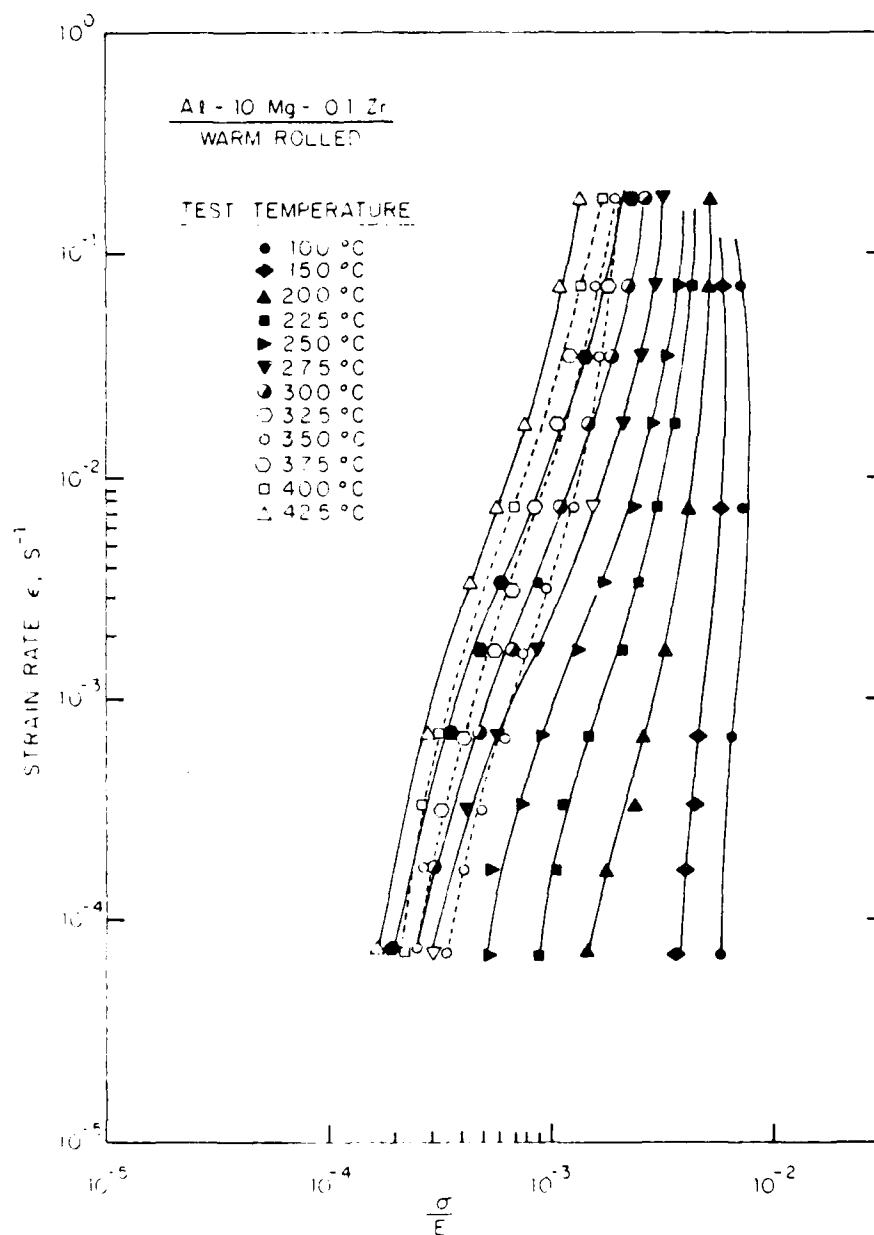
Figure 4.7. Modulus compensated stress at a true strain of 0.1 versus strain rate for the warm-rolled Al-10Mg-0.1Zr tested at different temperatures. The anomalous strengthening extends over the temperature range of 325°C–375°C for this processing condition.
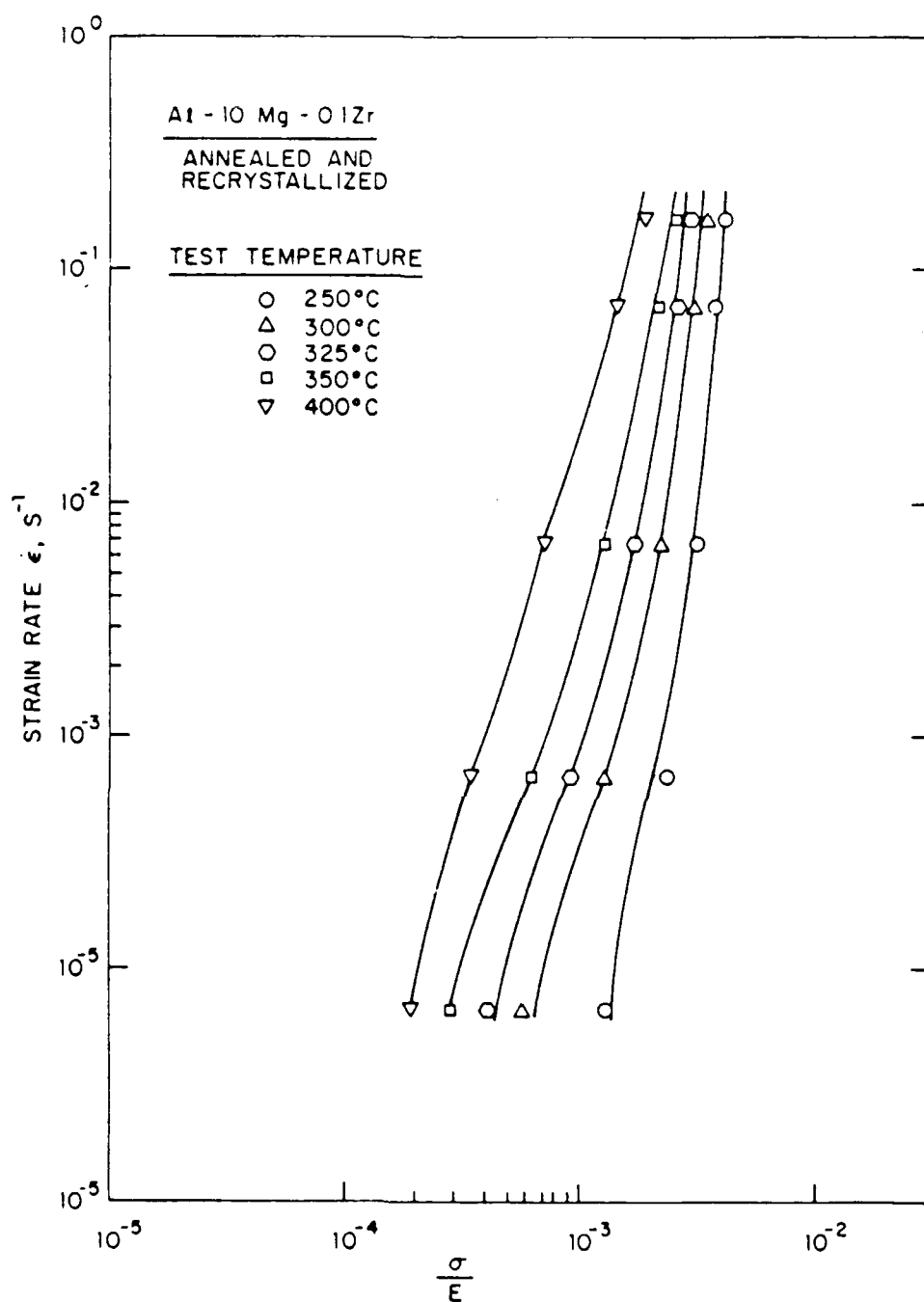
Figure 4.8. Modulus compensated stress versus strain rate for the Al-10%Mg-0.1%Zr alloy tested at temperatures from 250°C–400°C. No anomalous behavior is seen here.

77
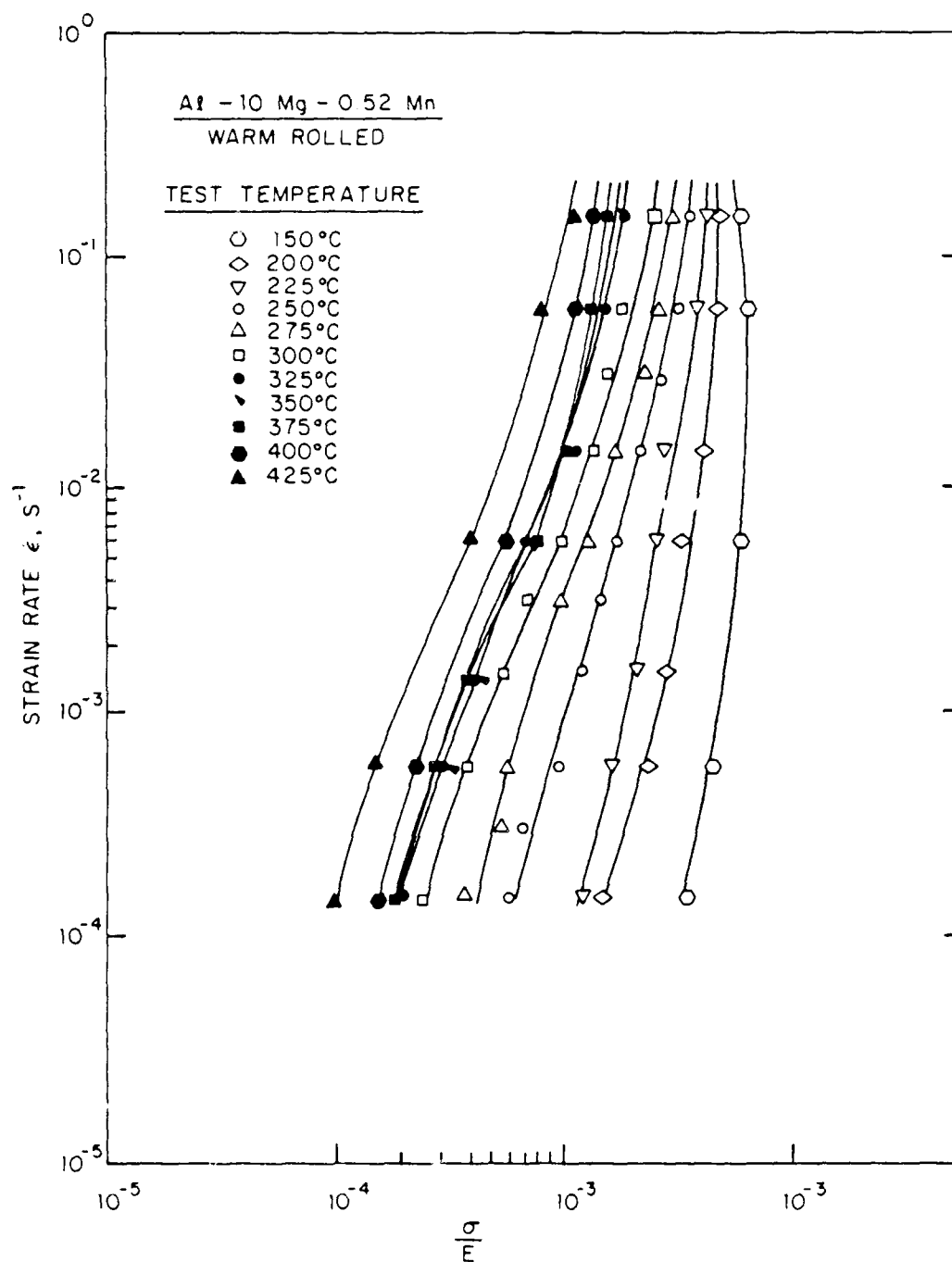
Figure 4.9. Modulus compensated stress at a true strain of 0.1 versus strain rate for the warm-rolled condition of the Al-10%Mg-0.5%Mn alloy. This material exhibits a similar regime of anomalous strengthening as seen in the Al-10%Mg-0.1%Zr alloy.
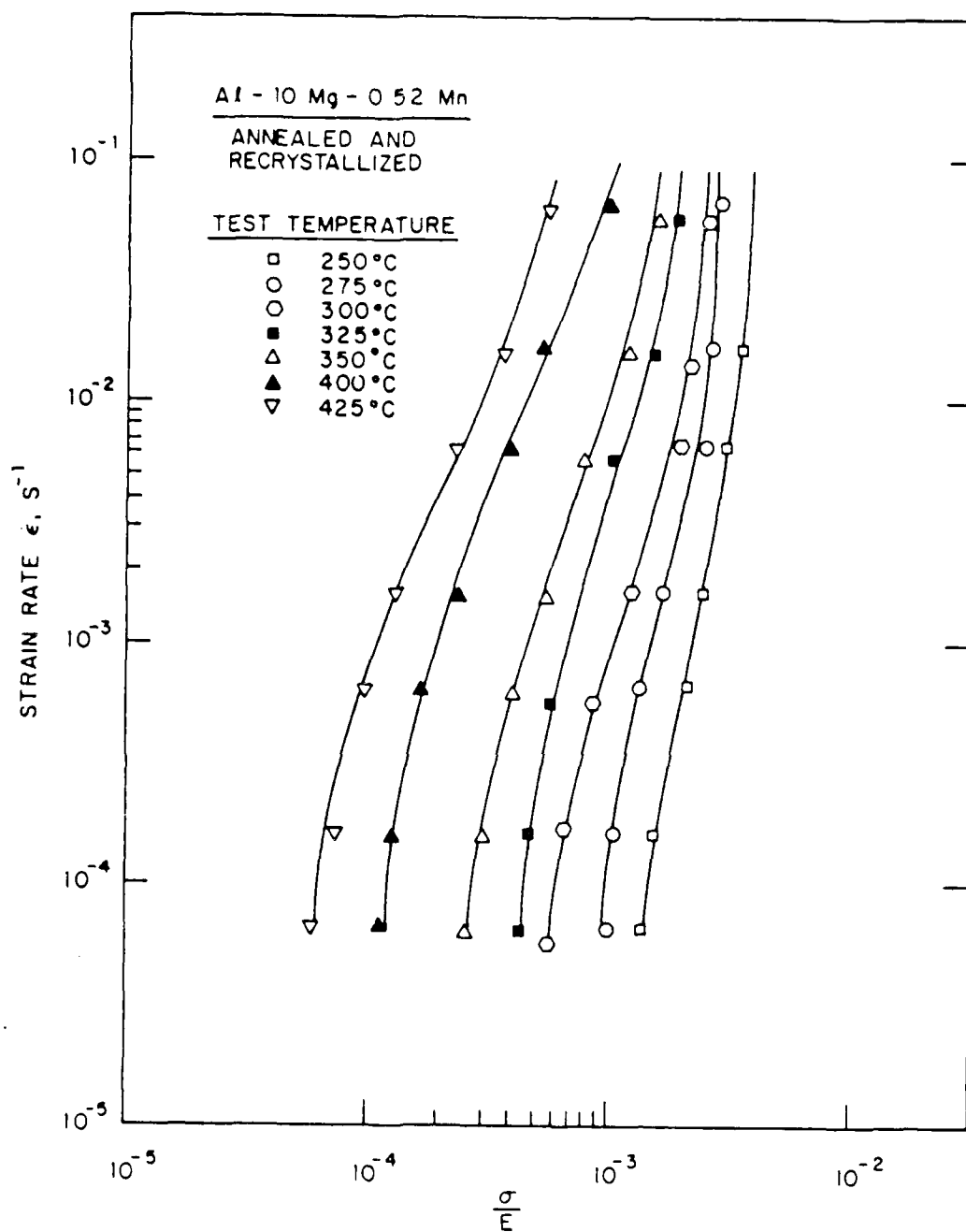
Figure 4.10. Modulus compensated stress at a true strain of 0.1 versus strain rate for the warm-rolled and recrystallized Al-10%Mg-0.5%Mn alloy. Again, no anomalous strengthening with increased temperatures is seen for this alloy after annealing above the Mg-solvus temperature.

79
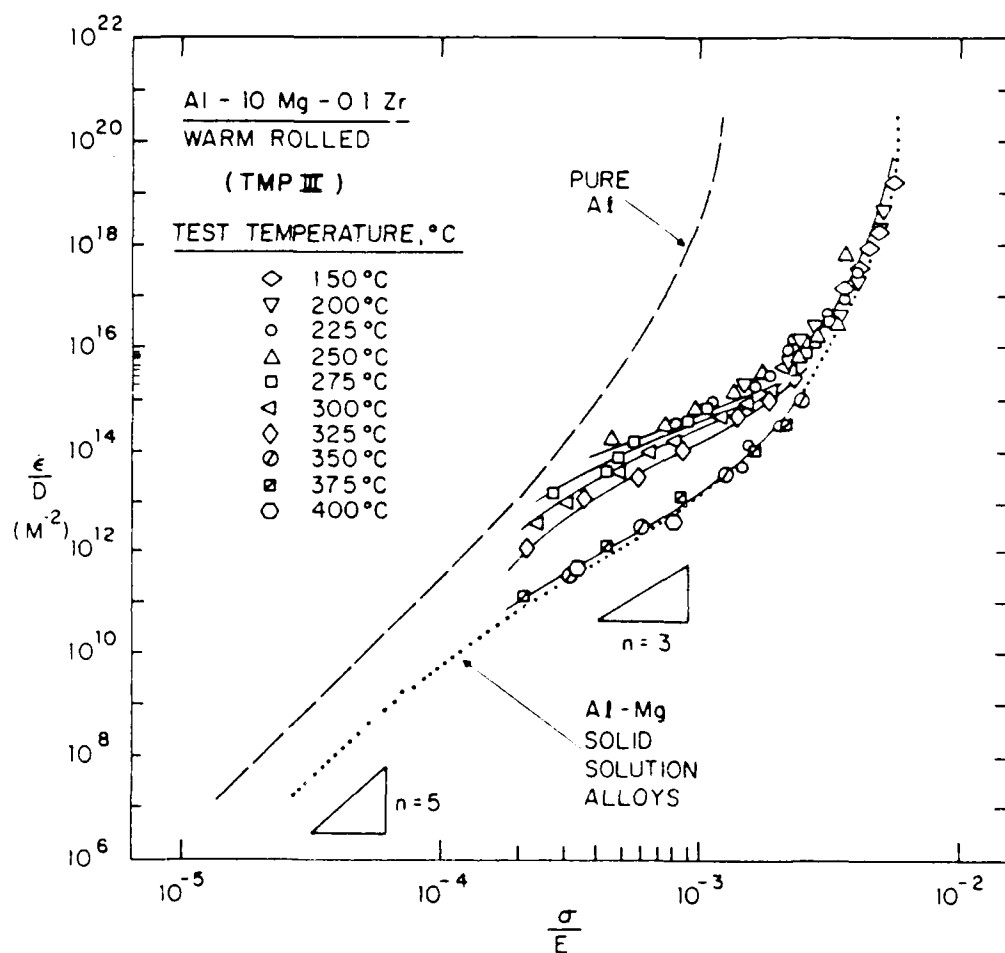
Figure 4.11. Diffusion-compensated strain rate as a function of modulus-compensated stress for warm-rolled Al-10%Mg-0.1%Zr tested at temperatures from 150° to 400°C. Below 325°C the material is weaker than solid solution alloys of Mg in Al. At temperatures above 325°C the data for the warm-rolled material falls on the curve for creep of Class 1 solid solution Al-Mg alloys.

80
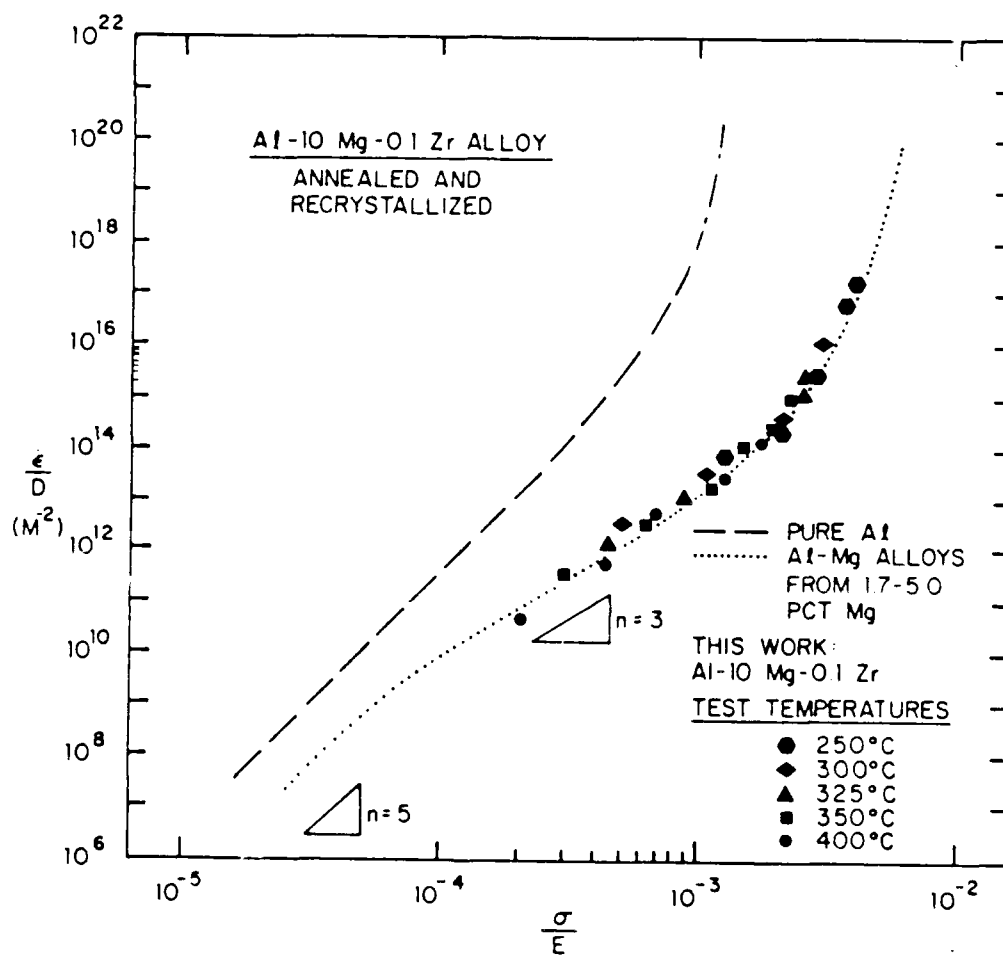
Figure 4.12. Diffusion-compensated strain rate versus modulus- compensated stress for the recrystallized Al-10%Mg-0.1%Zr alloy. The data falls on the curve for creep of Class I solid solution Al-Mg alloys.

81
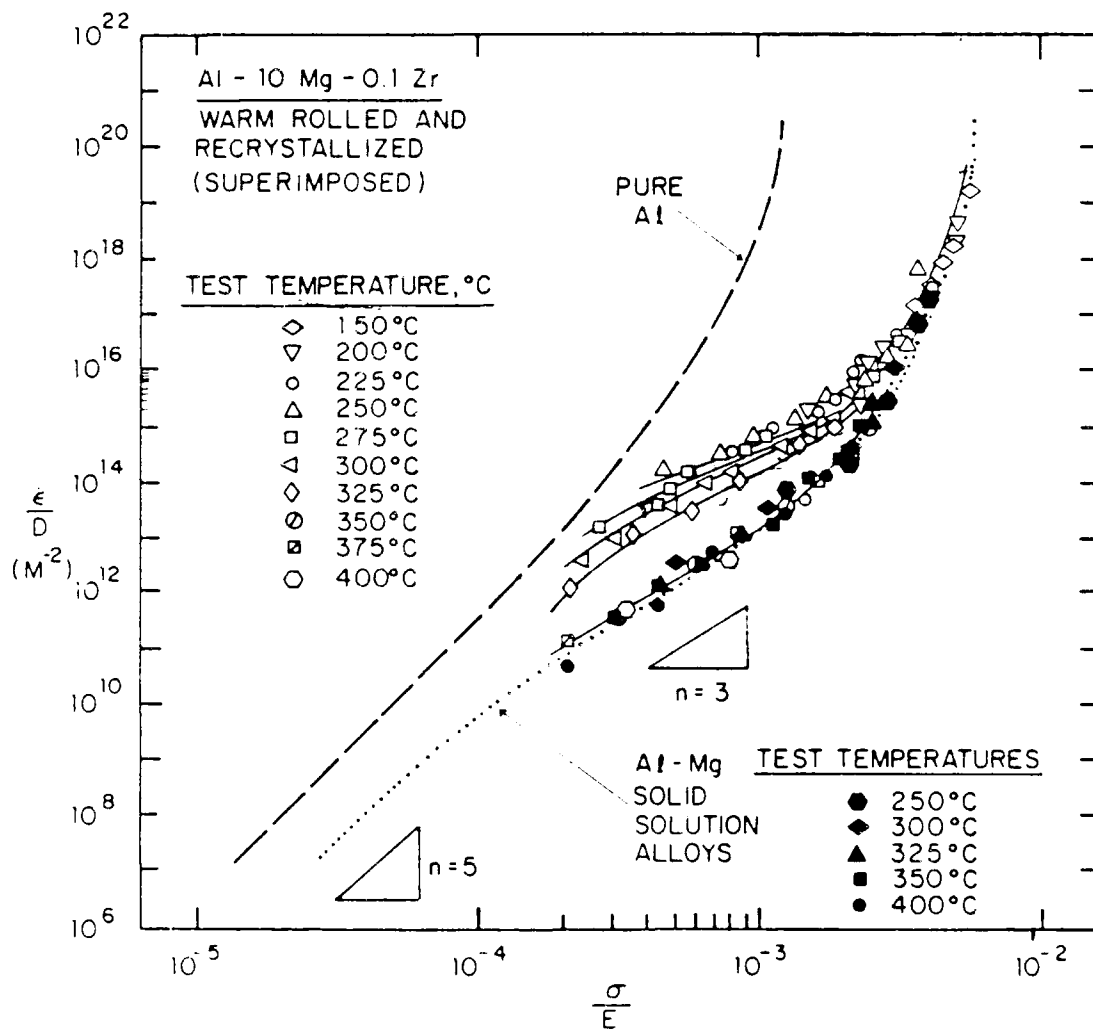
Figure 4.13. Diffusion compensated strain rate versus modulus compensated stress for the warm rolled and recrystallized Al-10%Mg-0.1%Zr superimposed. The behavior of the warm-rolled material tested at high temperature is identical to the behavior of the recrystallized material and both behave in the same manner as Al-Mg solid solution alloys.
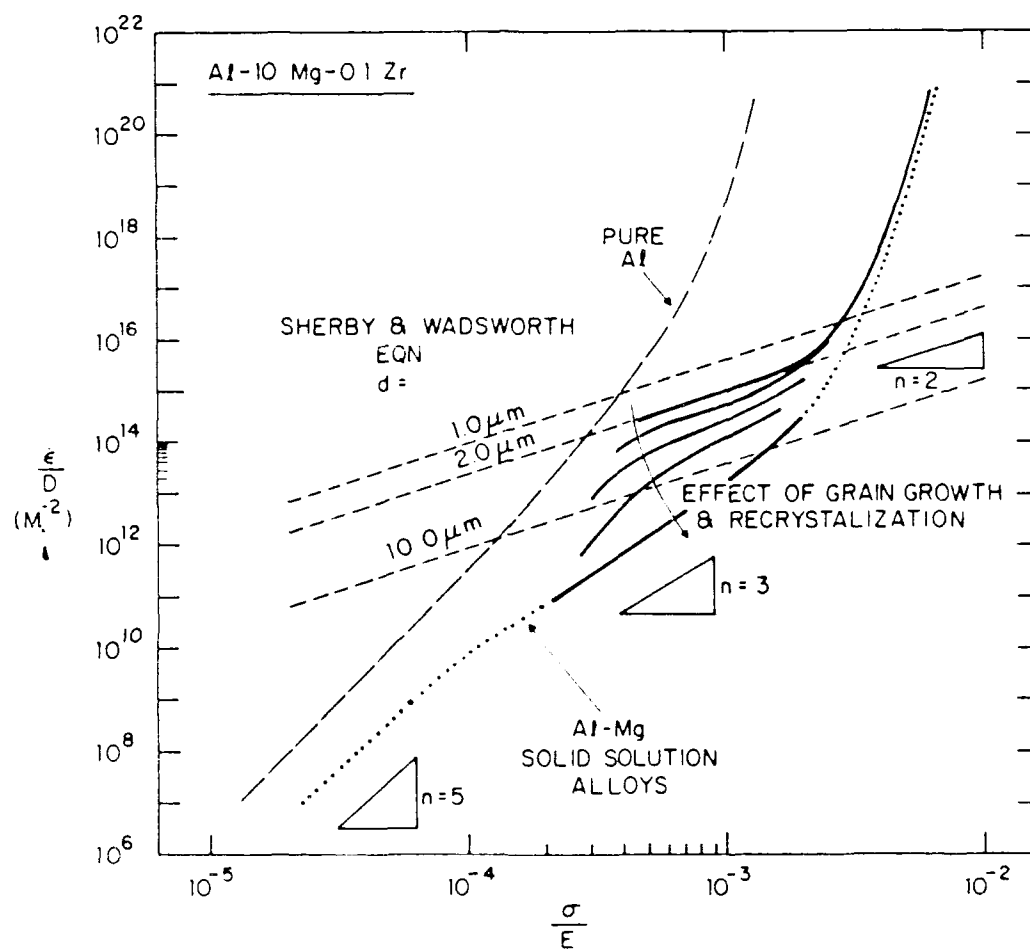
Figure 4.14. Schematic diagram illustrating the effect of grain growth. A series of curves were calculated, using the Sherby and Wadsworth relation (Eqn. (2.25)) for $d = 1.0; 2.0$; and 10μm. The effect of grain growth is more pronounced at lower strain rate; coarsening to a grain size of 30μm will lead to a transition to a solute drag mechanism.

83

series of curves were calculated based on Equation (2.25) and using $A = 2 \times 10^{12}$ as suggested by the analysis of Sherby and Wadsworth (1982). These are plotted on Figure 4.14 for $d = 1.0\mu$m; 2.0μm; and 10.0 μm. Comparison of Figure 4.14 with 4.11 reveals that Equation (2.25), if assumed to apply in an additive manner with a constitutive equation for the solute-drag mechanism, will describe the behavior of the warm rolled material up to 250°C. This is illustrated by the uppermost solid curve on Figure 4.14. The effect of grain growth is illustrated by the series of solid curves; these were determined based on the data of Lee and McNelley (1987) who demonstrated grain growth to occur more rapidly with strain at lower strain rates. Coarsening to grain sizes larger than 30μm will lead to a transition again to the solute drag mechanism, at least for the range of strain rates and temperatures examined in this research. This is indicated by the lower solid curve on Figure 4.14. A more detailed treatment of grain growth, and an analysis of its effect on the measured activation energy, is the subject of Chapter V.

A similar analysis was also done for the data on the Al-10%Mg-0.5%Mn alloy of McNelley, Lee and Mills (1986) and Lee, McNelley and Stengel (1986). The analysis of the warm rolled condition is presented in Figure 4.15. The same general behavior at lower temperatures is apparent here as was seen in the Zr-containing alloy. At and above 350°C, the material remains weaker than the Zr-containing alloy in a manner that suggests less grain growth. Indeed, the presence of $MnAl_6$ in this alloy was documented by McNelley, Lee and Mills (1986) in the form of rod-like particles 0.02μm in diameter and 0.1μm in length.

Retention of a finer structure even during reheating to the solution treating temperature is also evident for the annealed and recrystallized condition of this alloy (Figure 4.16). Microscopy data presented by Lee McNelley and Stengel (1986) did suggest grain size of about 10μm even after recrystallization, confirming a stabilizing effect of $MnAl_6$. Such a grain size, in conjunction with coarsening at lower strain rates, may explain the behavior of this condition of the Al-10%Mg-0.5%Mn alloy.

84
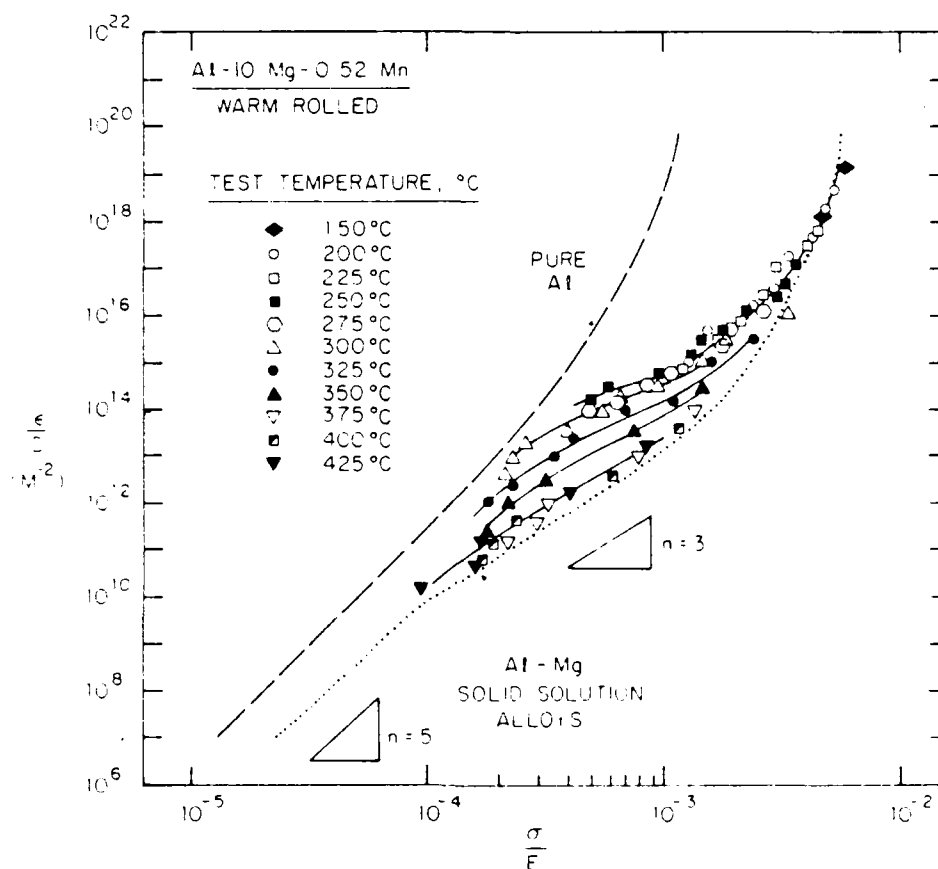
Figure 4.15. Diffusion compensated strain rate versus modulus- compensated stress for warm-rolled Al-10%Mg-0.52%Mn tested at temperatures from 150°C–425°. Below 250°C the data fits one curve. In the temperature range from 275°C to 375°C the data for each temperature fit on separate curves while above 375°C, the data again fall on one curve.

85
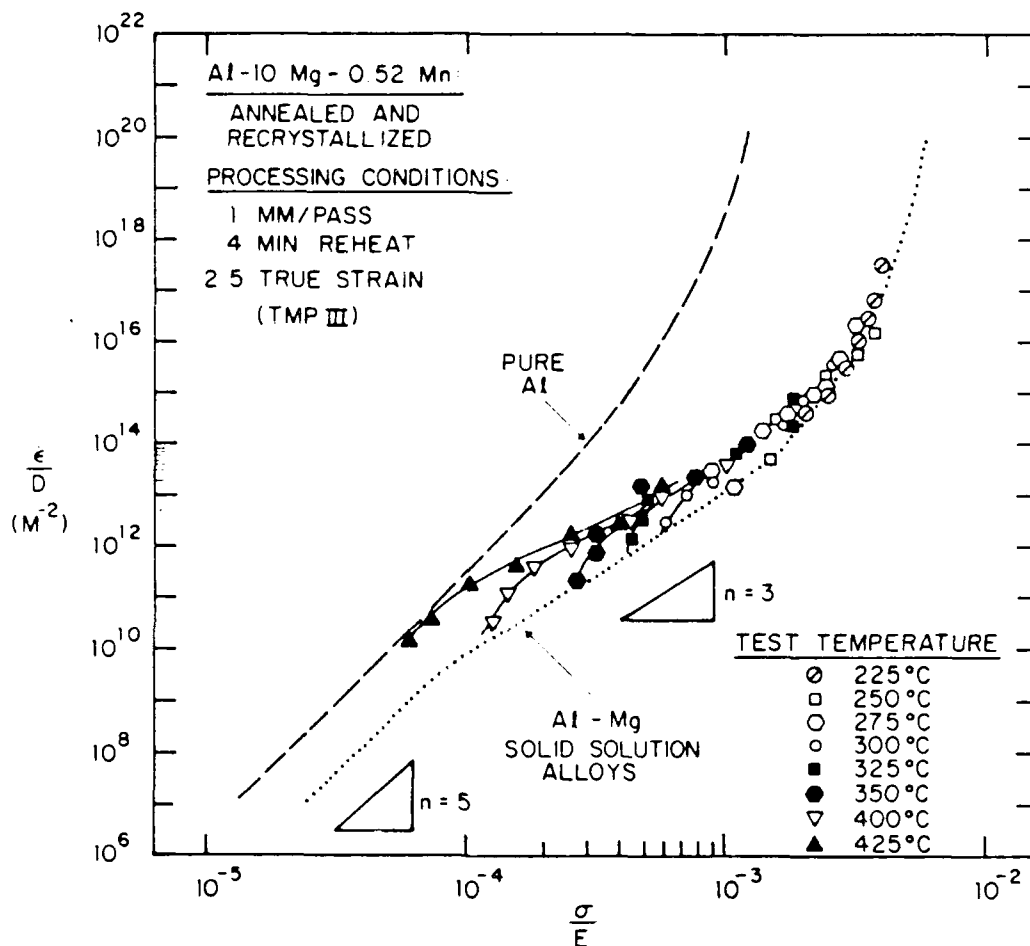
Figure 4.16. Diffusion compensated strain rate versus modulus- compensated stress of the recrystallized Al-10%Mg-0.52%Mn alloy tested at temperatures from 225° to 425°C. Superplastic ductility was seen at temperatures above 400°C.

C. AN ALTERNATIVE VIEW

It was noted earlier that there appears to be a regime of reduced activation energy for $\sigma = 50$ MPa and $T \simeq 300°$C in Figure 4.2. These data are at $\dot{\epsilon}/D \simeq 10^{16} m^{-2}$ on Figure 4.11, where the stress exponent $n \simeq 4$. As noted in Chapter II, control of accommodation by dislocation pipe diffusion will result in an apparent stress exponent $n = 4$ in conjunction with $Q = Q_p \simeq 2/3Q_L$. It is possible that such a pipe-diffusion controlled process is being observed as predicted by Equation (2.27). However, grain growth is also occurring in the regime (to be discussed in Chapter V) and this phenomenon may also influence the activation energy. As this possible pipe-diffusion controlled behavior is also being seen near the transition from the superplastic regime to a high-stress region of solute drag controlled deformation, alternative interpretations for both the stress exponent and activation energy are possible.

V. MICROSTRUCTURE INSTABILITY, GRAIN GROWTH AND THE ACTIVATION ENERGY

Microstructure instability in the form of gradual coarsening at lower temperatures and also recrystallization with subsequent growth at higher temperatures was examined by microscopy of both the Al-10%Mg-0.1%Zr and Al-10%Mg-0.52%Mn alloys. Most of the effort in this research was directed at the Al-10%Mg-0.1%Zr alloy.

A. INSTABILITY AND GROWTH IN Al-10%Mg-0.1%Zr

Microstructures in warm-rolled material deformed either at 250°C or 275°C are shown in Figure 5.1. Even at the lowest temperature (Figure 5.1a) the structure appears similar to the continuously recrystallized grain structures documented previously after heating at 300°C (Figure 4.6). The grain size obtained at 250°C is $1.1 \mu m$, and at 275°C is $1.5 \mu m$ (Figure 5.1b).

Optical microscopy of this alloy after deformation at 300°C is shown in Figure 5.2. This structure appears unrecrystallized as did the as-rolled condition when examined by optical microscopy (Figure 4.1a). Nonetheless, TEM of this condition revealed a continuously recrystallized grain size of $1.9 \mu m$ upon heating to 300°C (Figure 4.6a) which coarsened to $2.3 \mu m$ after deformation. Comparison of Figures 4.6 and 5.2 demonstrates the need for caution in assessing the microstructural condition of these alloys under conditions where continuous recrystallization produces such highly refined structures as obtained here. As temperature is increased to 300°C, the structure coarsens gradually. Upon heating to 325°C, instability is seen. In some cases, a grain structure of $\sim 2.0 \mu m$ grain size is observed as shown by TEM in Figure 5.3. An optical micrograph of this sample is shown in Figure 5.4a where the structure is seen to appear unrecrystallized. Other samples among those tested at 325°C exhibited the structure shown in Figure 5.4b. This appears to be a recrystallized structure much as seen in warm-rolled samples reheated to 440°C, the solution treatment temperature. Here, the grain size is $\sim 20 \mu m$. It is

88
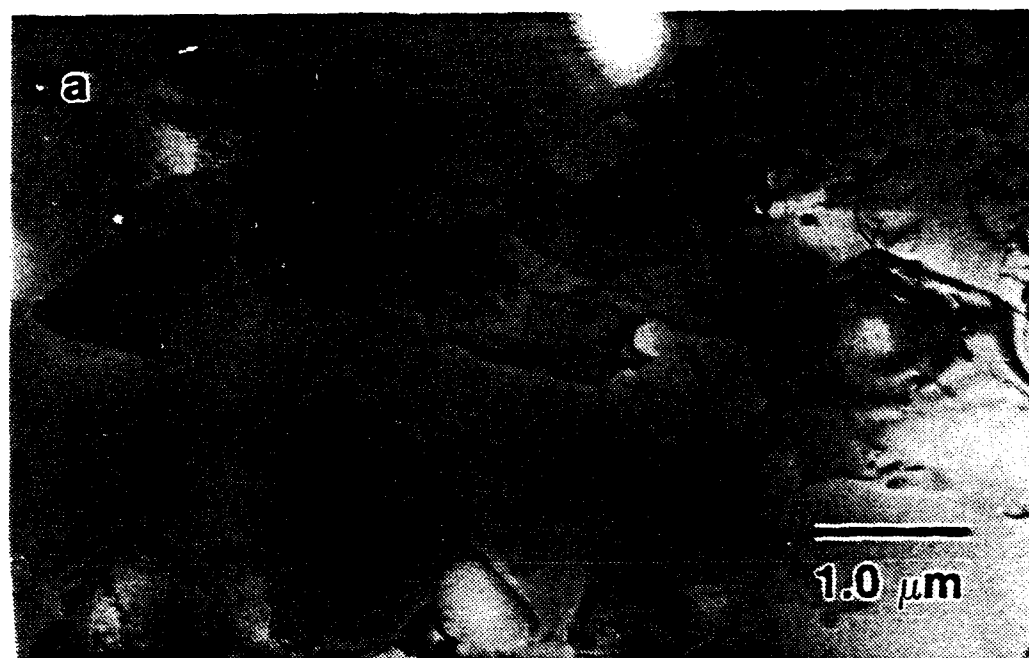
Figure 5.1. Bright field micrographs showing the Al-10%Mg-0.1%Zr alloy TMP III condition. The specimens were from grip sections: (a) test temperature 250°C (grain size = 1.1 μm) and (b) test temperature 275°C (grain size = 1.47 μm).
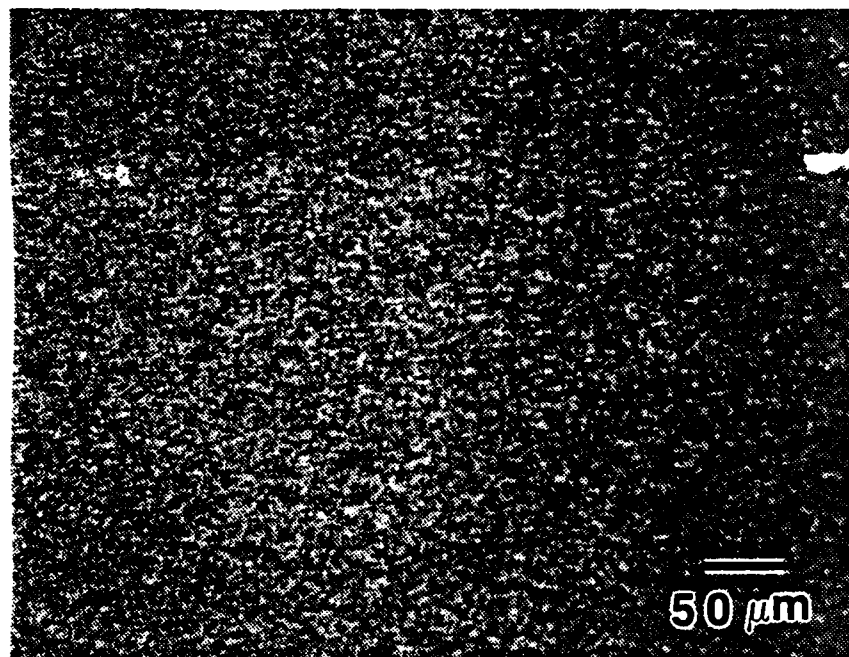
Figure 5.2. Optical micrograph obtained under crossed polarizers illustrating the refined structure in Al-10%Mg-0.1%Zr alloy in the warm-rolled condition and tested at 300°C and strain rate of $1.67 \times 10^{-3} S^{-1}$.

90

Figure 5.3. Bright-field TEM micrograph showing the alloy processed to TMP I.I. This is from the grip section of a test sample and represents the structure just prior to testing at 325°C. The grain size = 1.97 μm.

91
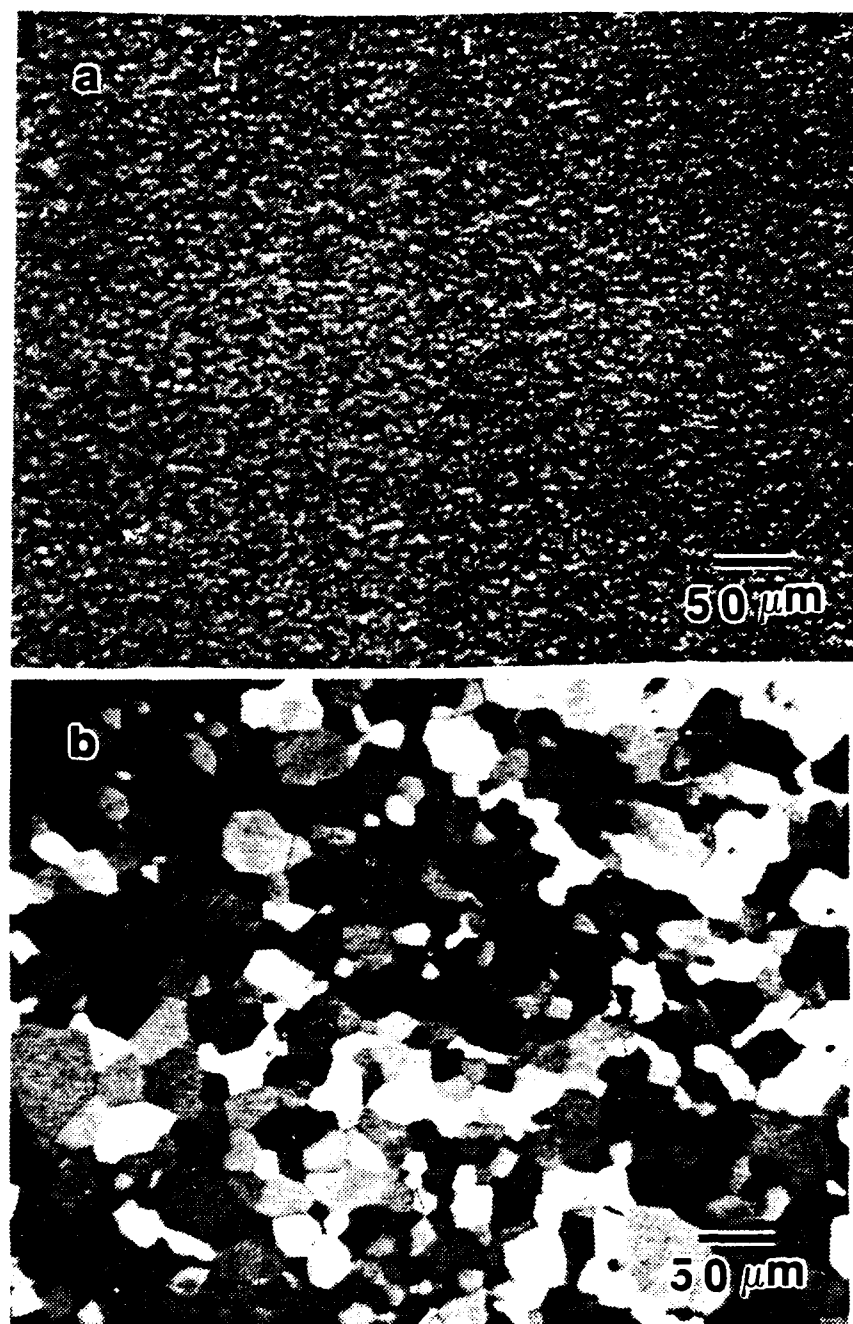
Figure 5.4. Optical micrographs of two different samples of the Al-10%Mg-0.1%Zr alloy tested at 325°C illustrating the instability of the structure at this temperature; (a) a refined structure and (b) a recrystallized, coarse structure (grain size = 20 μm).

possible that the differences in structure documented in Figure 5.4 may arise from small differences in heating temperatures not detected during testing; this suggests that the recrystallization process is extremely temperature sensitive.

The refined structures seen at lower temperatures evolve from the rolled condition by a process of continuous recrystallization. The details of structure evolution producing microstructures such as that of Figure 5.4b have not been studied in detail. Apparently recrystallized structures such as this may result from normal growth of continuously recrystallized grains formed during heating; the growth would be increasingly rapid as temperature approaches the solvus and the β dissolves. Alternatively, discontinuous recrystallization may be initiated if a sufficient density of unrecovered dislocations is present upon heating at temperatures above the prior rolling temperature, i.e., into region II or III of Figure 2.8. Further research will be necessary to resolve the mode.

Heating to still higher temperatures results mainly in increasing grain size as seen in Figure 5.5. Table III provides a summary of this investigation of grain size. Finally, it should be noted that these data were obtained from samples experiencing relatively slow heating upon being placed in the furnace on the mechanical testing machine. The recrystallized and annealed condition was produced by heating in a salt bath, a process involving much higher heating rates. Grain sizes obtained under the latter condition were consistently finer than those attained with slower heating. This may reflect different degree of recovery and possibly different modes of structural transformation.
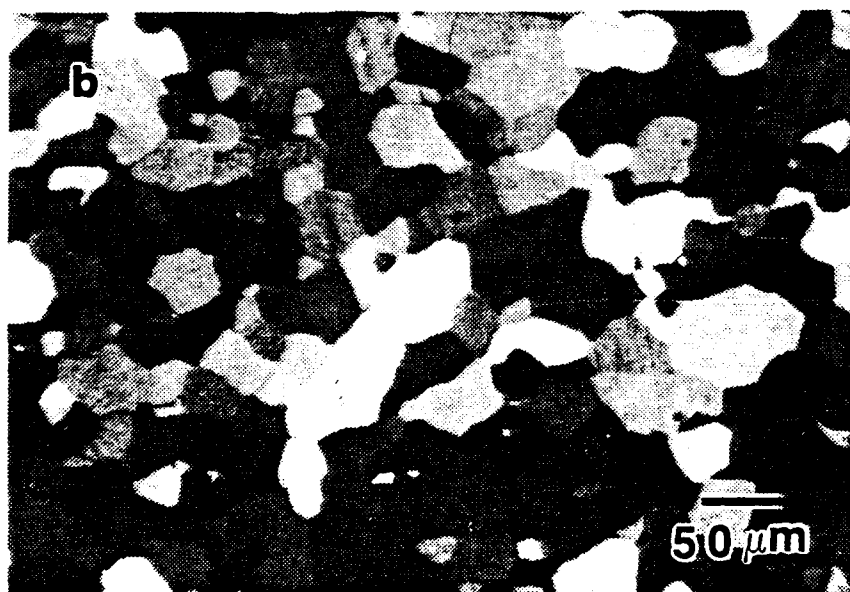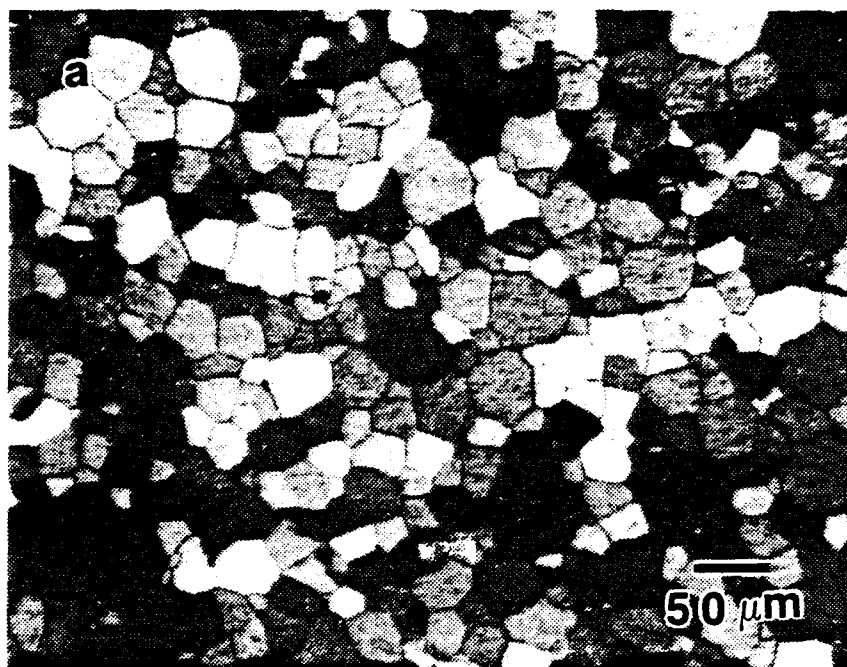
Figure 5.5. Optical micrographs of test samples of the Al-10%Mg-0.1%Zr alloy in the warm-rolled condition illustrating the recrystallized, coarse structure obtained upon heating to temperatures close to or above the Mg solvus: (a) test temperature 350°C (average grain size = 50 μm) and (b) test temperature 375°C (average grain size 64μm).

TABLE V-1
GRAIN SIZE - TEMPERATURE DATA FOR Al-10%Mg-0.1%Zr
PROCESSED BY TMP III.

Temperature, °C	Grain Size (μm)	
	Optical	TEM
250	–	1.1
275	–	1.47
300	–	2.3
325	–	1.97
325	30.0	
350	49.7	
375	63.8	
400	73.4	
425	83.4	

ANALYSIS OF GRAIN REFINEMENT AND SUPERPLASTICITY IN
ALUMINUM-MAGNESIUM ALLOYS(U) NAVAL POSTGRADUATE SCHOOL
MONTEREY CA A A ABOU-SALAMA DEC 87

UNCLASSIFIED

F/G 11/6.1   NL
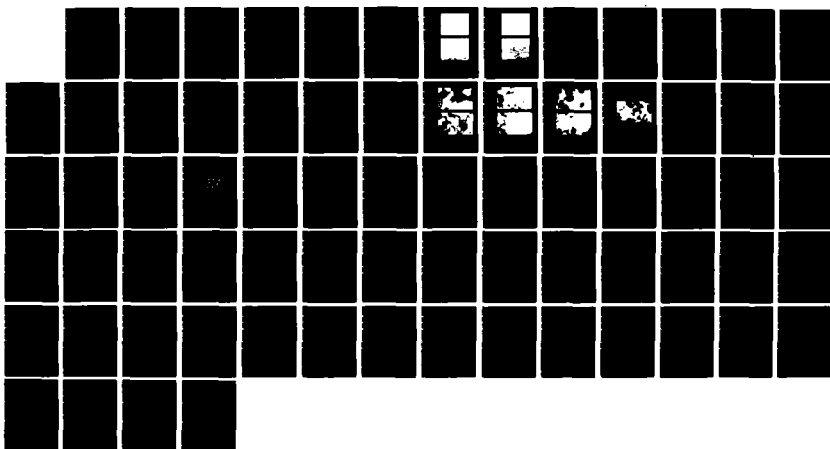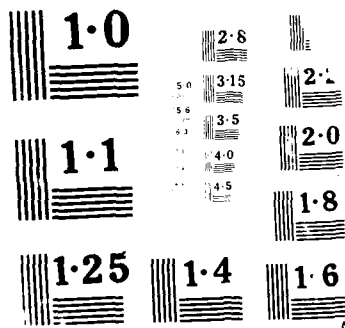
B. EFFECT OF COARSENING ON ACTIVATION ENERGY DATA

Suery and Baudelet (1978) have provided an analytical basis to estimate the effect of microstructural on deformation parameters such as the activation energy. Their result was given earlier in Equation (2.31) as

$$Q = \frac{\bar{Q} + \bar{a}Rh_{\epsilon,\dot{\epsilon}}}{1 + \bar{a}g_{\epsilon,T}}$$

where Q is the observed activation energy, i.e. $Q_{obs,\sigma}$ in Equation (4.1). $\bar{Q}$ is the activation energy of the underlying diffusional process, $\bar{a}$ is the exponent in grain size (the symbol p was used in Equation (2.17)), and $h_{\epsilon,\dot{\epsilon}}$ and $g_{\epsilon,T}$ are parameters describing the coarsening of the structure with temperature and strain rate, respectively.

Data on coarsening with strain rate during testing at 300°C was obtained by Lee and McNelley (1987). They reported data at two strain rates differing by one order of magnitude, $6.67 \times 10^{-4}s^{-1}$ and $6.67 \times 10^{-3}S^{-1}$. Their data indicated a grain size of $1.9\mu m$ at the initiation of straining and coarsening to $2.0\mu m$ at the lower strain rate upon reaching a strain $\epsilon = 0.1$ (the value at which data for activation energy evaluation was obtained). Also, Lee and McNelley (1987) recorded an unchanged grain size of $1.9\mu m$ upon straining to $\epsilon = 0.1$ at the higher of these strain rates. Therefore

$$\begin{aligned} g_{\epsilon,T} &= \frac{\delta \log d}{\delta \log \dot{\epsilon}} \\ &= \frac{\log \frac{d_2}{d_1}}{\log \frac{\dot{\epsilon}_2}{\dot{\epsilon}_1}} \end{aligned} \tag{5.1}$$

where $d_1, d_2, \dot{\epsilon}_1$ and $\dot{\epsilon}_2$ are grain sizes and strain rates, respectively, at which data were obtained. Inserting the values reported by Lee and McNelley (1987)

$$g_{\epsilon,T} \cong \frac{\log \frac{2.0\,\mu m}{1.9\,\mu m}}{\log \frac{6.7 \times 10^{-4}s^{-1}}{6.7 \times 10^{-3}s^{-1}}},$$

and hence

$$g_{\epsilon,T} = -0.02 \tag{5.2}$$

96

In Chapter IV, it was demonstrated that the superplastic regime of behavior can be described by a constitutive equation like that of Equation (2.25), which predicts a $(1/d)^2$ dependence of strain rate on grain size, i.e. $\bar{a} = 2$, and a lattice diffusion dependence for the strain rate, i.e., $\bar{Q} = Q_L$. Therefore the result obtained in Equation (5.2) may be inserted in Equation (2.31) to give

$$Q = \frac{Q_L + 2Rh_{\epsilon,\dot{\epsilon}}}{1 + 2(-0.02)} \quad \text{or}$$
$$Q \simeq 1.05(Q_L + 2h_{\epsilon,\dot{\epsilon}}). \tag{5.3}$$

From this, it is seen that increased coarsening at lower strain rates introduces only a five percent error in the activation energy data, at least for the extent of coarsening noted by Lee and McNelley (1987).

The effect of the parameter $h_{\epsilon,\dot{\epsilon}}$ is much greater for these data. This is given by

$$h_{\epsilon,\dot{\epsilon}} = \frac{\delta \log d}{\delta \left(\frac{1}{T}\right)}.$$

This relation may be used in conjunction with the data of Table III to estimate the influence of coarsening and instability documented in the previous section.

This is done in Figure 5.6. The grain size data is shown as $\log d$ versus $(1/T)$ in the lower plot; in this form, the parameter $h_{\epsilon,\dot{\epsilon}}$ may be determined directly from the slope of the smooth curve through the data points. The experimental data for $\sigma = 50$ MPa was used to establish a point on the upper plot representing the behavior predicted by Equation (2.25). This point was from data at 225°C and $\dot{\epsilon} = 1.7 \times 10^{-4} s^{-1}$, well below the range of rapid grain size change. At this point, the slope of the $\log \dot{\epsilon}$ versus $(1/T)$ curve was assumed to be given by $Q_L = 140$ KJ/mol (Lundy and Murdock, 1960).

The dotted curve, representing the effect of grain coarsening and instability on activation energy, was then calculated by applying Equation (5.3) to determine an apparent slope Q on the upper plot. This slope represents the observed activation energy $Q_{obs,\sigma}$ determined earlier by applying Equation (4.1) to the experimental data. The suppression of the superplastic mechanism due to the rapid grain growth

97
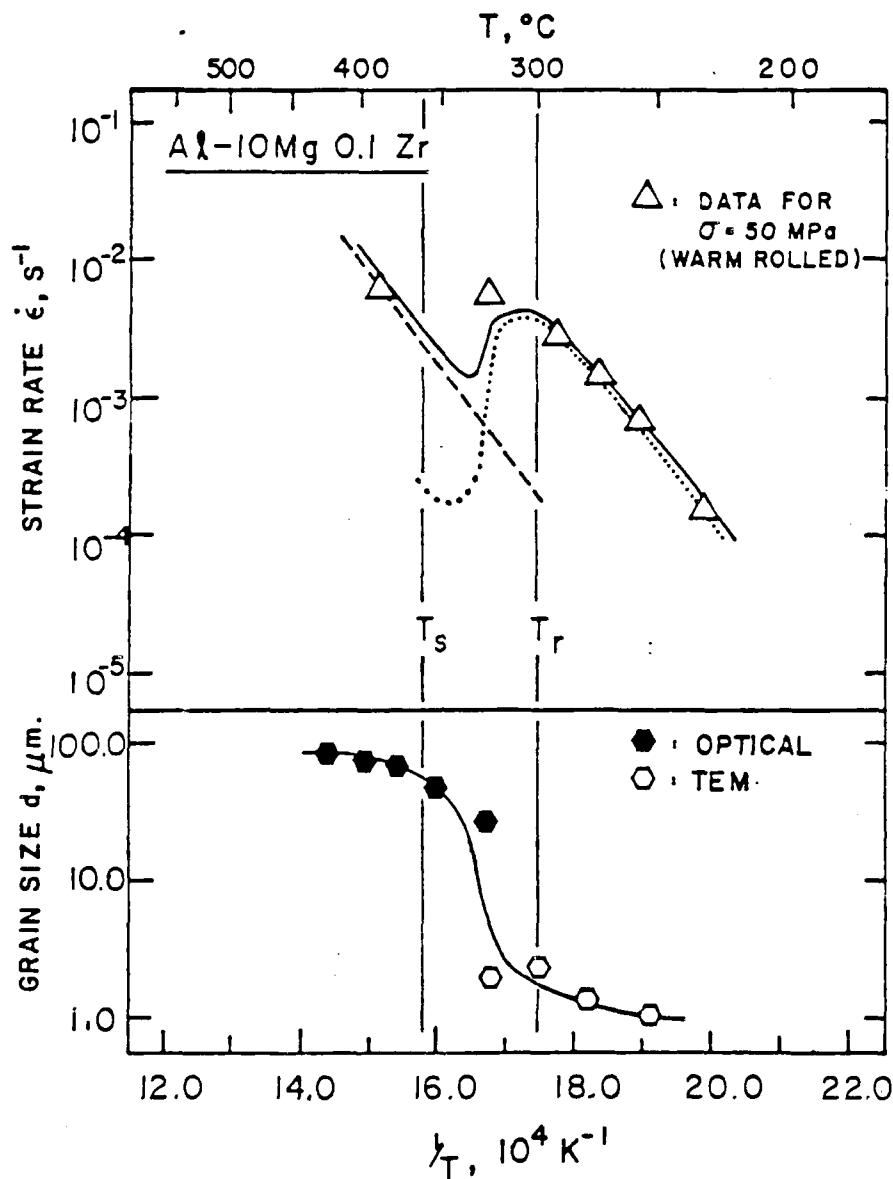
Figure 5.6. The influence of grain coarsening upon the activation energy. The grain growth data (bottom plot) were used to calculate the apparent dependence of $\ln \dot{\epsilon}$ on $(1/T)$ including grain coarsening effects as given by Eqn. (5.3). this is the dotted curve (upper plot). This is assumed to act additively with the solute drag mechanism (dashed curve) to predict the apparent behavior seen in the solid curve. This is seen to describe the data at 50 MPa very accurately.

98

at about 325°C is apparent as is the prediction of even negative activation energy values.

It was noted earlier that the constitutive relation being assumed to describe the superplastic response, Equation (2.25), is assumed to act additively with the solute-drag mechanism. Data describing this latter mechanism, for $\sigma = 50$ MPa, was obtained from Figure 4.3b. When the strain rates are added, the result, given by the solid curve on the upper plot of Figure 5.6, is seen to provide an accurate, quantitative description of the behavior in this system. In particular, this strongly supports the conclusion of the analysis of Hales and McNelley (1987) that the boundary structures attained in this alloy by TMP III, involving misorientation of $2°$-$7°$, are in fact capable of sustaining superplastic flow processes as described by Equation (2.24).

It was noted earlier that the coarsening occurs rapidly in a narrow temperature interval. Hillert (1965) has analyzed grain growth in the presence of particles such as the β precipitated during the rolling done here. Following his analysis, grains smaller than

$$d_1 = \frac{\bar{d}}{1 + \frac{3f}{2d_p}\bar{d}} \tag{5.4}$$

will shrink, being consumed, while grains greater in size d than

$$d_2 = \frac{\bar{d}}{1 - \frac{3f}{2d_p}\bar{d}} \tag{5.5}$$

will grow. In these equations, $\bar{d}$ is the average grain diameter, f is the volume fraction of particles and d_p is the particle diameter. The ratio $3f/2d_p$ is the Zener drag term. Thus, grain growth is inhibited when

$$\bar{d} = \frac{2d_p}{3f} \tag{5.6}$$

and there is a size range in which grains neither grow nor shrink. This may be seen in Equation (5.5) for the upper limit d_2; as growth proceeds, d_2 increases and fewer and fewer grains are able to grow.

Upon heating above the rolling temperature, the β, precipitated during the rolling, should begin to redissolve. Thus, f will begin to decrease upon heating above the rolling temperature and this may be accompanied by particle coarsening. Experimentally, the coarsening is seen to be especially rapid near $325°C$, a temperature above the rolling temperature but below the β solvus. It is concluded that the β is the primary factor stabilizing the grain size in this alloy and that the microstructure instability is the result of dissolution of the β and loss of its stabilizing effect on the grains.

C. COARSENING IN Al-10%Mg-0.5%Mn

A similar study of coarsening in the Al-10%Mg-0.5%Mn alloy is summarized in Figures 5.7 and 5.8. Here, it is seen that heating of warm-rolled material above the prior rolling temperature for mechanical testing produces far less notable coarsening (Figure 5.7b compared to Figure 5.7a). Even material initially annealed and recrystallized (Figure 5.8) remains highly refined. This increased stability due to $MnAl_6$ was seen in the mechanical property data (Figures 4.15 and 4.16); grain size data obtained by TEM on this material in the annealed and recrystallized condition showed it to have a grain size of $8 - 10\mu m$ (Lee, McNelley and Stengel, 1986).
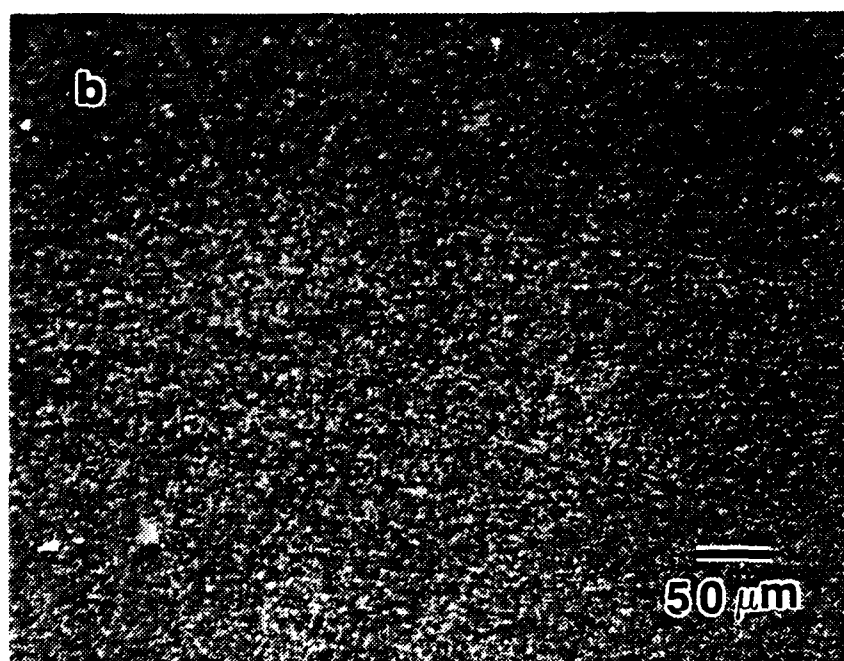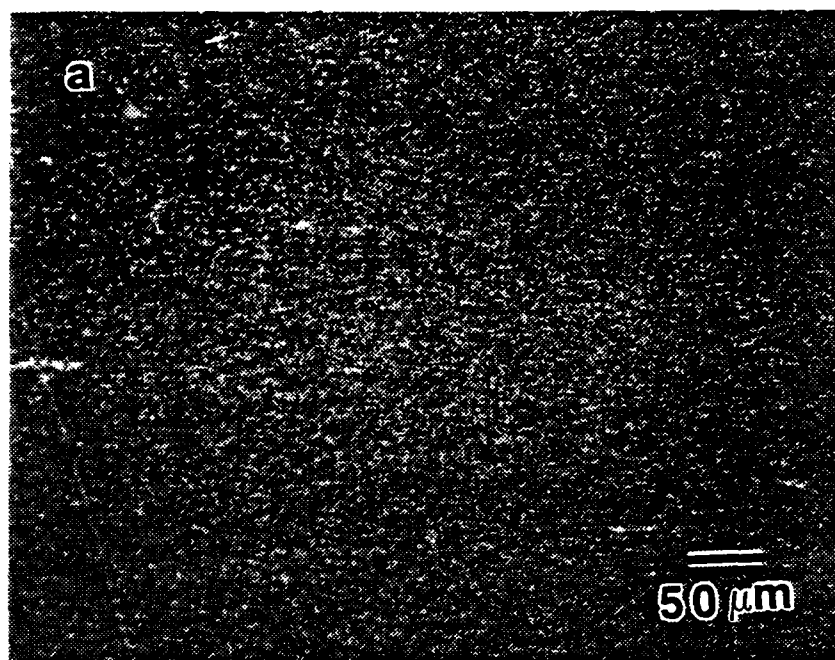
Figure 5.7. Optical micrographs under crossed polarizers illustrating the fine structure of Al-10%Mg-0.52%Mn in the warm-rolled condition; (a) test temperature 300°C and (b) test temperature 450°C.

101
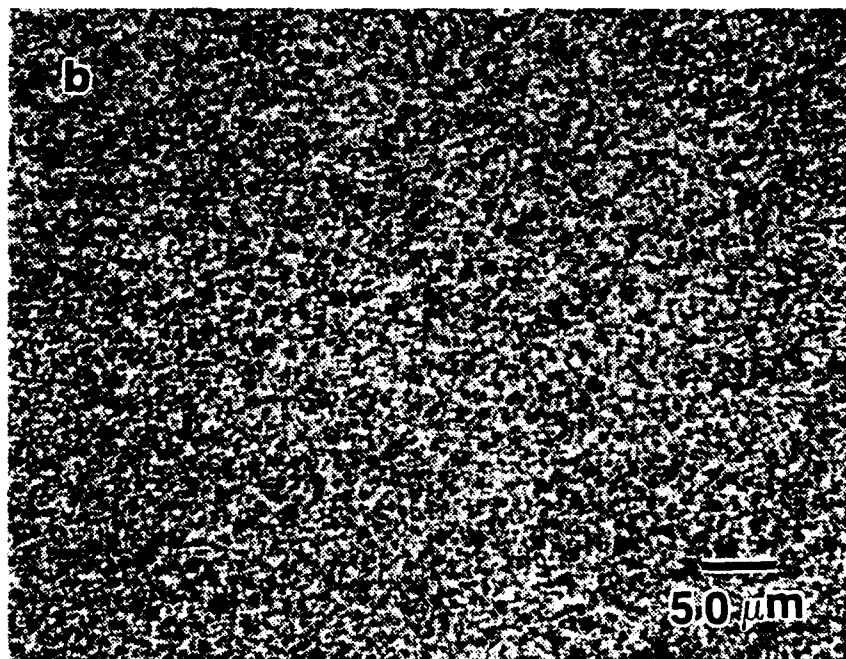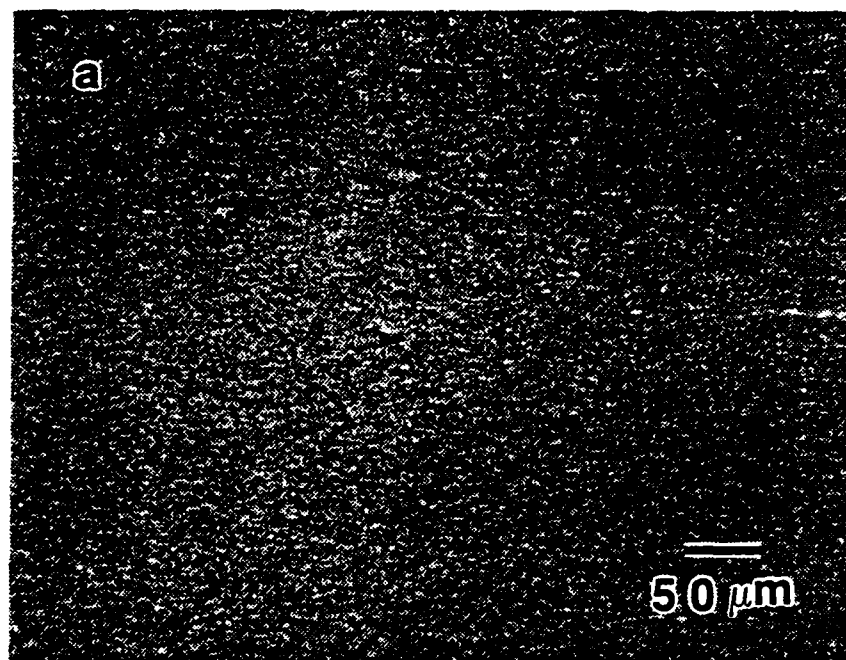
Figure 5.8. Optical micrographs under crossed polarizers illustrating the fine structure Al-10%Mg-0.52%Mn in the recrystallized condition; (a) test temperature 350°C and (b) test temperature 450°C.

102

VI. EFFECT OF THERMOMECHANICAL PROCESSING VARIABLES

Microstructures sufficiently fine to sustain superplasticity in these materials have been assumed in this work to evolve by continuous recrystallization. Most of the data examined thus far was obtained on material processed by TMP III, a process involving rolling with relatively small reduction per pass and short reheating time between passes. Continuous recrystallization is often described in terms of subgrain coalescence leading to increases in boundary misorientation and also to subgrain growth. It is usually thought to occur mainly during the early stages of superplastic deformation when observed in superplastic aluminum alloys (Nes, 1985). In work by Hales and McNelley (1987), it was demonstrated to occur in the initial heating prior to superplastic deformation, where an initially nonrecrystallized structure recovered to form boundaries of $2^{\circ} - 7^{\circ}$ misorientation. These misorientations were then seen to increase significantly with superplastic deformation.

In deformation processing, the straining of the material results in an increased dislocation density. The subsequent microstructure evolution occurs by the recovery of these dislocations to form boundaries and so it was surmised that increasing the reduction per pass, which should increase the dislocation density generated, would in turn lead to an increase in the misorientation of the resultant subboundaries and consequently enhance the superplastic response. It was also surmised that increased total strain attained during rolling would result in a higher dislocation density and thus also to enhanced superplasticity.

A thermomechanical process was therefore devised in which the reduction per pass was increased from 1 mm per pass, used in TMP- III, to 2.5 mm per pass, keeping the reheating time between rolling passes constant at 4 minutes. The results obtained were not what had been anticipated. Increasing the reduction per

103

pass drastically <u>diminished</u> the ductility in subsequent testing to evaluate the superplastic response. Increased total strain did, on the other hand, result in enhancement of superplastic response.

The recovery processes responsible for the substructure development take place during rolling itself (by dynamic recovery) and during the reheating time between passes and heating prior to superplastic deformation (by static recovery). In the study by Hales and McNelley (1987), where only the static recovery prior to superplastic straining was investigated, the structural changes appeared to take place in the first 10 minutes of annealing after which the interior of the grains appeared clear. Annealing for a longer times, up to 50 mins., did not increase the misorientations appreciably and they remained at $2^{o} - 7^{o}$. From these results, it therefore appears that reheating for four minutes between rolling passes may not be sufficient for recovery processes to become complete and hence the subboundaries formed were not well defined. Thus, a reheating period substantially longer than four minutes was selected, (30 minutes), as during this time recovery and substructure formation would be expected to be complete.

These considerations lead to the matrix of thermomechanical processes given earlier in Table II. Table VI indicates possible comparisons where the effect of the thermomechanical processing variables may be isolated.

TABLE VI-1

TMP COMPARISONS TO EXAMINE THE EFFECTS
OF THE PROCESS VARIABLES

	Variable	TMP Comparisons
1.	Strain	I vs III; II vs V
2.	Reheating time between passes	III vs IV; V vs VI
3.	Reduction per pass	I vs II; III vs V; IV vs VI
4.	Rolling temperature	V (220°C, 300°C, 380°C)

The effect of these thermomechanical processing variable may be seen by comparing the stress versus strain rate response or ductility versus strain rate response during subsequent stress strain tests.

A. ROLLING STRAIN

Figure 6.1 compares the stress versus strain rate data obtained at 300°C for TMP I ($\epsilon_{rolling} = 1.5$) and TMP III ($\epsilon_{rolling} = 2.5$). This comparison in terms of $\dot{\epsilon}/D$ versus σ/E. Both thermomechanical processes used the same reduction per pass (1 mm) and reheating time between passes (four minutes). Peak ductility for TMP III (Figure 4.5, Chapter IV) was about 500 percent while that for TMP I (data not shown) was only 170 percent.

B. REHEATING TIME BETWEEN PASSES

Figures 6.2, 6.3, and 6.4 provide data for a detailed comparison of reheating time between passes for TMP V (four minutes) and TMP VI (30 minutes). Both processes employed 2.5 mm reduction per pass and were rolled to a strain of 2.5. TMP V is stronger and of lesser m value compared to TMP VI for temperatures from 250° C to 400° C and also is consistently only slightly weaker than this same material in an annealed and recrystallized condition. TMP VI is of lesser strength and exhibits greater m value except at temperatures greater than 400° C where recrystallization before straining leads to a coarse grained material. Detailed comparison in Figure 6.4 of only 300° C data reveals the decreased m value with the longer reheating time between rolling passes. Ductility data for these two processing conditions is included in Figure 6.5 where the increased reheating time is seen to lead to a dramatic increase in ductility, from the lowest seen (peak $\sim 200\%$ for TMP V) to the highest ($\sim 600\%$ for TMP VI). For that matter, comparison of TMP III and TMP IV indicates a similar but much less pronounced trend.

C. REDUCTION PER PASS

Figure 6.5 also allows comparison of the ductility data obtained at 300° C for TMP III (1 mm reduction per pass) and TMP V (2.5 mm reduction per pass). Both processes involved four minutes reheating between passes and rolling to 2.5
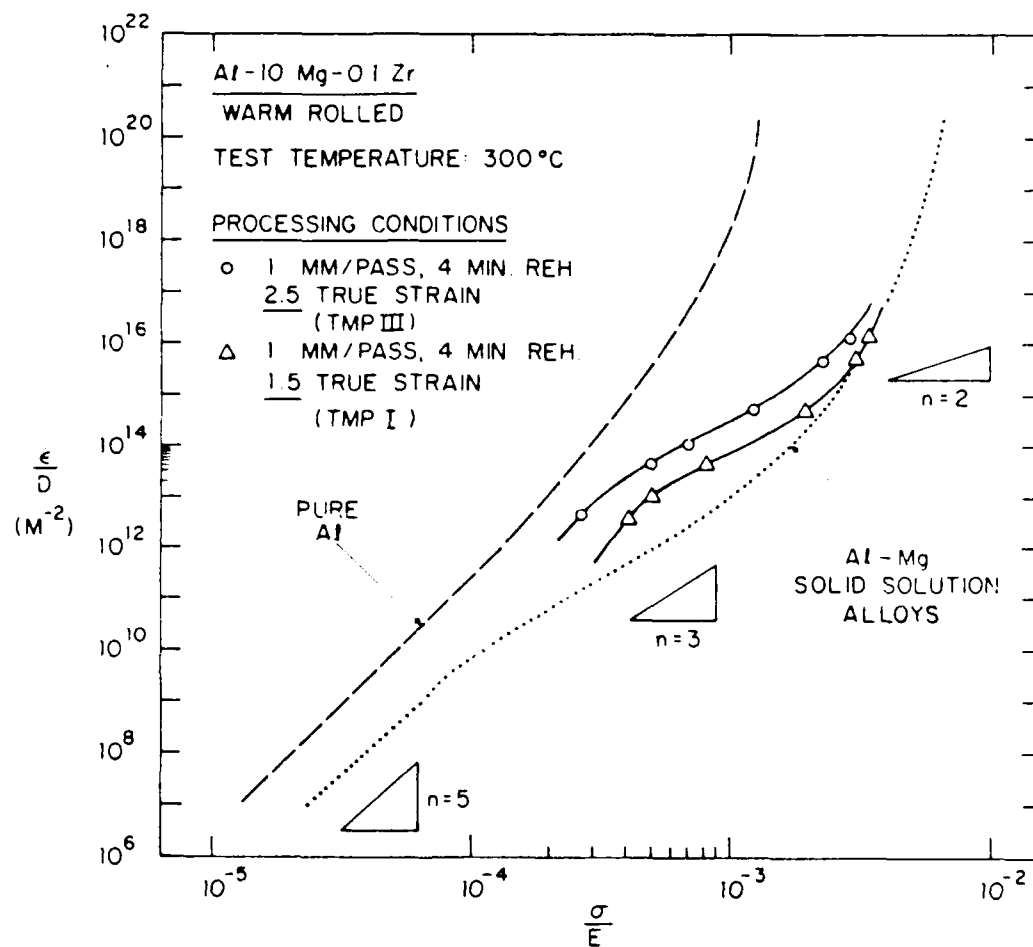
Figure 6.1. Diffusion-compensated strain rate versus modulus-compensated stress for TMP I and TMP III illustrating the effect of total strain. Processing by TMP III, with 2.5 true strain, results in a better superplastic response than TMP I, with 1.5 true strain.
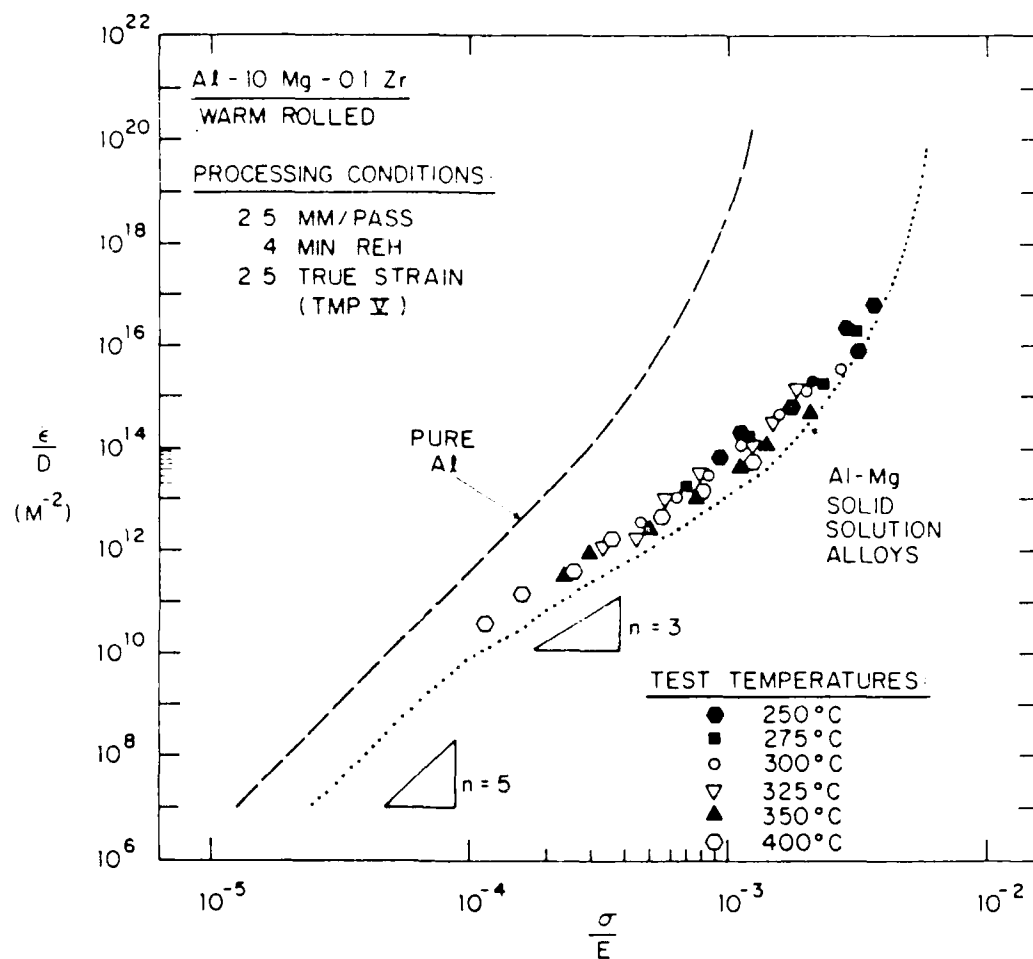
Figure 6.2. Diffusion-compensated strain rate versus modulus-compensated stress for TMP V. The data in the temperature range (250°-300°C) fits one curve near that of Al-Mg solid solution alloys. The material has a high stress exponent close to 3 (m ≈ 0.33). The material shows a low ductility and no superplastic response.
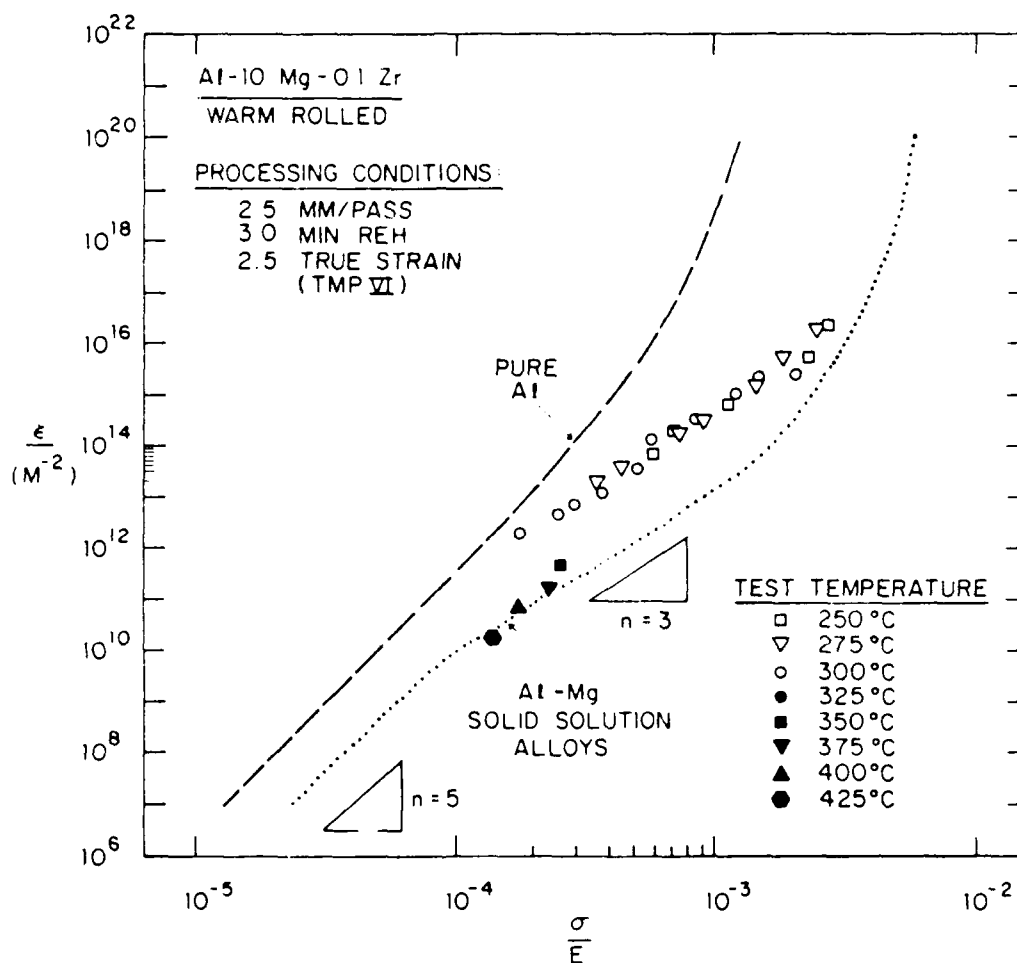
Figure 6.3. Diffusion-compensated strain rate versus modulus-compensated stress for TMP VI. The data in the temperature range $(250^{\circ}C-200^{0}C)$ fits a single curve. The material shows a higher strain rate sensitivity and smaller stress exponent than TMP V, and thus has a higher ductility and enhanced superplastic response.
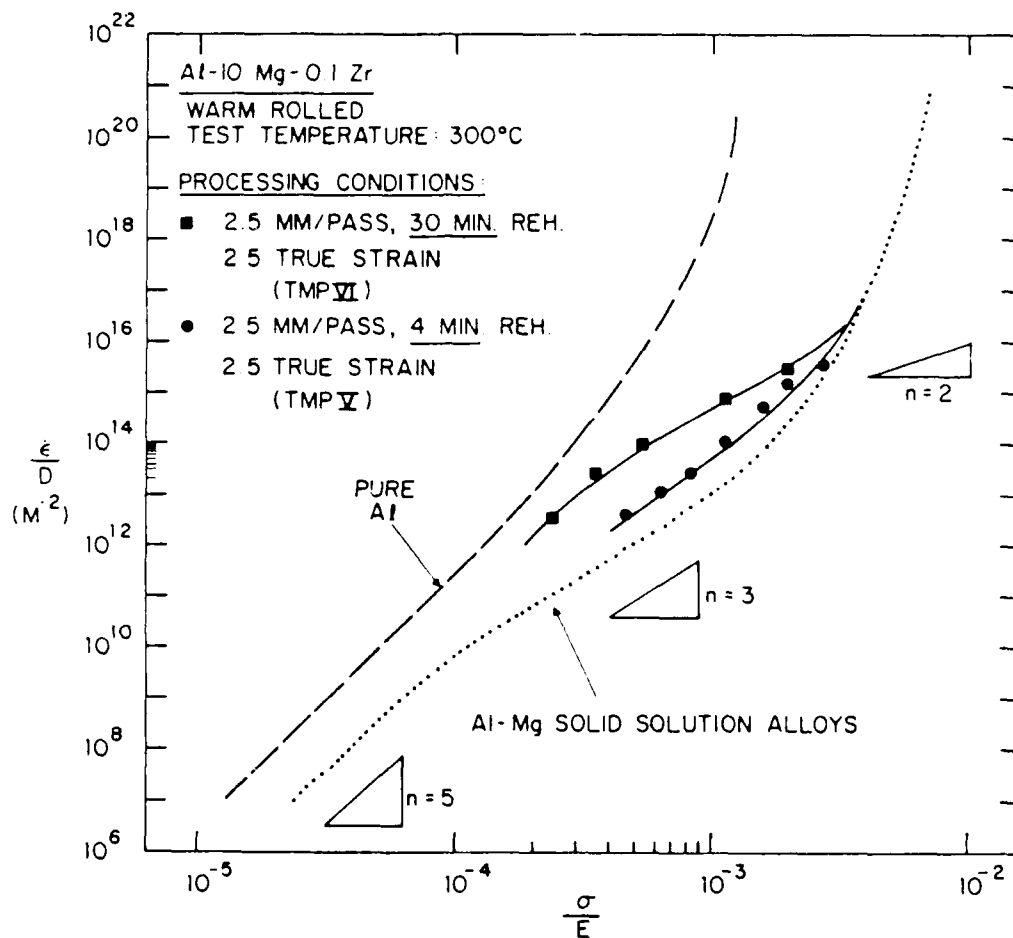
Figure 6.4. Diffusion-compensated strain rate against modulus-compensated stress for TMP V compared with that for TMP VI illustrating the effect of reheating time between passes. TMP VI, with 30 minutes reheating time, shows enhanced superplastic properties compared to TMP V.
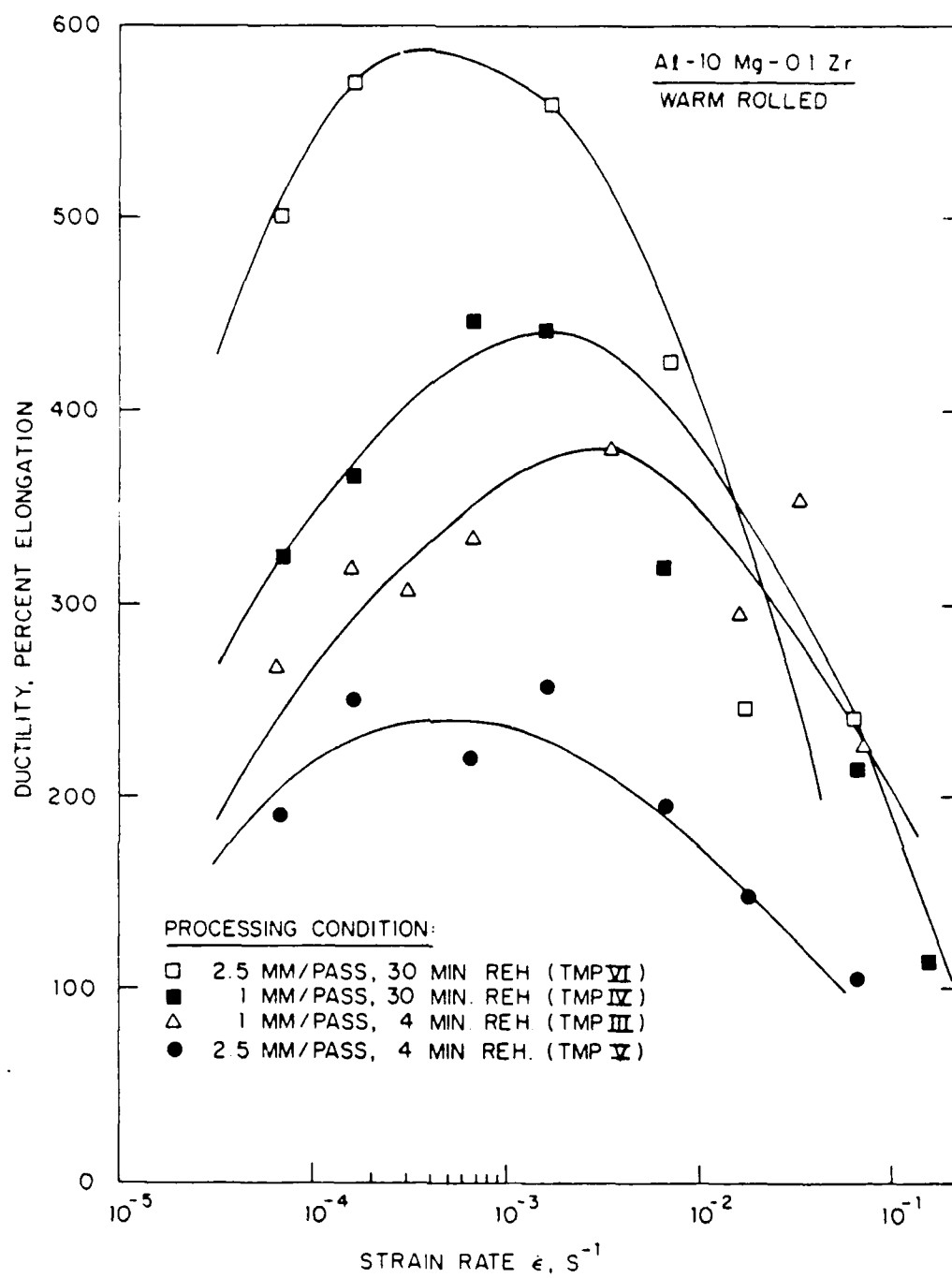
Figure 6.5. Ductility as percent elongation versus strain rate for the different thermomechanical processing conditions.

110

true strain. Comparison is also possible between TMP IV and TMP VI, which were reheated 30 minutes between passes and rolled to 2.5 true strain. It is obvious from these comparisons that increasing the reduction per pass substantially increases the ductility seen in the subsequent superplastic response.

D. ROLLING TEMPERATURE

The effect of rolling temperature may be seen and is given in Figures 6.6 and 6.7. The data is for material processed by TMP V but at different rolling temperatures. All data was obtained by tension testing at 300° C after completion of the rolling. Figure 6.6 provides stress versus strain-rate data for evaluation of rolling at 220° C, 300° C, and 380° C. Rolling at 220° C gives a stronger material and lesser m value, and increased rolling temperature results in both decreased strength and increased m value up to the highest rolling temperature employed, 380° C. The trend in ductility clearly reflects the strength data in that ductility is higher for high rolling temperatures under this TMP V processing condition. Figure 6.7 shows the corresponding ductility data for these rolling temperatures.

E. TRANSMISSION ELECTRON MICROSCOPY

Transmission electron microscopy (TEM) was used to assess the effect of the processing variables on microstructure by measurement of the grain or subgrain size. The results are summarized in Table V for the different thermomechanical processes.

TABLE VI-2

GRAIN/SUBGRAIN SIZE FOR VARIOUS
THERMOMECHANICAL PROCESSES

TMP	SampleLocation	
	Gage	Undeformed (Grip)
TMP III	2.30μm	1.9μm
TMP IV	2.70μm	2.0μm
TMP V	1.82μm	1.67μm
TMP VI	2.36μm	1.75μm
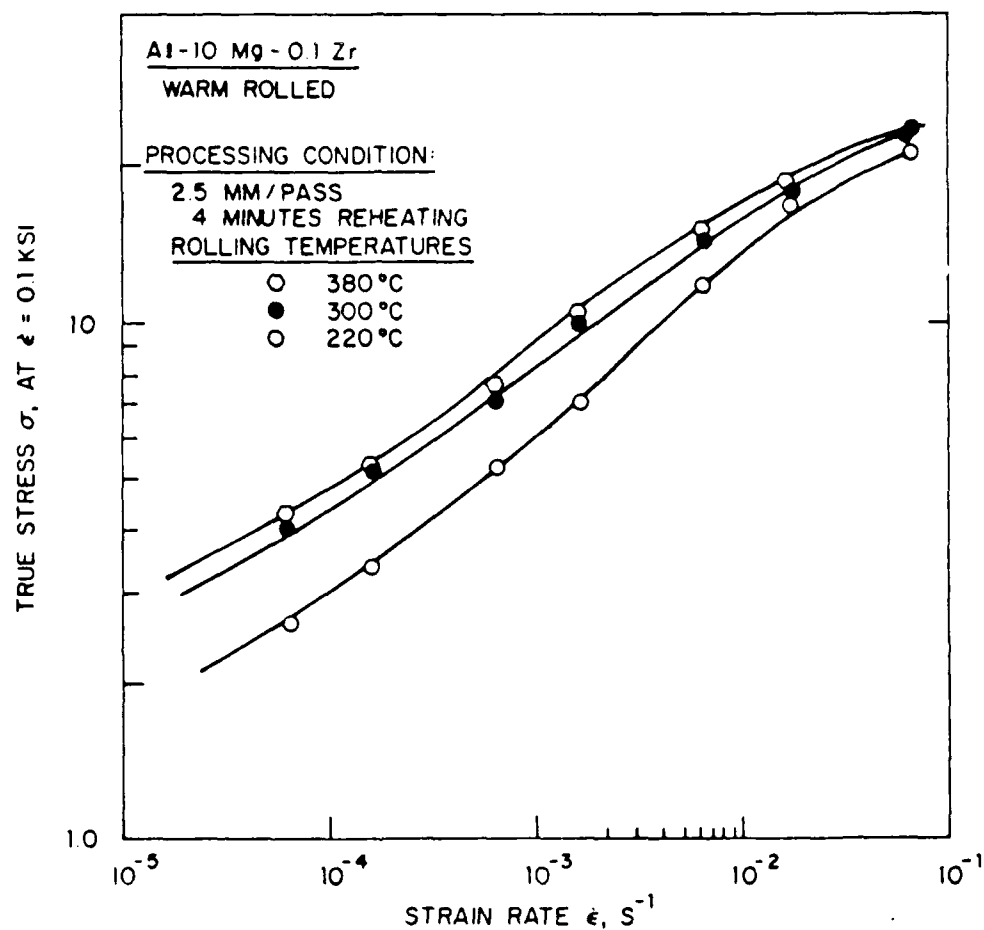
Figure 6.6. True stress at 0.1 true strain versus strain rate for warm-rolled material under TMP V condition, illustrating the effect of rolling temperature on ductility and superplastic properties. Under this TMP the lower rolling temperature results in less ductility and superplastic response.

112
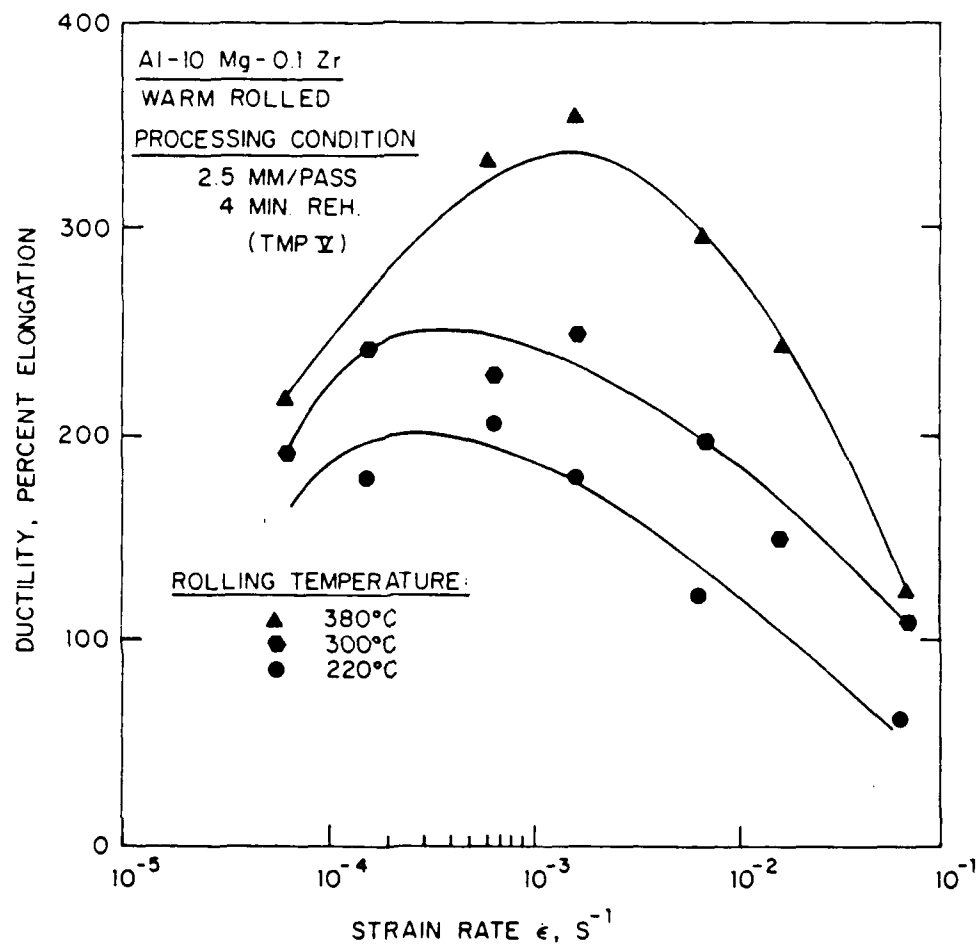
Figure 6.7. Ductility in percent elongation versus strain rate for warm rolled material under TMP V condition illustrating the effect of rolling temperature. Under this TMP condition, high rolling temperature result in higher ductility and better superplastic properties.

All the samples had been tested at $300°$ C and a at strain rate of $1.67 \times 10^{-3} s^{-1}$. Figures 6.8 - 6.11 present the TEM photomicrographs for samples processed by TMP IV, V and VI, respectively and then heated and tested at $300°C$. Microscopy for TMP III was shown in Figure 4.6. The subgrain or grain size of the undeformed material is smaller for material rolled with larger reductions and also for material rolled at low temperatures. Also, the grain size in deformed gage sections is always larger than in the undeformed material which reflects the grain growth during superplastic deformation. The grain or subgrain size is larger for longer reheating time and the maximum average grain size measured is $2.7 \mu m$.

In summary, increasing the rolling strain increases the ductility and superplastic response. The effect of rolling strain is more pronounced in material rolled with 1 mm reduction per pass than in material rolled with 2.5 mm reduction per pass. Increasing the reheating time between rolling passes improves the ductility and superplastic response. The improvement is more significant in material rolled with larger reductions per pass. Increasing the reduction per pass apparently increases the potential for superplastic behavior. To exploit this, however, a long reheating time between passes is necessary. If insufficient time is allowed between passes, then the larger reduction will result in a lower ductility and lesser superplastic properties. Finally increasing the rolling temperature increased the ductility and superplastic response for TMP V, a process involving short reheating time.

114
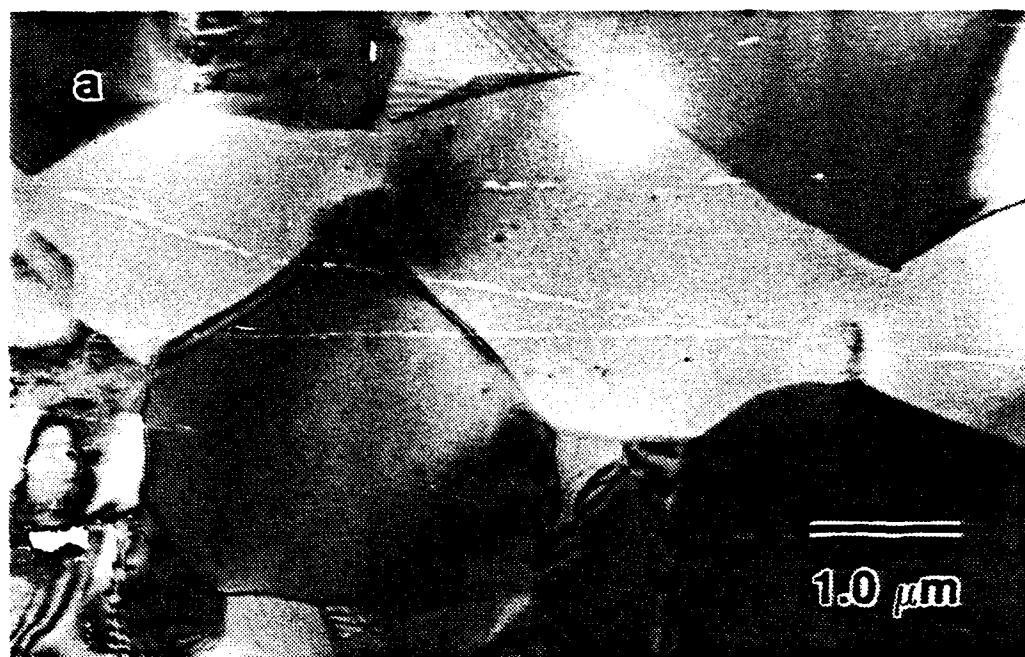
Figure 6.10. Bright field TEM micrographs showing the alloy in the TMP VI condition: (a) grip section (grain size = 2.0 μm) and (b) gage section (grain size = 2.7 μm).

117

Figure 6.9. Bright field TEM micrographs showing the alloy in the TMP V condition: (a) grip section (grain size = 1.67 μm) and (b) gage section (grain size = 1.82 μm).

116
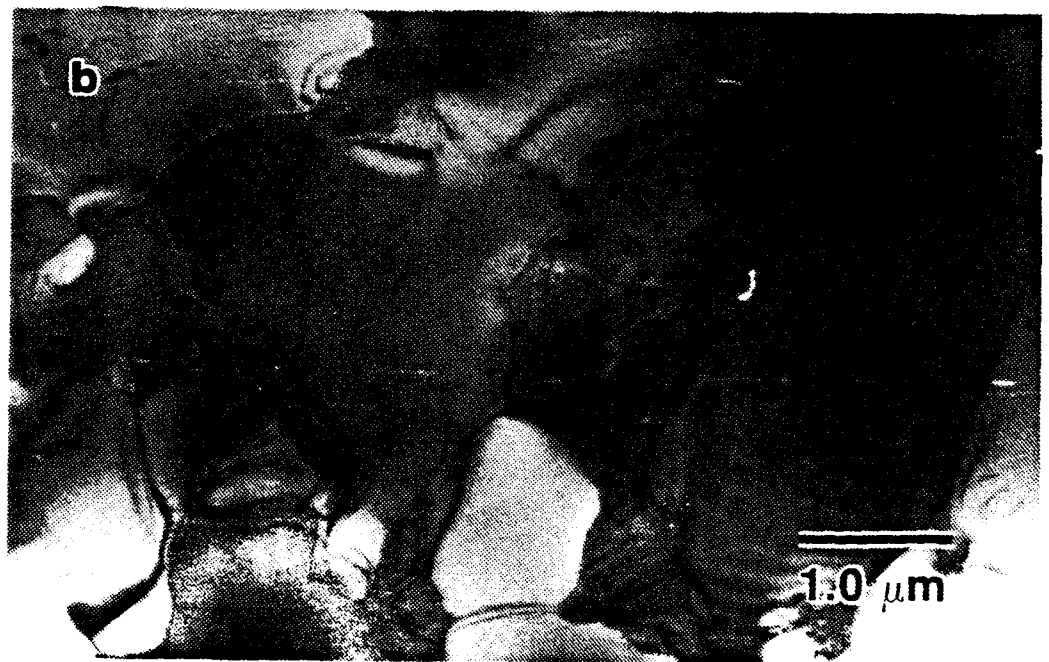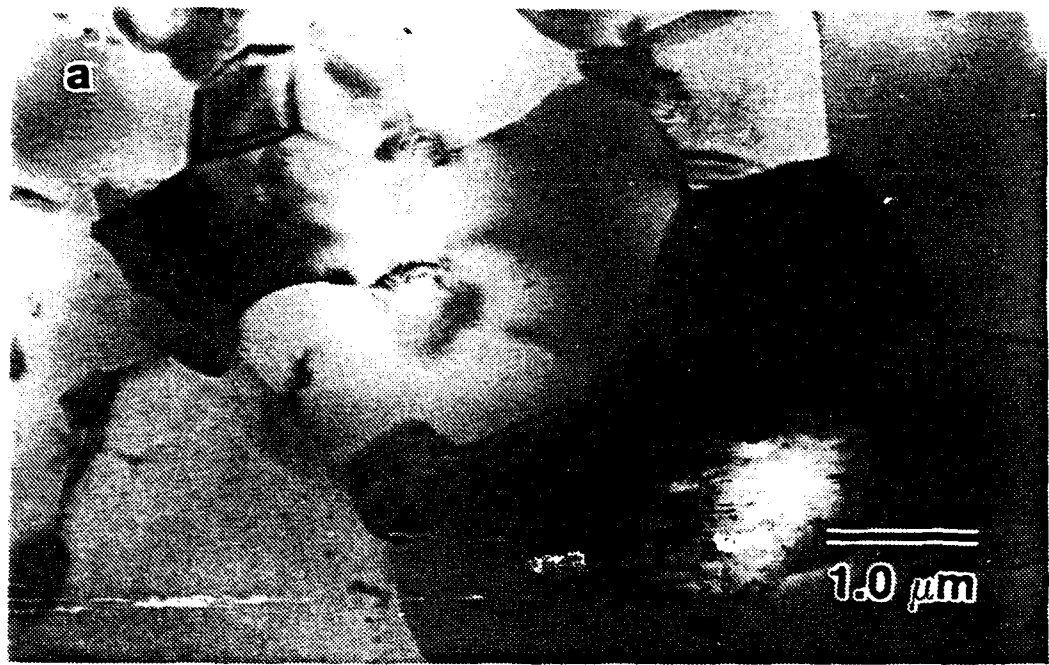
Figure 6.8. Bright field TEM micrographs showing the alloy in the TMP IV condition: (a) grip section (grain size = 1.75 μm) and (b) gage section (grain size = 2.36 μm).

Figure 6.11. Bright field TEM micrograph showing the alloy in the TMP V condition; rolling temperature is 220°C. the specimen is from a gage section (grain size = 1.37 μm).

VII. <u>PHYSICAL MODEL FOR MICROSTRUCTURE EVOLUTION</u>

It is important to understand the evolution of the microstructure from the moment the material enters the roll gap during a rolling pass, on through the reheating periods between rolling passes, cooling after rolling and finally heating for superplastic deformation. The effect of rolling parameters (which are reduction per pass, the rolling temperature, the reheating time between passes and the total strain) on the nature of the microstructure is necessary. Especially important are the size of the grains or subgrains and the nature of their boundaries, i.e. their misorientation. A model is suggested to explain the effect of the various thermomechanical processes evaluated in this research.

A. MICROSTRUCTURE EVOLUTION DURING A ROLLING PASS

Al is a high stacking fault energy material. When Al is deformed at a temperature above one-half of its melting point a polygonized structure results (Jonas et al., 1969; McElroy, 1972; McQueen and Jonas, 1973; McQueen and Jonas, 1973; McQueen, 1977). Dislocations are generated by the plastic deformation, with grain boundaries acting as important dislocation sources. As a result of interaction of mobile dislocations with each other and with other dislocations stored within the grains, the dislocation density increases very rapidly. As the dislocation density increases recovery and annihilation start to take place. At first, the rate of annihilation is smaller than the rate of dislocation generation, and accumulation of dislocations occurs, causing the strain hardening of the material. Eventually, the rates of the two processes become equal and the dislocation density then attains an equilibrium value (Jonas et al., 1969; Sellars and Tegart, 1972; McQueen and Jonas, 1975). This equilibrium dislocation density depends on the rolling conditions.

During dynamic recovery the dislocations become arranged into regular arrays or subboundaries. These boundaries surround regions now depleted in dislocations and the resultant structure consists of subgrains. The subgrain size is mainly determined by the rate of straining during rolling and also the rolling temperature

119

(Jonas et al., 1969). The Mg content of the alloy in this case will also affect the subgrain size, reducing it as the alloy content increases.

The dislocation rearrangements required to attain an equilibrium subgrain size occur very fast (Exell and Warrington, 1972; Sheppard et al., 1985). An equilibrium structure may not be attained, however, during a rolling pass and the resultant structure may be incompletely recovered. If equilibrium is attained, the subgrains would remain constant in size during the subsequent steady state period (McQueen et al., 1967; Jonas et al., 1968; Fulop and McQueen, 1972; McQueen and Jonas, 1975). The dislocation density inside the subgrains and in the subgrain walls would remain constant and so the and thus the misorientation of the subboundaries would also remain constant.

B. EFFECT OF TEMPERATURE AND REDUCTION PER PASS ON MICROSTRUCTURAL EVOLUTION

The dynamic recovery which takes place during each rolling pass is the first step in the microstructure evolution process. Increasing the temperature makes the dislocation motion easier, because cross slip and climb processes are easier at high temperatures. This easier dislocation motion increases the annihilation rate and thus decreases the dislocation density. On the other hand, increasing the rate of straining by increasing the reduction per pass increases the generation rate and thus increases the equilibrium dislocation density.

It was shown in Chapter VI that both increased reduction per pass and lower rolling temperature both result in a smaller substructure size; conversely the smaller reduction per pass results in a larger substructure, as does rolling at a high temperature.

The subgrain size has been shown to be related to the rolling variables by the relation

$$d^{-1} = a + b \ln Z \qquad (7.1)$$

120

where a and b are constants (McQueen et al., 1967; McQueen, 1968; Sherby et al., 1977; Jonas et al., 1969; McElroy, 1972; McQueen and Jonas, 1973, 1975); Z is the temperature compensated strain rate or Zener Hollomon parameter given by

$$Z = \dot{\epsilon}\exp^{Q/RT} \tag{7.2}$$

where $\dot{\epsilon}$ is the strain rate during the rolling, Q is the activation energy for the recovery process, and R and T have the usual meaning.

From these equations, it is evident that an increase in strain rate has the same effect as the decrease in temperature (McQueen, 1977) because both result in an increase in Z. Since the subgrain size d is inversely related to Z, the subgrain size will be larger for higher temperature and lower rate of straining.

C. EFFECT OF REHEATING BETWEEN PROCESS

The rolling process also includes reheating periods between passes. During these periods, static recovery takes place. Static recovery is a relatively slow process involving many sequential steps. It slows as the recovery process proceeds and the dislocation density decreases, thereby decreasing the driving force (McQueen, 1976). During static recovery, annihilation of redundant dislocations takes place. These are dislocations which do not annihilate during dynamic recovery process due to the short time available.

An additional important feature of structure evolution in these Al-Mg alloys is precipitation of the intermetallic β. This occurs concurrently with the rolling process (McNelley and Garg, 1984). Microscopy results, e.g. as reported by Hales and McNelley (1987), indicate that this precipitation occurs on nodes of the substructure, stabilizing the boundaries of the structure. The static recovery takes place by the redundant dislocations moving to subgrain boundary walls and being absorbed in them, increasing the number of dislocations per unit length in the boundaries and therefore their misorientation.

Subgrain growth may also take place during static recovery. This growth takes place through the decomposition of thinly populated dislocation walls. The dislocation of these walls are added to other, more thickly populated walls, also

increasing the dislocation density in the remaining boundaries and their misorientation as well as the size of subgrains. This build up of misorientation in cell walls can lead to nucleation recrystallization (Perrymann, 1956; Beck et al., 1959; Lyton et al., 1965; McElroy and Szkopiak, 1972; McQueen and Jonas, 1975). Finally, as a result of recovery processes, the density of dislocation inherited from the rolling tends to decrease to that of an annealed condition; this cleaning of the interior of the subgrains prepares the scene for a new cycle of dislocation generation.

D. CONTINUOUS VERSUS DISCONTINUOUS RECRYSTALLIZATION

Any recrystallization process whether it is continuous or discontinuous includes the formation of nuclei and the growth of these nuclei. A nucleus can form and grow only if its size exceeds a minimum value and if it has boundary misorientation higher than a critical angle (Hu, 1963), or (for discontinuous recrystallization) is surrounded, at least in one part, by a high angle boundary. This prerequisite regarding the boundaries arises because of the low mobility of the low angle boundaries (Doherty, 1978). The nucleation process takes place through the growth of a polygonized subgrains (Cahn, 1950, and independently by Beck, 1949) or through subgrain coalescence which leads to increases in size and misorientation (Smith, 1948; Fujita, 1961; Li, 1962; Hu, 1963; Li, 1966).

In a fully polygonized substructure obtained by TMP, all subgrains could become nuclei if they have sufficient size and boundary misorientation to enable them growth. The subgrain growth can be treated in the same manner as grain growth (Rhines and Craig, 1974; Martin and Doherty, 1976). It can be divided into two categories: one, normal subgrain growth and two, abnormal subgrain growth, analogous to normal and abnormal grain growth.

The structure formed during the rolling process has grains elongated in the direction of flow. The elongated grains then contain equiaxed subgrains inside (Figure 7.1). If the TMP conditions result in subgrains of size larger than the critical size necessary for nucleation and of sufficient misorientation (Figure 7.2a), most or all of these subgrains may be able to grow simultaneously. The attainment

122

of the misorientation may be facilitated by the precipitated β in these alloys if the β stabilizes the boundaries and yet allows dislocation recovery to them. This is continuous recrystallization (Figure 7.2b).

On the other hand, if the thermomechanical processing (TMP) conditions result in subgrains with sizes smaller than the critical size for nucleation or misorientation less than the minimum angle for growth, the subgrains will not be able to grow (Figure 7.3a). There are then two possibilities. First, if the material contains enough fine, second-phase or dispersoid particles, i.e., fine β phase and $ZrAl_3$ or $MNAl_6$, of size less than $0.1\mu m$, the dispersoids may pin the subboundaries and the subgrain growth is then controlled by the rate of dissociation of these particles. Since the original size and misorientation of the subgrains are small, the growth rate, although uniform, is slow and the increase in misorientation is low, the net result is limited grain boundary sliding and hence a low superplastic response and ductility in subsequent testing.

Second, if the material does not contain a sufficient amount of dispersoid or second phase, a few subgrains may be able to grow and increase in misorientation and become nuclei. This is analogous to the abnormal grain growth. The nucleation process in this case is difficult because the mobility of the low angle boundaries is low. Thus subgrains which are able to grow are those of large size and which have at least one boundary in contact with a coarse second phase particle, prior grain boundary or deformation band. This is the case of discontinuous recrystallization (Figure 7.3b). This results ultimately in a coarse grain structure (Figure 7.3c).

E. FEATURES OF THE PHYSICAL MODEL

Based on the above analysis a model is proposed. Figures 7.4 and 7.5 are schematic representations of this model. The model is based on the events which take place during the rolling, the reheating periods between passes, and the subsequent heating for superplastic deformation: dislocation generation, dynamic recovery, static recovery and annihilation processes. Previous models for microstructural evolution have dealt primarily with the events occurring during the early stages of superplastic deformation. They were not concerned with the effects of events

SECOND PHASE
PARTICLE   SUBGRAIN   ELONGATED GRAIN
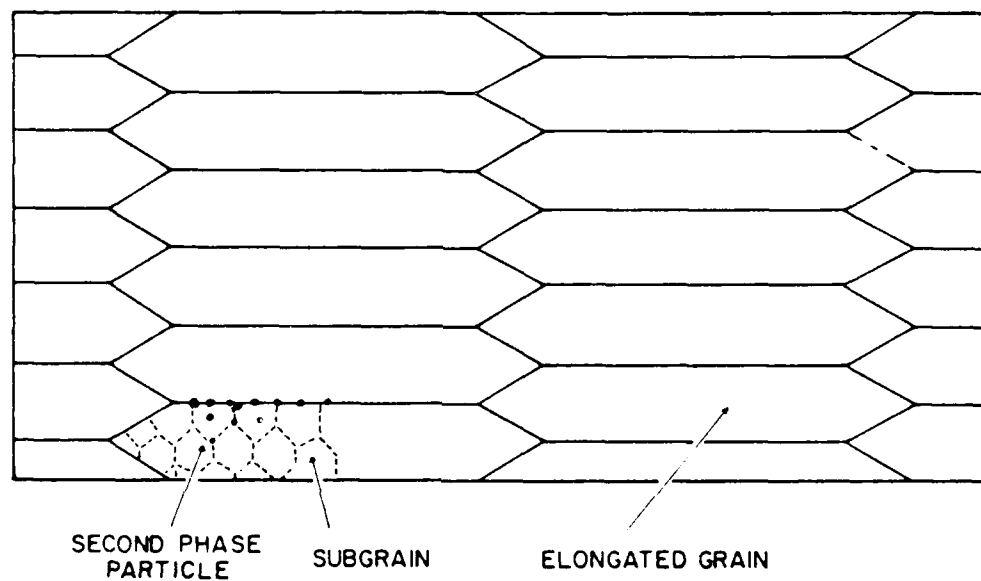
Figure 7.1. Structure formed during the rolling process. The grains elongate
in the rolling direction and do not recrystallize. The elongated grains contain
equiaxed subgrains.

124
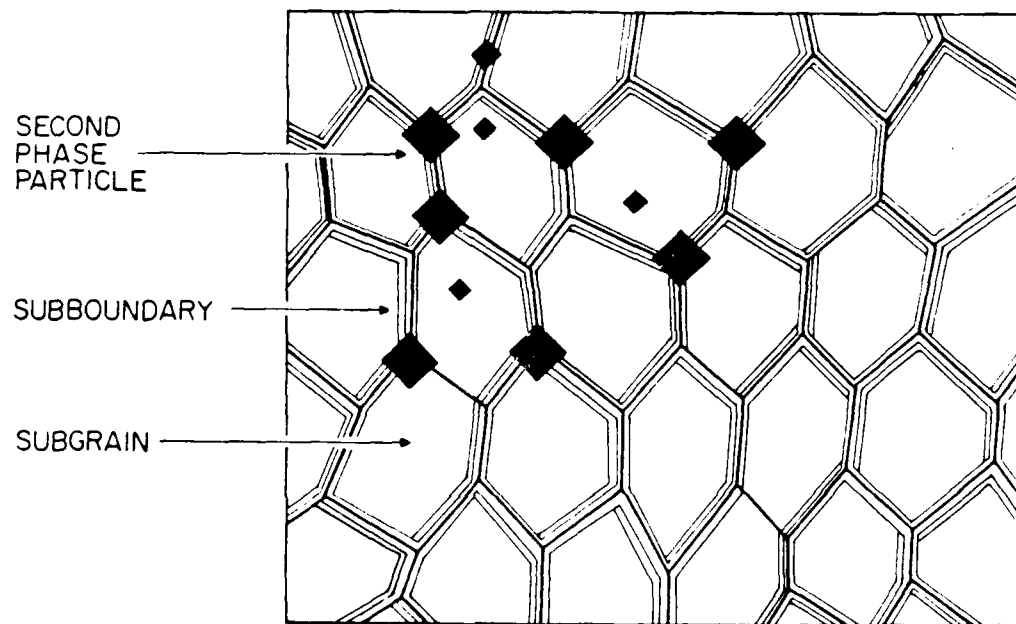
Figure 7.2a. Substructure of subgrains of a size larger than the critical size and misorientation larger than the critical angle for nucleation. Most or all subgrains are able to grow simultaneously. The second phase particles pin the subboundaries and stabilize the substructure. The result is a structure shown in Figure 7.2b.

125

SECOND PHASE PARTICLE

FINE GRAIN FORMED BY CONTINUOUS RECRYSTALLIZATION

MODERATE ANGLE BOUNDARY ($\vartheta < 7°$)
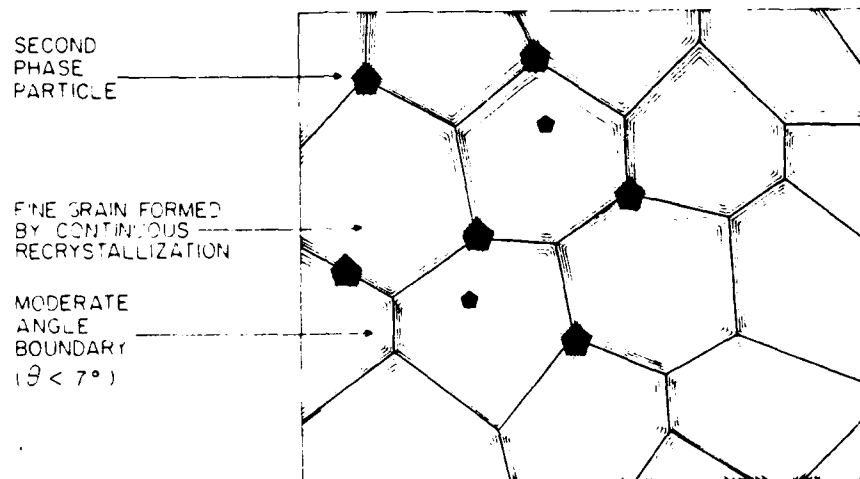
Figure 7.2b. Structure formed by a continuous recrystallization process. If the conditions for nucleation and growth are fulfilled, the subgrains increase in size and the subboundaries have a higher dislocation density, the misorientation increases, reaching that of high angle boundaries.

126

SECOND
PHASE
PARTICLE

SUBGRAIN

SUBBOUNDARY
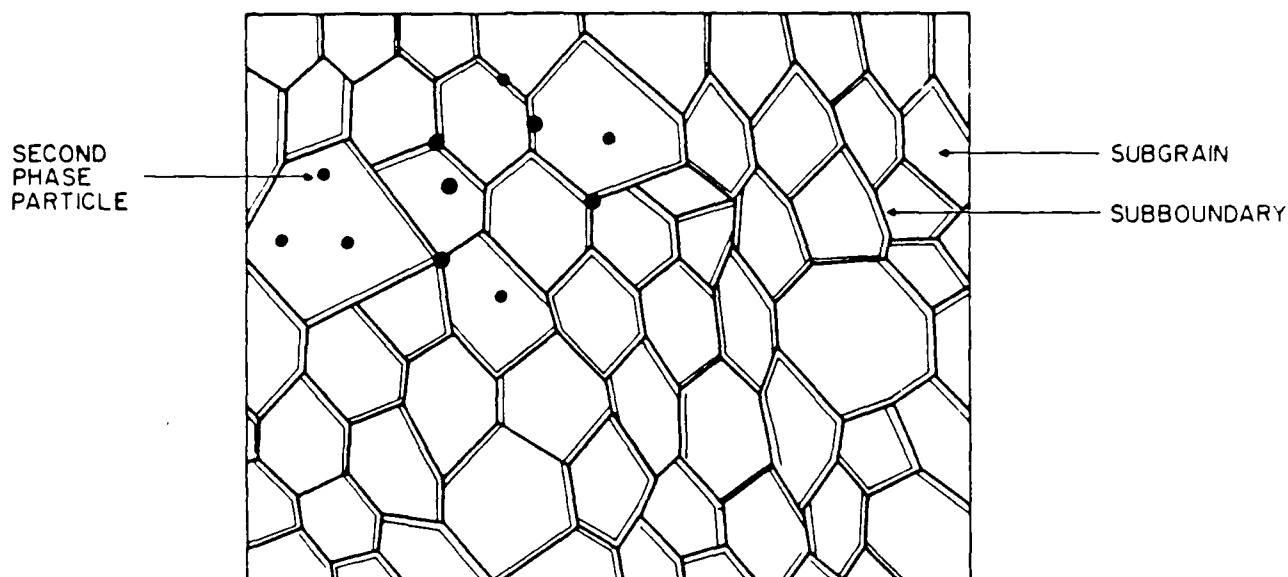
Figure 7.3a. Subgrains smaller than the critical size and misorientation smaller than the critical angle necessary for nucleation. In this case there are two possibilities: (i) if the structure contains sufficient dispersoid of small size which can pin the subgrain efficiently, the growth is slow and controlled by the dissolution of the particle. The result is a limited grain boundary sliding; (ii) if the structure does not contain enough particles and because most of the grains are not able to grow, a selective growth occurs and a discontinuous recrystallization takes place.

127
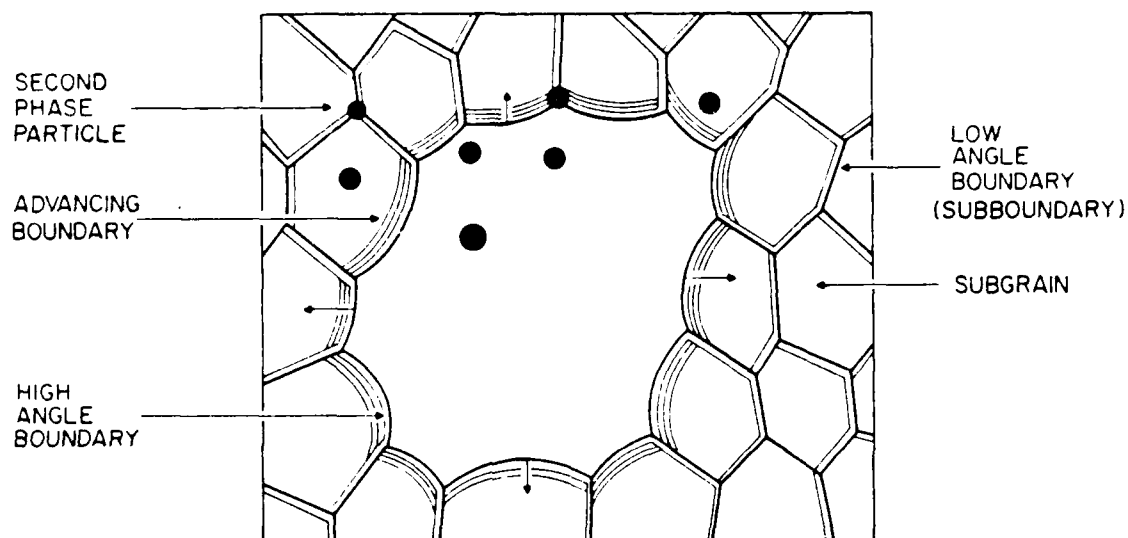
Figure 7.3b. Discontinuous recrystallization. If the conditions are such that only few of the subgrains are able to grow, the grains with size larger than the critical size for nucleation and having one side in contact with a high angle boundary, slipband, or second phase particle discontinuous recrystallization takes place. The result is a coarse structure shown in Figure 7.3c.

COARSE GRAIN FORMED BY DISCONTINUOUS RECRYSTALLIZATION

HIGH ANGLE BOUNDARY
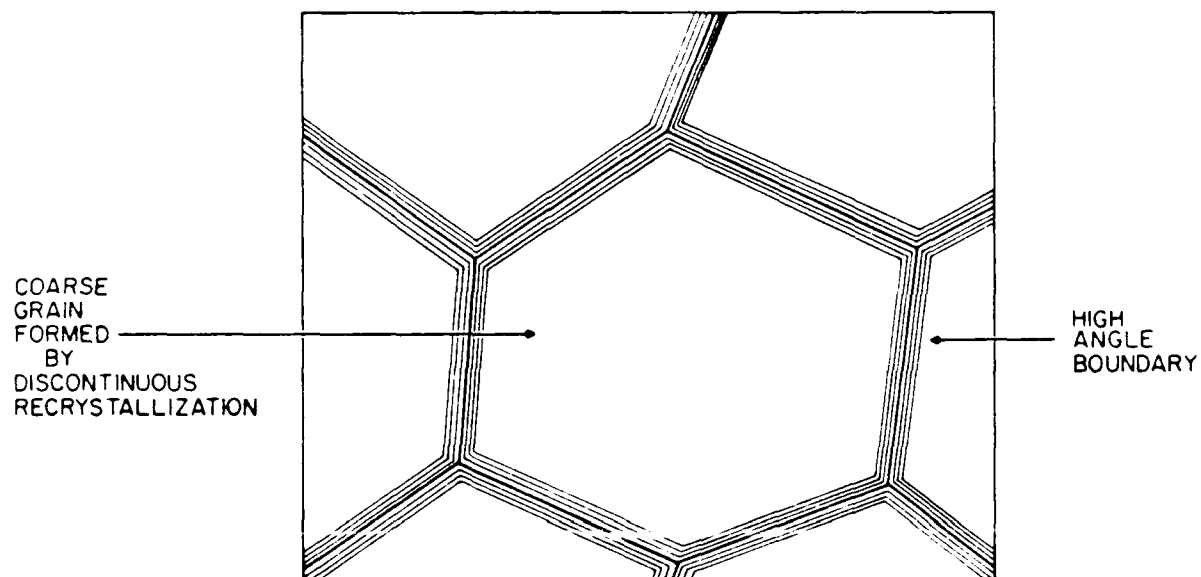
Figure 7.3c. Coarse grain structure which results by discontinuous recrystallization. Compare this with the finer structure produced by continuous recrystallization mechanism in Figure 7.2b.

129

occurring before superplastic deformation on the microstructural evolution and superplastic behavior.

The most important feature of the thermomechanical process used is that it consists of multiple passes separated by reheating periods. Each cycle includes the events previously described, leading to continuous recrystallization during the process. Essentially, a rolling pass produces dislocations; depending upon the temperature and strain rate during the pass, the dislocations undergo dynamic recovery, with additional, i.e., redundant, dislocation remaining. These later undergo further static recovery during reheating time between passes. Also as deformation proceeds, precipitation of 0.5–1.0μm β occurs at triple points in the evolving structure.

The critical feature of the model is that the boundary misorientation increases as recovery processes allow the redundant dislocations to be absorbed into pre-existing subboundaries. Misorientation sufficient to sustain superplastic deformation mechanisms, including grain boundary sliding, can be developed if the subboundaries remain stabilized by the precipitated β and if recovery processes are facilitated, e.g., by increased time at temperature or rolling with a greater number of small reductions, by increasing temperature within the range of this mechanism, or by alloy modifications to enhance recovery, again within the range of the continuous recrystallization process.

Consider first the initial rolling pass on annealed material. If the reduction is large (2.5 mm as in TMP II, V and VI), the strain rate will be high leading to a large dislocation density (Figure 7.4a). If the reheating interval is short (4 mins.), time may be insufficient for recovery to produce well-defined subgrains. Longer reheating will result in better-defined subgrain boundaries. On subsequent passes further dislocation generation takes place followed by recovery in the reheating interval between passes. With the longer interval, the redundant dislocations recover more completely, lodging in the subboundary walls. As β precipitation occurs at nodes, the boundaries become stabilized such that the absorption of dislocations in them results in more dislocations per unit length and hence increased misorientation. This is illustrated in the diagrams of Figure 7.4a by comparing structures

130
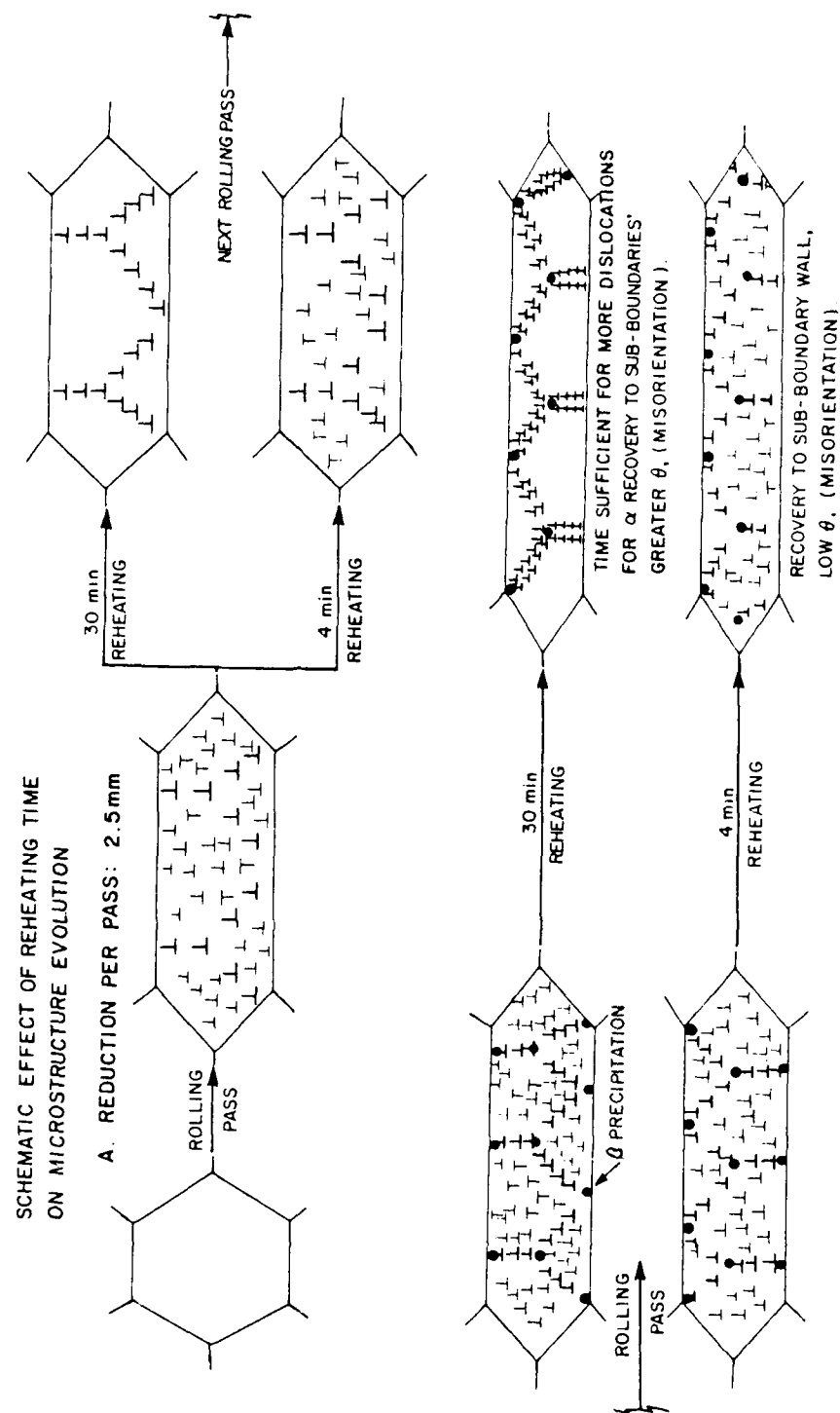
Figure 7.4a. A schematic representation of the evolution of microstructure through a sequence of rolling passes. These diagrams compare structures anticipated to result from rolling with a large reduction per pass and with either a short reheating interval (4 mins.) or a long reheating interval (30 mins.).

131
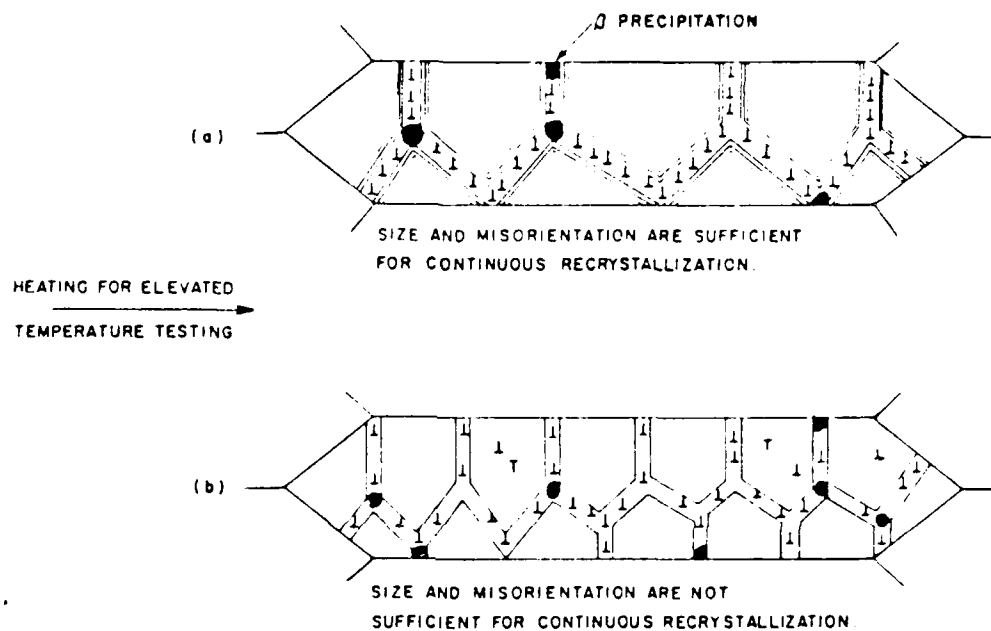
Figure 7.4b. Upon reheating prior to tension testing, recovery processes facilitate further increase in misorientation. With the longer reheating interval, the structure is better able to sustain grain boundary sliding and is thus more highly superplastic.

132

developed in materials rolled with longer reheating intervals (upper diagrams - TMP-VI) to those rolled with shorter reheating intervals (lower diagrams - TMP V). As total strain is increased, the subboundaries are better able to sustain grain boundary sliding and the resultant superplasticity will be enhanced (i.e., TMP II is less superplastic than TMP V or VI). With The longer reheating time and processing to larger total strain ($\epsilon_{rolling} = 2.5$) the bounaaries have attained sufficient misorientation and behave as high angle boundaries upon subsequent heating and straining (Figure 7.4b).

If the reduction is small (1.0 mm as in TMP-I, III or IV), the strain rate will be low and thus the equilibrium dislocation density lower than for a large reduction (2.5 mm as in TMP-II, V, or VI). Subsequent recovery during reheating between passes results in a greater subgrain size for the smaller reduction processing. This effect is illustrated in Figure 7.5 and may be seen by comparing the microstructure shown in Figure 4.6 (TMP III) to that in Figure 6.10 (TMP V).

With sufficient passes to attain a total strain of 2.5, the material rolled with the short reheating interval and smaller reduction per pass, 1.0 mm (TMP - II), does achieve a superplastic microstructure while that with the larger reduction, 2.5 mm (TMP V), does not. In terms of the model being proposed, this result occurs because the short reheating interval does not allow the high density of redundant dislocations, produced with the 2.5 mm reduction, enough time to recover to subgrain boundaries and thereby increase the boundary misorientation. Indeed, these dislocations remain and are able to move in subsequent passes, thus diminishing the need for fresh dislocation generation on each pass. The structure in essence is like that of a cold worked metal. With a smaller reduction per pass, more passes are required to reach a strain of 2.5 and thus more time is accumulated at the rolling temperature. Recovery of dislocations to prior subboundaries would be facilitated. Following the final pass and reheating for mechanical testing, this condition, TMP-III, was shown to have attained boundaries of $2^o - 7^o$ misorientation (Hales and mcNelley, 1987), evidently sufficient to sustain superplastic mechanisms.

Continuous recrystallization in Aluminum (Matsuki, et al., 1977) has been proposed to occur either statically or dynamically (Watts, et al., 1976). The details of the mechanism have not been established but it is usually suggested to occur by a process of subgrain boundary coalescence, either during initial heating or during subsequent deformation. The material is usually presumed to be in a cold worked condition prior to heating and thus the details of the processing to induce the cold worked state are not important. Usually, only the initial dislocation density is considered, and a finer structure assumed to result from a higher dislocation density. Such a line of reasoning is not entirely satisfactory when applied to the situation of interest here. As noted previously, material rolled to the final strain of 2.5 by a process consisting of a large number of small passes (TMP III) was more highly superplastic than one rolled with a small number of large reductions (TMP V). This latter process would be presumed to result in a higher dislocation density and thus yield boundaries of greater misorientation and ability to sustain superplastic flow processes. In fact, the opposite is seen; the mechanism proposed, involving recovery to pre-exisitng subboundaries, is better able to explain the observed results.

This may also be seen in the results concerning the effect of reheating time between rolling passes. Comparison of the mechanical property data for TMP V to that for TMP VI reveals the latter to be more superplastic at 300°C, even though material processed to TMP VI was reheated 30 minutes between passes while that of TMP V was reheated only 4 minutes. Microstructure data for VI shows it to be slightly coarser; it is expected, however, to have greater misorientation between adjacent grains to account for its greater degree of superplastic response.

F. EFFECT OF Mg CONTENT AND ROLLING TEMPERATURE

Al is a high stacking fault energy (SFE) material. Addition of Mg lowers the SFE (Cotner and Tegart, 1969). The effect of Mg on Al is not as clear regarding the effect of alloying elements as is the case in other, similar solid solutions, for example, in Cu-Zn and Zr-Sn (Pollard and Nuttins, 1964; Jonas et al., 1969; Luton and Jonas, 1972; McQueen and Jonas, 1975; McQueen, 1977; Sherby et al., 1977). In

these latter alloys,the dynamic recovery and polygonization processes are strongly impeded (McQueen, 1977). Al-Mg alloys still develop a well defined substructure, which means that the addition of Mg to Al is not as effective in retarding the recovery process. McQueen (1977) has mentioned that the effect of Mg is through "dynamic strain hardening" and the dynamic interaction between the Mg atoms and the dislocations in the subgrain formation process (Morris, 1974, 1976). Sheppard has indicated that because of the activation energy for diffusion Mg is less than the self-diffusion of Al, the Mg atoms move faster and surround dislocations (Sheppard, 1985). This decreases the the rate of the annihilation processes. This Mg atom-dislocation interaction varies according to the strain rate. In creep processes where the strain rate is very small, the dislocation velocity is low and the Mg atoms surround dislocations easily. In hot working processes, where the rate of straining is high, the dislocations must move faster and the Mg atoms are less able to surround them and impede their motion. The higher the rate of straining the less effective will be the Mg atoms. Sheppard (1985) has also noted that the binding energy between the Mg atoms and vacancies is very strong. Because dislocation climb depends mainly on availability of vacancies, it will be impeded due to the presence of Mg atoms. The net result of these two effects is reduced dislocation recovery and annihilation. Mg-content does not seem to influence the generation rate, rather, by changing the balance between annihilation and generation, the equilibrium dislocation density is increased.

Data was obtained on the Al-8%Mg-0.1%Zr alloy, processed by either TMP III or TMP V. When evaluated for superplastic response at 300°C, the opposite trend to that obtained for the 10 wt. pct. Mg alloy was noted. For the 8% Mg alloy, TMP-V (2.5 mm per pass with 4 minutes reheating) exhibited greater ductility during testing at 300°C than TMP-III (1.0 mm per pass, also with 4 minutes reheating time). Comparison of data for this alloy and the 10% Mg alloy for identical processing conditions is provided in Figures 7.6 and 7.7. In terms of this recovery model, such a result reflects enhancement of recovery in the lower Mg alloy sufficient to offset the effect of the short reheating time. A similar result was shown in the 10%Mg-0.1%Zr alloy by varying the rolling temperature. TMP

135

V (Figures 6.6 and 6.7) was employed and rolling was done at 220°C and 380°C as well as 300°C. Based solely on consideration of boundary coalescence evolving from an initially cold worked condition it would have been anticipated that the lower rolling temperature would have produced the highest ductility in subsequent 300°C testing. The opposite result was obtained.

In summary, the following parameters must be considered:

- reduction per pass
- total strain
- Mg-content
- rolling temperature
- reheating time between passes.

The first three result in increased dislocation density as any or all increase in value. As any of the first three are increased then either or both of the latter parameters must also be increased to an extent sufficient to facilitate recovery of dislocations to subboundaries stabilized by the intermetallic β precipitates. Finally, it must be kept in mind that these considerations apply only insofar as the alloy composition and the rolling temperature fall within Region IV on Figure 2.8.

B REDUCTION PER PASS — 1mm

ROLLING PASS

4 MIN REHEATING

MISORIENTATION INCREASES AT A SLOWER RATE

PRECIPITATION

RECOVERY TO WALLS

HEATING FOR ELEVATED TEMPERATURE TESTING

AFTER MANY PASSES THE MISORIENTATION INCREASES AND THE NUMBER OF DISLOCATIONS PER UNIT LENGTH INCREASE

THE FINAL STRUCTURE HAS SUBGRAINS OF SUFFICIENT SIZE AND MISORIENTATION FOR CONTINUOUS RECRYSTALIZATION

Figure 7.5. With smaller reduction per pass, fewer dislocations are generated on each pass and more recovery time is available as more passes are required to complete the rolling. A shorter reheating interval may therefore be sufficient to attain a superplastic response.

137
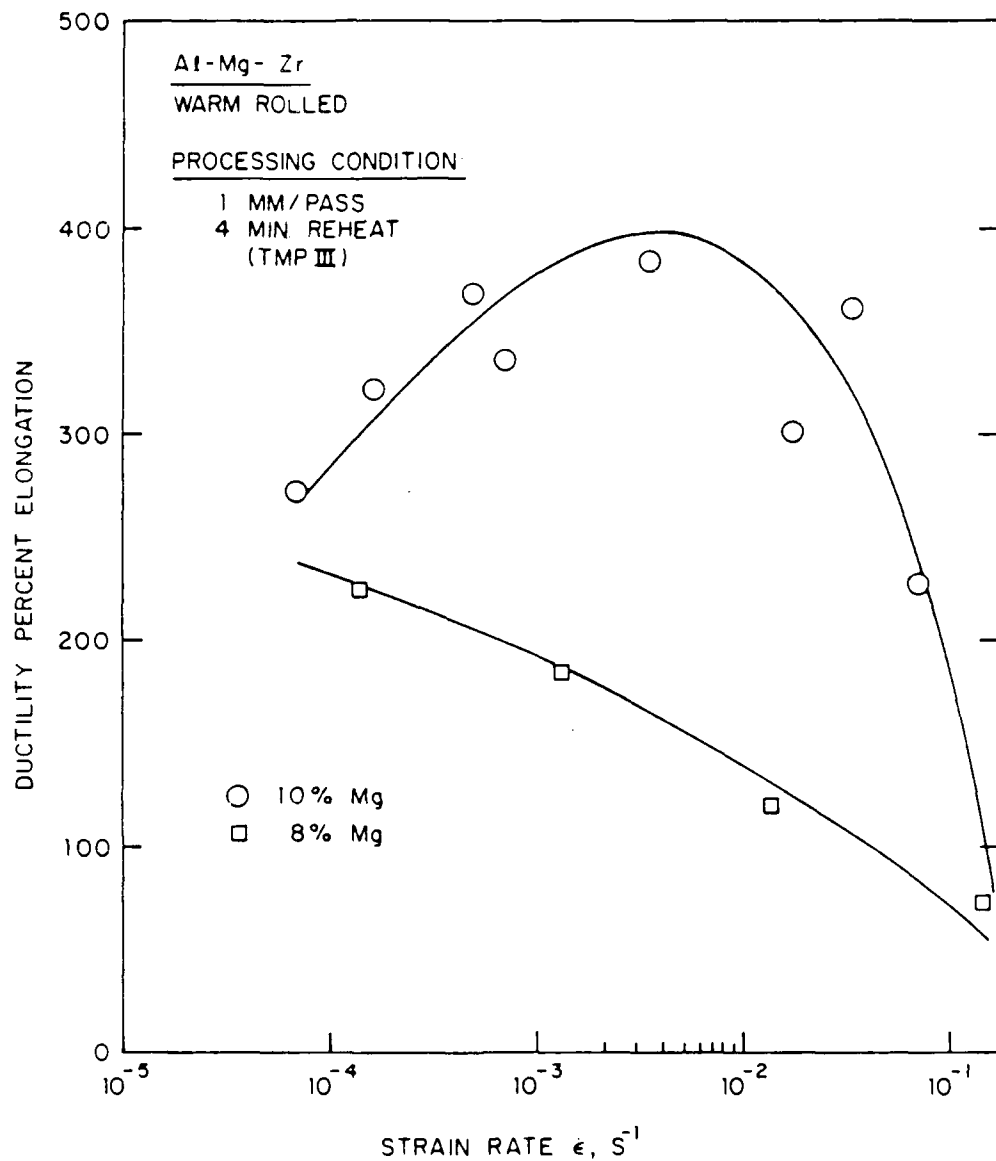
Figure 7.6. Ductility in percent elongation versus strain rate for Al-10%Mg-0.1%Zr and Al-8%Mg-0.1%Zr under TMP III processing conditions. Al-10%Mg-0.1%Zr shows higher ductility.

138
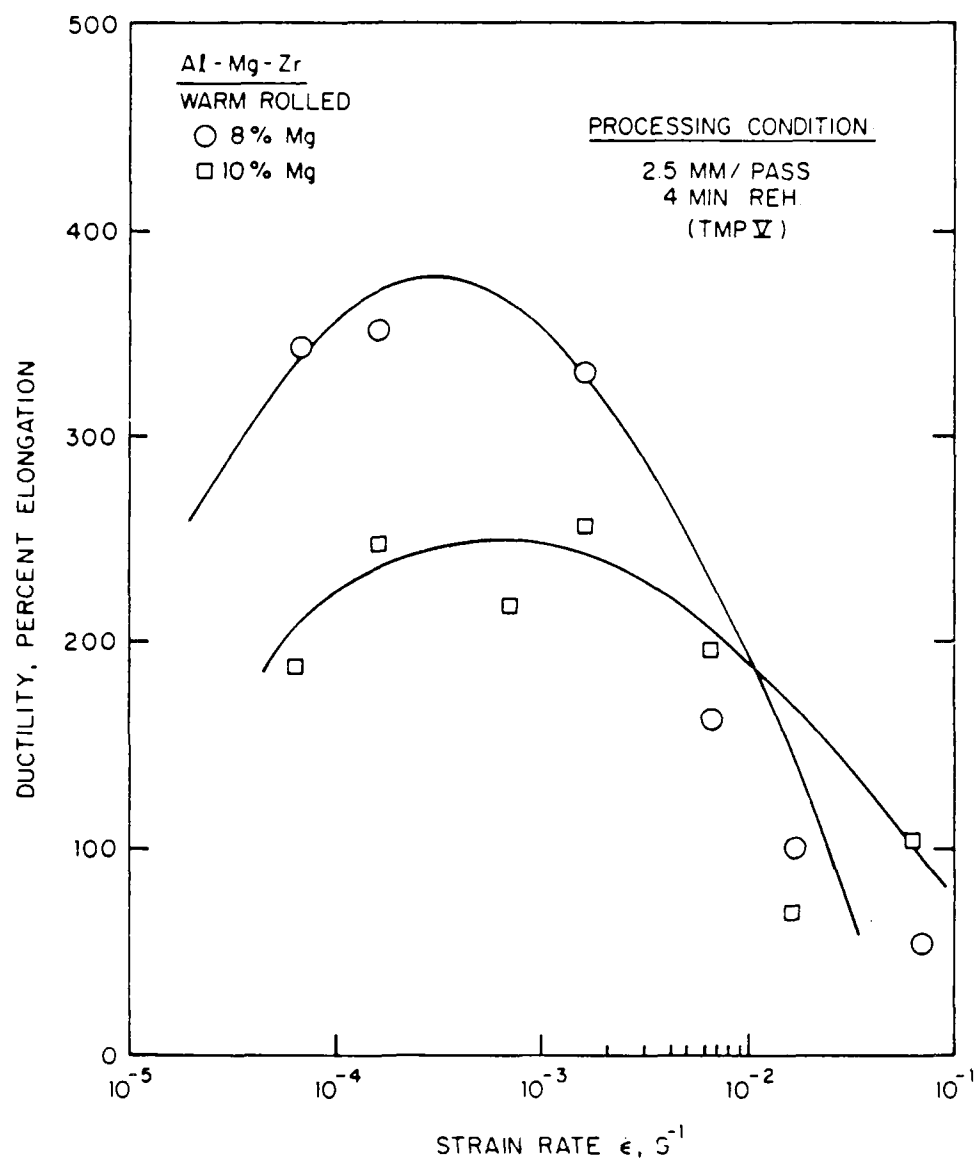
Figure 7.7. Ductility in percent elongation versus strain rate for Al-10%Mg-0.1%Zr and Al-8%Mg-0.1%Zr under TMP IV processing condition. Al-8%Mg-0.1%Zr shows higher ductility.

139

VIII. APPLICATION TO DEVELOPMENT AND ASSESSMENT OF SUPERPLASTIC ALUMINUM ALLOYS

The concepts developed in this research are used for assessment and to consider development of other superplastic Al alloys. Two types of superplastic materials are chosen, one which shows superplasticity at high temperatures, and the second at low temperatures.

A. ALUMINUM ALLOYS EXHIBITING SUPERPLASTICITY AT HIGH TEMPERATURES

1. Al-5% Mg-1.2% Cr

A fine grained (3μm grain size) Al-5% Mg - 1.2% Cr alloy was developed by Shin, et al., (1985) through a powder-metallurgy, thermomechanical processing route. The fine grain size was obtained by discontinuous recrystallization before superplastic deformation at 520°C. The tensile and superplastic properties of this material were evaluated in the homologous temperature range of 0.75 to 0.98 Tm (370°C–550°C). The data obtained by tensile testing at five temperatures over four orders of magnitude of strain rate (10^{-4} to 1 S^{-1}) at each test temperature are shown in Figure 8.1. Several points are apparent. The superplastic behavior of this material starts at a low modulus compensated stress value compared to the continuously recrystallized superplastic Al-10%Mg-0.1%Zr alloy. Also, the material shows superplastic response at higher temperatures than the Al-10%Mg-0.1%Zr alloy. The material shows a threshold stress and the value of the threshold stress is seen to vary with temperatures, decreasing in magnitude with increase in temperature. At high modulus compensated stress values, the behavior of this fine grain material is identical to that observed in Al-Mg solid solution alloys, namely, that of a class I solid solution alloy.

140

The m value for this material in the superplastic range is larger than that for low-temperature superplastic materials and does not show the anomalous temperature dependence of the strength and ductility. This likely is because the structure retains its stability over the whole test temperature range. At the highest test temperature (550°C) the deformation rates of this material are as high as those observed in pure aluminum. The rate, however, does not exceed that for pure aluminum. At stresses where the creep rate of fine-grained material and of pure aluminum are equal, the creep rate diminishes rapidly, decreasing with stress and resulting in a region of high stress exponent. At stresses below this, the behavior coincides with that of class I solid solution alloys.

The activation energy was measured at different $\frac{\sigma}{E}$ values. Shin, et al., (1985) have reported the value of Q where $n = 2$ to be about 135–139KJ/mole. This is essentially equal to the activation energy for lattice diffusion of aluminum in aluminum, Q 140KJ/mole. Grain boundary sliding with lattice diffusion control is likely the dominant deformation mechanism.

They reported the value of Q at low stresses equal to 180 KJ/mole, a value which is higher than that for lattice self diffusion. They mentioned that, although the origin of this high value of Q is not known, it has also been observed in a class I solid solution alloy (Al-1% Mg) at low stresses where dislocation climb is believed to be the rate controlling process. As shown in Figure 8.2, the activation energy curves are continuous at low $\frac{\sigma}{E}$ values, while at high $\frac{\sigma}{E}$ there is a change in the slope of the log $\dot{\epsilon}$ vs. $\frac{1}{T}$ curves. This discontinuity suggests the high value of activation energy measured by Shin, et al., to be a result of a threshold stress.

2. Al-6Mg - 0.37Zr

This material was developed by Matsuki et al., (1976). After cold working and recrystallization the material has a grain size $\approx 7.6\mu$m. Tensile testing was carried out at high temperatures 400 - 500°C. The stress versus strain rate data were analyzed and the results are shown in Figure 8.3. The following can be predicted seen in the data. The material starts to exhibit superplasticity at lower $\frac{\sigma}{E}$ values than for the low temperature superplastic materials of this research and also below the material developed by Shin, et al. The slope of the curve for this fine

141

Figure 8.1. Modulus-compensated stress versus diffusion-compensated strain rate for the data of Shin, et al., (1985).

grained material is equal to 2; the m value is greater than for any other material tested. This is an indication that the material has a high stability and low rate of grain growth during superplastic deformation.

The material also shows a threshold stress which is temperature dependent and decreases as the temperature increases. The deformation rates are less than for pure Al for all temperature below 520°C. The data for 520°C was found to cross the curve for pure Al. At this very low stress, the subgrain size in pure Al may become larger than the grain size of this fine- grained material since the subgrain size increases as stress decreases. Activation energy is equal to that for lattice self diffusion of aluminum.

3. Aluminum Alloy 7475

A commercial aluminum alloy, 7475, was processed to achieve fine grain size. The material was tested at temperatures from 437°C to 516°C. The stress versus strain rate data were analyzed and the results are shown in Figure 8.4. The material tested at high temperature also shows show a deformation rate greater than pure Al at low stress. This trend is similar to the behavior shown by Al-6% Mg-0.37%Zr, alloy investigated by Matsuki et. al., (1976).

4. Al-6.3%Mg-0.5%Mn

Al-6.3%Mg-0.5% Mn was developed by Valiyev, et al., (1981). Superplastic flow was observed in this alloy at 420°C, when the initial grain size obtained after cold rolling followed by recrystallization was $\approx 5\mu$m. Their data were analyzed and the results are shown in figure (8.5). The data coincide with the data for the Al-10%Mg-0.52%Mn in the recrystallized condition. This indicates that the two materials have a similar structural state. The material also shows a threshold stress at low stress values. The stress value at which the superplastic behavior starts is higher than that given for the high temperature superplastic materials developed by Shin, et al., (1985) and by Matsuki et al., (1976) but lower than given for the lower temperature superplastic material of this research. The material shows an m value of about 0.4 which is typical value for materials showing superplasticity in this temperature range.

143

STRAIN RATE $\dot{\epsilon}$, s^{-1}

10^0

10^{-1}

10^{-2}

10^{-3}

10^{-4}

10^{-5}

Al – 6 Mg.– 1.2 Cr ALLOY
RECRYSTALLIZED

$\frac{\sigma}{E} =$

○ 1×10^{-3}
□ 8×10^{-4}
▲ 6×10^{-4}
◔ 4×10^{-4}
● 2.75×10^{-4}
▽ 2×10^{-4}
◇ 1.5×10^{-4}
△ 1×10^{-4}
● 6×10^{-5}
■ 4×10^{-5}

1.2   1.3   1.4   1.5   1.6

$\frac{1}{T} \times 10^{-3}$
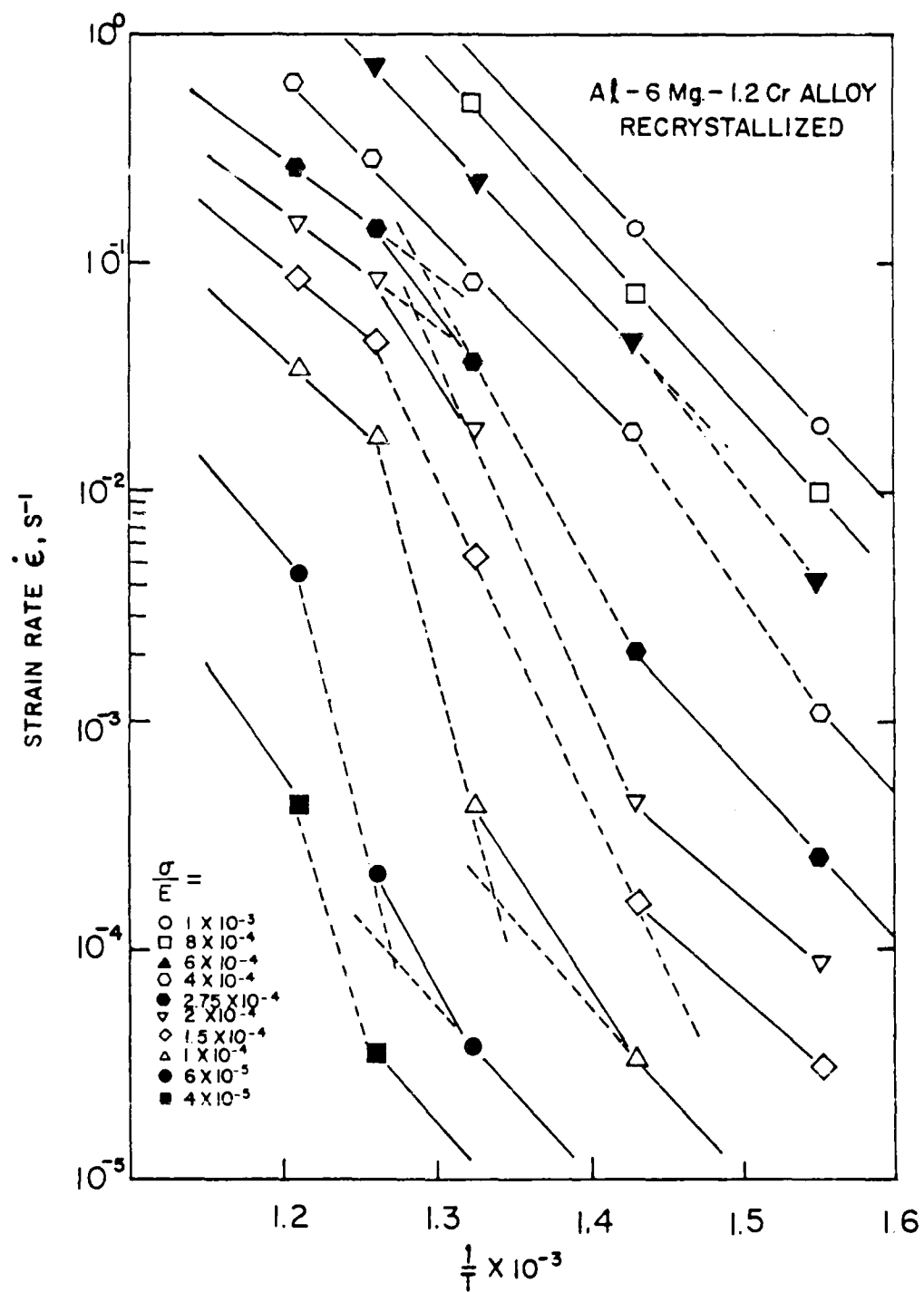
Figure 8.2.   Activation energy data reported by Shin, et al., (1985).

144
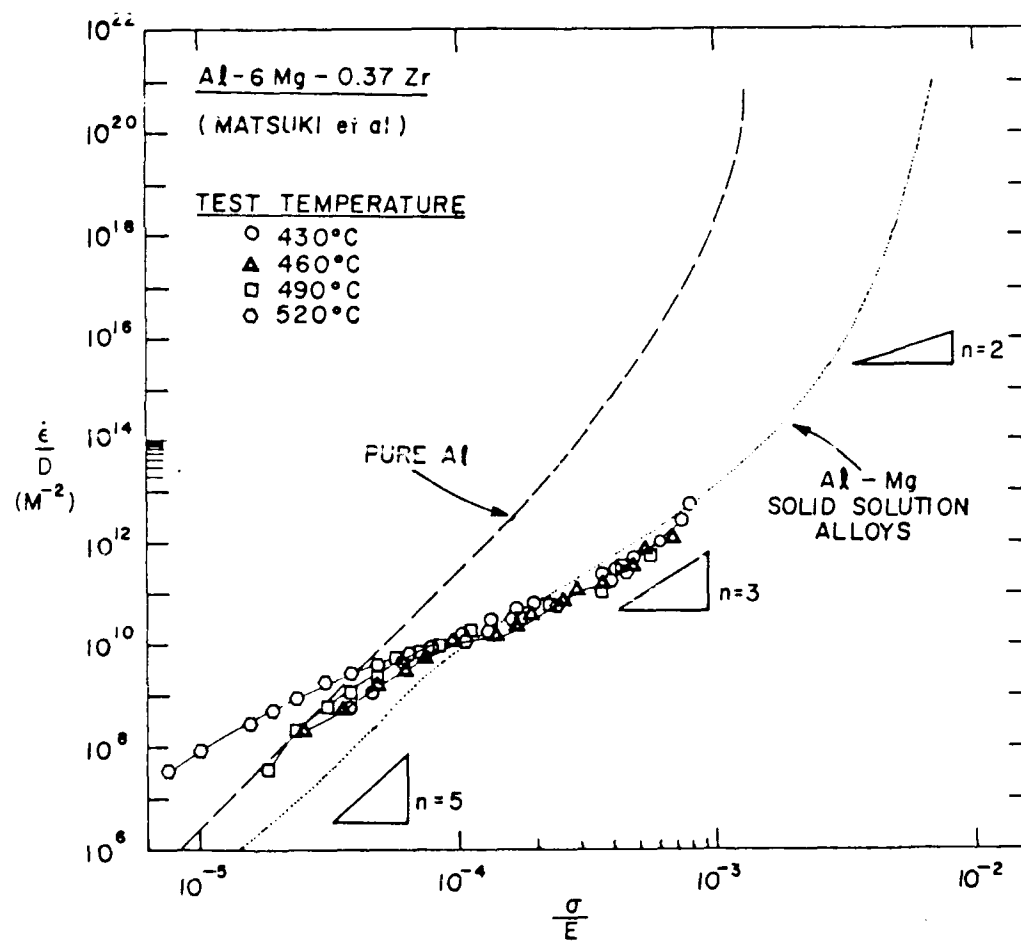
Figure 8.3. Modulus-compensated stress versus diffusion-compensated strain rate for the data of Matsuki, et al., (1976).

145
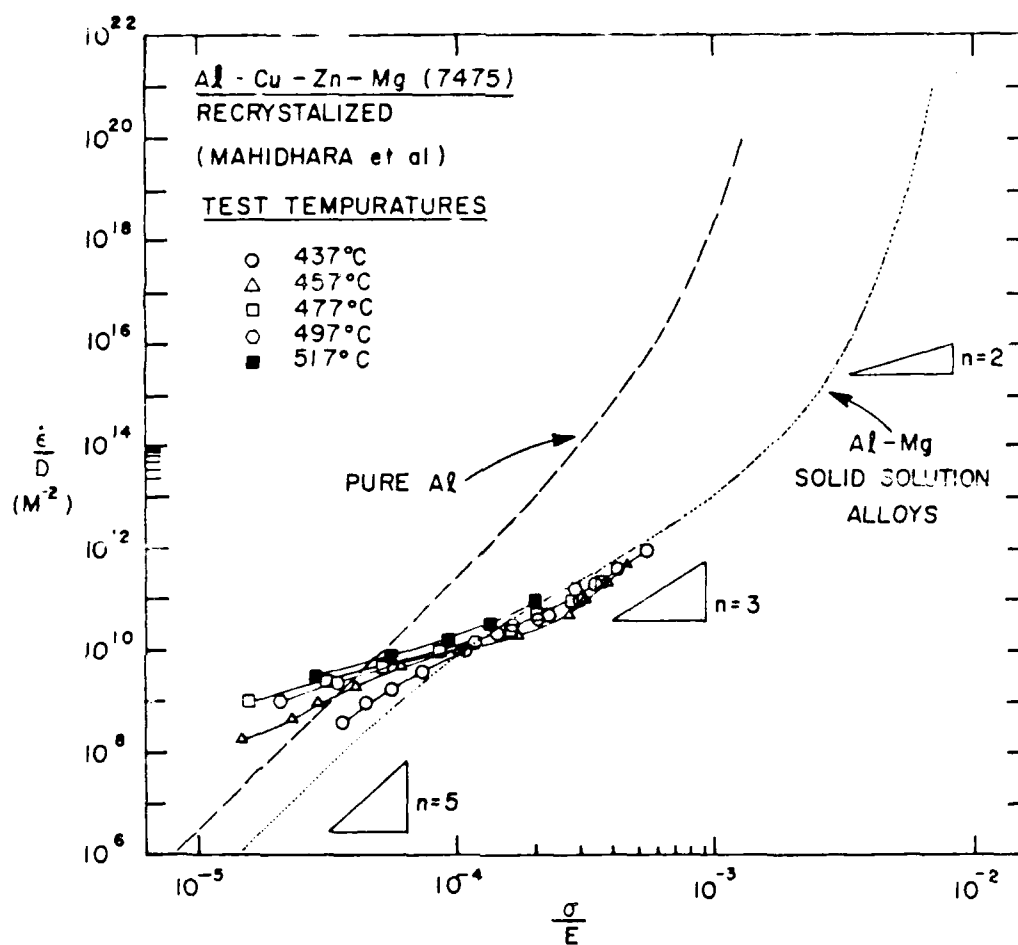
Figure 8.4. Modulus-compensated stress versus diffusion-compensated strain rate for the data of Mahidhara et al., (1986)

146
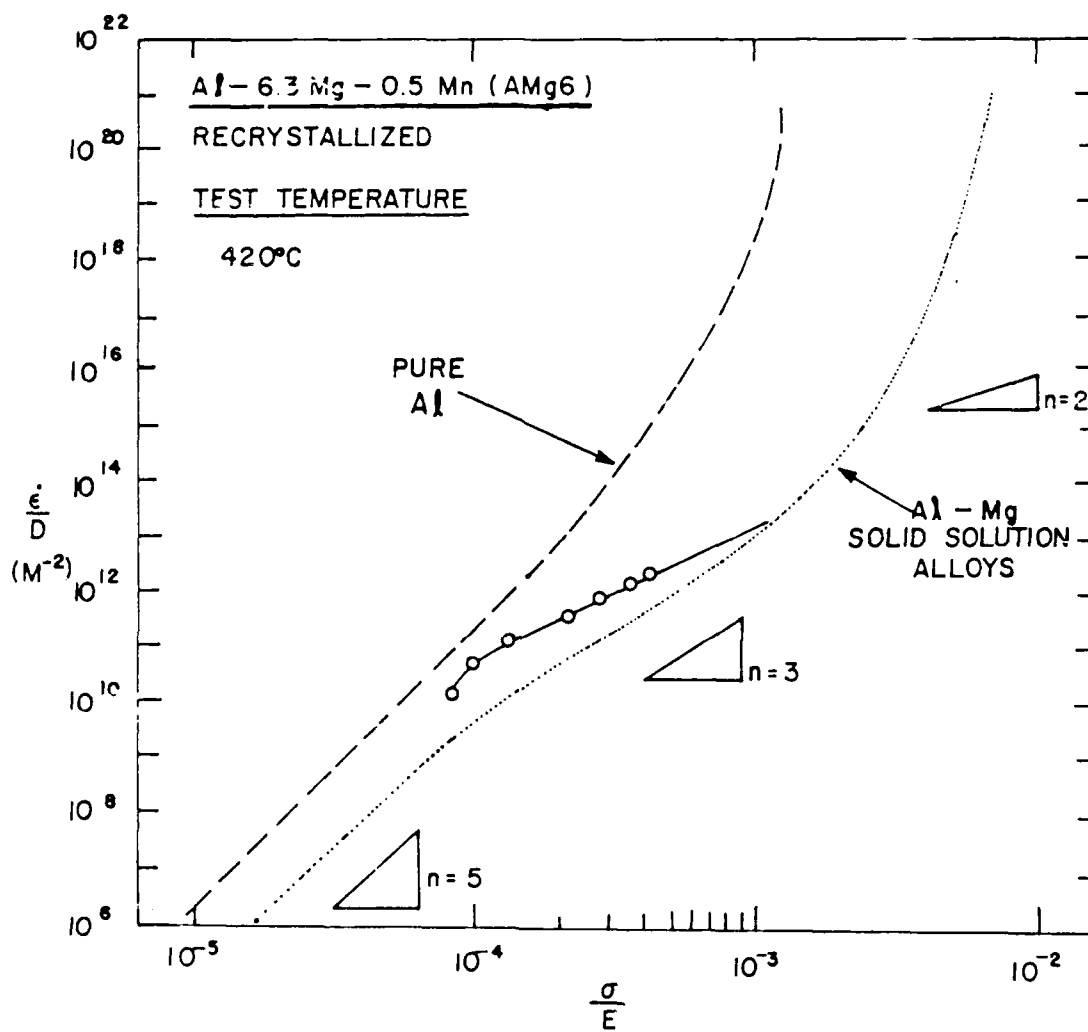
Figure 8.5. Modulus-compensated stress versus diffusion compensated rate for the data of Valiyev, et al., (1981).

B. AN ALUMINUM ALLOY EXHIBITING LOW TEMPERATURE SUPERPLASTIC BEHAVIOR.

Data for an alloy exhibiting relatively low temperature superplastic behavior was analyzed. This was Al-67%Mg-1.6%Li developed by Zhang and Grand (1984). Very fine grain sizes resulting from rapid solidification resulted in superplastic deformation. The Al-6.7%Mg-1.6%Li alloy exhibits superplastic behavior at temperatures near 325°C (Figure 8.6). An elongation of 182% was achieved for strain rates of about $10^{-2} S^{-1}$. The material was tested at temperatures 300°C, 325°C, and 350°C. The m value is about 0.4. The curves of log stress versus log strain rate at various temperatures are straight over the entire range of strain rates, confirming the presence of a stable grain size. A transmission electron micrograph for the Al-6.7%Mg-1.6%Li alloy in the aged condition shows that the average grain size is about 2μm, with Mg_2Al_3 precipitates less than 0.1 μm in diameter. This material does not show very high ductility, however, the material shows superplastic behavior under the same conditions as 10%Mg- 0.1%Zr alloy. Also, the material does not show microstructure instability in this temperature range but has an m value of ≈ 0.35 and no threshold stress. It is noteworthy that microstructures as fine as those attained in the wrought alloys of the research by continuous recrystallization have only been attained by powder methods elsewhere. Then, ductilities are much less than attainable by the methods developed here.

C. DISCUSSION OF HIGH AND LOW TEMPERATURE SUPERPLASTIC BEHAVIOR

Following Sherby and Wadsworth (1982), two independent processes contribute to the superplastic flow. The first grain boundary sliding accommodated by slip in the mantle region; the second is slip in the core region. These are two independent processes and thus the fastest controls deformation. Superplastic response is expected when mantle processes dominate. Conditions which facilitate mantle deformation and at the same time slip in the core region more difficult, if possible, will lead to superplasticity at high strain rates. The principal microstructural feature which influences superplasticity is the grain size. Superplastic flow is enhanced with a decrease in grain size. Fine grain size shifts the transition from
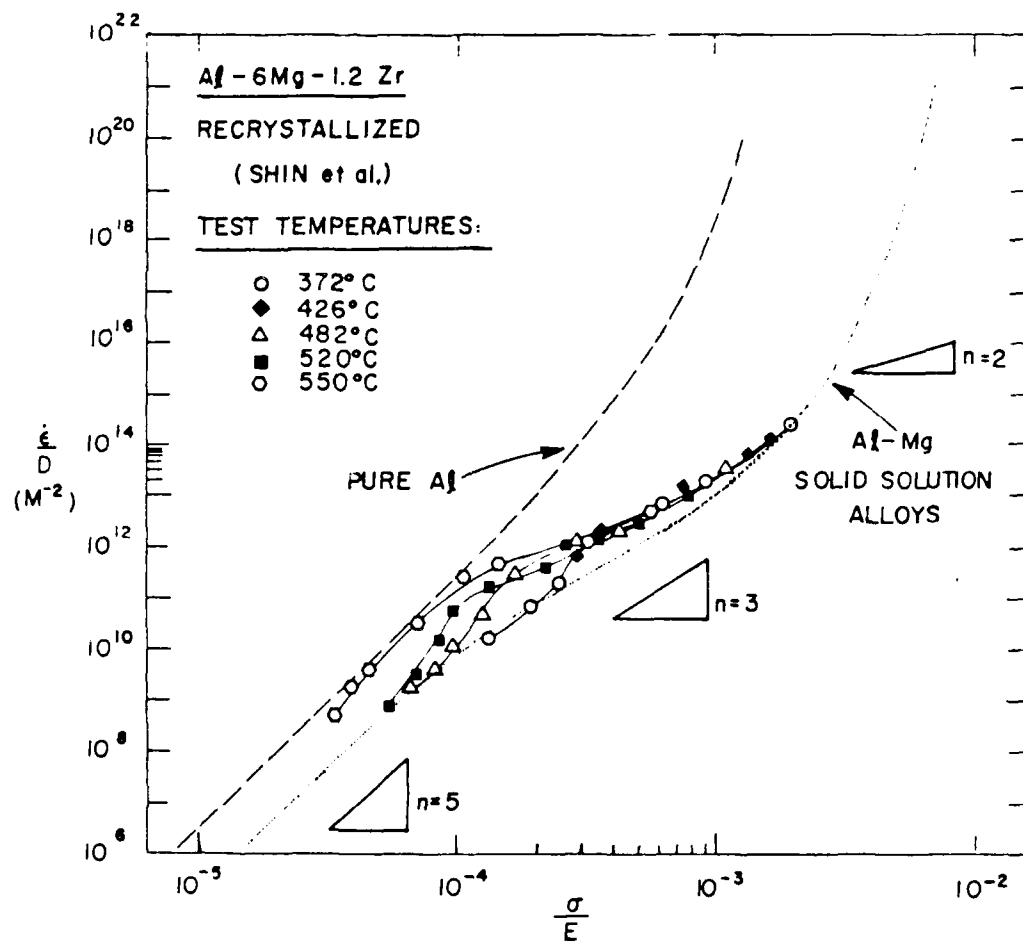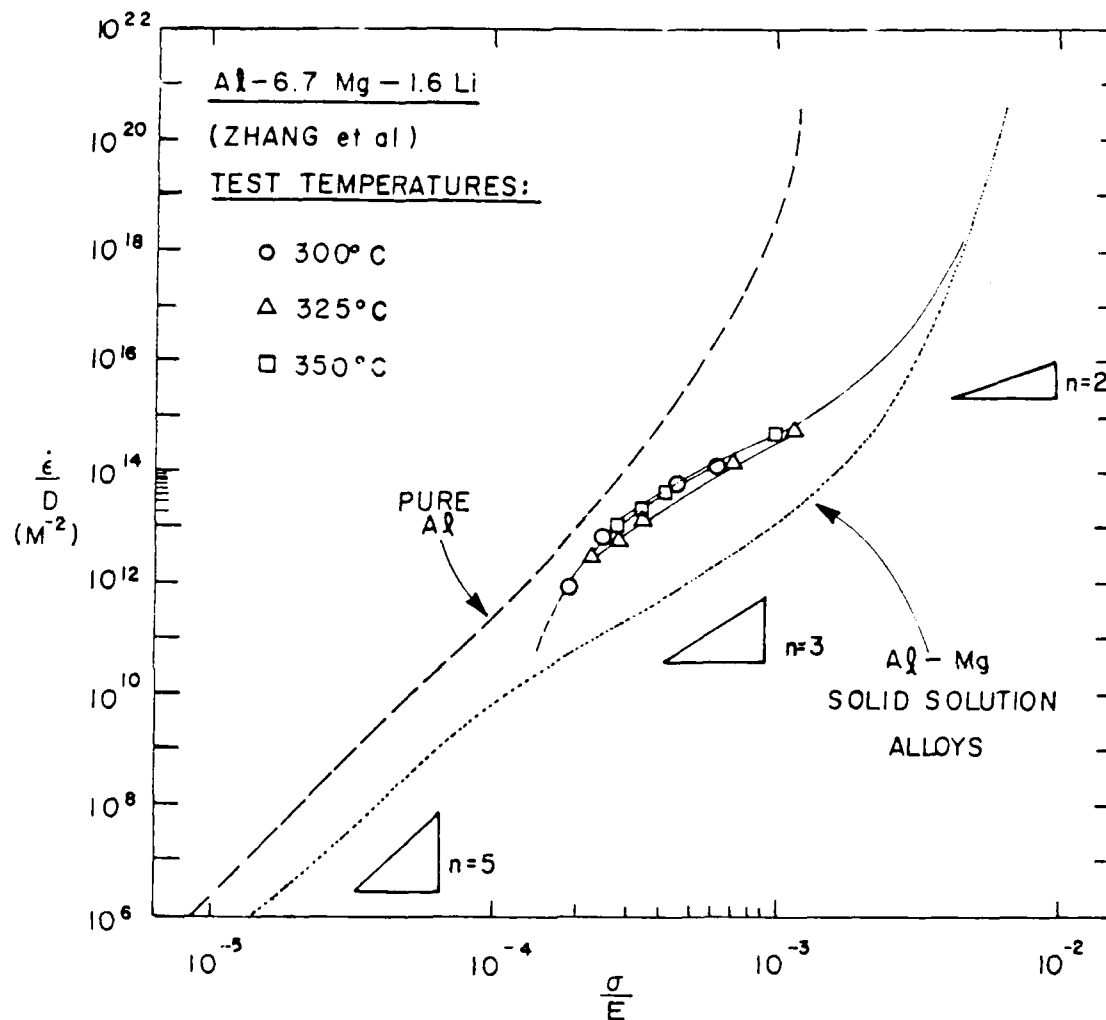
Figure 8.6. Modulus-compensated stress versus diffusion-compensated strain rate for the data of Zhang, et al., (1984).

149

dislocation creep to superplastic flow to higher strain rates. According to Gifkins (1976), for fine grain size and a fixed mantle width, the mantle region will dominate. According to Arieli and Mukherjee (1980), the width of both the core and mantle change with grain size. They assumed that the width of the mantle zone is yd where y is a constant and d is the grain size. The dislocation density in the mantle region is a function of strain rate it increases with strain rate.

The accommodation process (slip) in the mantle depends on the availability of dislocations in this region. Any factor which obstructs the dislocations in the mantle will slow the accommodation process, and hence diminish the superplasticity. Slip is grain size independent. All fine-grained superplastic materials likely deform by the same slip processes as coarse grain material, while each has a characteristic superplastic response depending on structure. This is evidence that the core deformation does not change much with grain size while the mantle deformation is affected by changing the structure (grain size, particle volume fraction, type and size).

If the material contains a large amount of stable dispersoid which can effectively pin dislocations in the mantle regions, the accommodation process may be diminished seriously and the grain boundary sliding and superplasticity shifted to a lower strain rate and higher temperature. The low temperature and high strain rate superplasticity shown by fine-grained Al-Mg alloys is achieved because first, a very fine structure of the order of 1–3 μm evolves by a continuous recrystallization process. Second, a limited amount of particles, just sufficient to keep the structure stable in the temperature range for superplastic deformation but not so high to pin the dislocation in the mantle region is present. Finally, the intermetallic β, important in establishing the fine grain size, is also able to deform with them.

In the deformation of fine-grained materials, for a given temperature there is a range of strain rate in which superplastic flow by grain boundary sliding is expected. When the strain rate increases above this limit, normal dislocation deformation (slip creep) takes place, and for strain rates below the lower limit, superplasticity is also lost. In terms of the core and mantle model, when the strain rate increases, the dislocation density increases in the mantle region and in the grain interior as well.

Some of these lattice dislocations arrive at the mantle, climb to the boundary and participate in the accommodation process. Thus the accommodation process and the grain boundary sliding go on unrestricted. Increasing the strain rate further, more sources are activated in the grain interior, increasing the dislocation density in the grain interior, and the number of dislocations arriving in the mantle region increases. When strain rate reaches a certain value, and the dislocation density increases in the mantle area, the back stress of these dislocations makes it more difficult for dislocation in the mantle region to climb into boundary sinks. The climb of dislocations inside the grain cores become the rate-controlling step. This climb is controlled by lattice diffusion and the normal dislocation creep starts to be the dominant deformation mechanism.

At low strain rates, the equilibrium dislocation density in the mantle region becomes low. Below a certain value, the accommodation process becomes restricted and the grain boundary sliding cannot proceed. Hence superplasticity will be diminished. Increasing the temperature will move the equilibrium dislocation density in the mantle region to a higher value and, at the same time, more dislocations arrive from the grain interior and help in the accommodation process. Thus grain boundary sliding and superplasticity can extend to a lower strain rate. Fine grained Al-Mg alloys superplastically deformed at 300°C do not show a threshold stress. This likely is related to the relatively high strain rate at which this material is deformed; the equilibrium dislocation density in the mantle region will be high, the accommodation process and the grain boundary sliding will go unobstructed.

Ruano, et al., (1981), showed that the fine-grained Pb-Cd alloy studied by Alden (1968), the fine-grained copper base alloy and the austenitic stainless steel investigated by Shei and Langdon (1978) show pipe diffusion controlled grain boundary sliding. They indicated that the pipe diffusion may control the creep rate at intermediate stresses and temperatures. This study of fine- grained, Al-Mg alloys has shown that grain boundary sliding starts at a high modulus-compensated stress in the power law breakdown range. Comparison to data given by Alden (1968), Shei and Langdon (1978) and by Ruano, et al., (1981), reveals these materials show the same trend, and that grain boundary sliding with pipe diffusion control starts

151

in the power law region when $n \geq 7$. Thus, the behavior of the Al-Mg alloys may in fact be pipe diffusion controlled for $\dot{\epsilon} \simeq 10^{16} m^{-2}$ (Chapter IV).

To summarize, grain boundary sliding and hence the superplastic deformation starts at high stresses in low temperature superplastic materials. The transition from slip to grain boundary sliding occurs at high stress. This is due to the limited amount of dispersoid, which is just sufficient to ensure the stability of the structure, but not so high that it inhibits grain boundary sliding at high stress. These materials have very fine grain sizes, evolved by continuous recrystallization processes, a large volume fraction of very stable and fine dispersoids would be needed which may then inhibit grain boundary sliding. Through continuous recrystallization processes it is possible to get a very fine grain size 1-2μm with a small volume fraction of fine particles and thus move the transition between slip and grain boundary sliding to high stress and strain rate.

IX. SUMMARY AND CONCLUSION

The superplastic behavior of high Mg, Al-Mg alloys can be understood using a phenomenological model relating diffusion-compensated strain rate to modulus-compensated stress. This relation was originally proposed by Sherby and Wadsworth (1982). At high stress, the behavior is identical to the creep behavior of coarse grained Al-Mg solid solutions where dislocation climb is the deformation controlling mechanism.

The warm-rolled material becomes fine grained by a continuous recrystallization mechanism at relatively low temperatures (0.58 - 0.64 T_M) leading to evolution of a very fine grain structure of the order of 1 - 2 μm grain size. Garofalo's (1963) hyperbolic type relation can be used to describe the creep behavior of coarse grained Al-Mg solid solutions over both dislocation glide and power law breakdown regions.

The warm-rolled, fine-grained material shows microstructural instability at about $325^{\circ}C$, where the balance between the very fine grains evolved by continuous recrystallization and the stabilizing β particles is disturbed and grain growth or discontinuous recrystallization takes place. The material may either loose superplasticity completely as in Al-10%Mg-0.1%Zr alloy or it may continue to show superplasticity at high temperatures as in Al-10%Mg-0.52%Mn depending on the ultimate grain size reached after the secondary recrystallization process. The phenomenon of microstructure instability shown by this material does not occur so markedly in eutectic or eutectoid materials where the stabilizing phase remains to the melting point or in materials in which the fine grain structure is evolved by a discontinuous recrystallization process before starting the superplastic deformation.

The microstructure instability and grain growth causes a change in the stress versus strain rate response and anomalous behavior in the activation energy data. The annealed and recrystallized material does not show the anomalous behavior exhibited by the warm rolled materials because the mircrostructures are stable in the range of temperatures examined.

The superplastic behavior of the fine grained Al-Mg alloys can be controlled by changing the thermomechanical processing variables, namely, the total strain, the reduction per pass, the reheating time between passes, the rolling temperature and the alloy content, i.e. Mg. Increasing the total strain, the reduction per pass and the Mg content as well as warm rolling at relatively low temperature and increasing the reheating time between rolling passes will enhance the superplastic response.

A physical model based on the recovery and annihilation of individual dislocations during rolling passes, reheating time between passes, cooling after rolling and heating for superplastic deformation can be used to describe the microstructural evolution and the effect of thermomechanical processing variables on resultant superplastic response. According to this model, the microstructure evolution occurs throughout the rolling by individual dislocations recovering into subboundaries, increasing the boundary misorientations and leading to well-defined boundaries able to sustain grain boundary sliding. According to this model, thermomechanical processes which lead to generation of more dislocations (large total strain, large reduction per pass, low warm rolling temperature and high Mg content) at the same time giving these dislocations sufficient time for recovery, will lead to subboundaries having enough dislocations per unit length and thus sufficient misorientations constitute continuous recrystallization to a very fine grain structure able to sustain grain boundary sliding.

The results of this investigation can also be applied to assessment and to development of new superplastic materials and to study the behavior of fine grained materials in conjunction with the creep behavior of pure metals and of coarse grained solid solutions alloy.

154

REFERENCES

Ahlborn, H., Hornbogen, E. and Köster, U., *J. Mat. Sci.*, Vol. 4, pp. 944-950, 1969.

Alcamo, M. E., "Effect of Strain Rate on the Microstructure of a Superplastically Deformed Al-10% Mg-0.1% Zr Alloy", Master's Thesis, Naval Postgraduate School, Monterey, CA, June 1985.

Alden, T. H., Treatise on Materials Science and Technology, Vol. 6, edited by R. J. Arsenault, p. 225, *Academic Press*, New York, 1975.

Alden, T. H., Fundamental Aspects of Structural Alloy Design, edited by R. T. Jaffee and B. A. Wilcox, p. 411, Plenum Press, 1977.

Alden, T. H., *J. Aust. Inst. Metals*, Vol. 14, pp. 207-216, 1969.

Alden, T. H., and Schadler, H. W., *Trans. A.I.M.E.*, Vol. 242, p. 825, 1968.

Alden, T. H., *Acta. Met.*, Vol. 15, pp. 469-480, 1967.

Alden, T. H., *Trans. A.I.M.E.*, Vol. 236, pp. 1633-1634, 1966.

Arieli, A., and Mukherjee, A. K., *Mat. Sci. Eng.*, Vol. 45, pp. 61-70, 1980.

Ashbey, M. F., and Verrall, R. A., *Acta. Met.*, Vol. 21, pp. 149-163, 1973.

Avery, D. H., and Backofen, W. A., *Trans. Quart. A.S.M.*, Vol. 58, p. 359, 1966.

Avery, D. H., and Backofen, W. A., *Trans. Quart. A.S.M.*, Vol. 58, p. 551, 1965.

Backofen, W. A., Murty, G. S., and Zehr, S. W., *Trans. A.I.M.E.*, Vol 242, p. 329, 1968.

Backofen, W. A., and Zehr, S. W., *Trans. A.S.M.*, Vol.61., p. 300, 1968.

Backofen, W. A., and Lee, D., *Trans. A.I.M.E.*, Vol. 239, p. 1034, 1967.

Backofen, W. A., Turner, I. R., and Avery, D. H. *Trans. A.S.M. Quart.*, Vol. 57, pp. 981-989, 1964.

Ball, A., and Hutchinson, M. M., *J. Met. Sci.*, Vol. 3, pp. 1-6, 1969.

Barrett, C. R., Muchleisen, E. C., and Nix, W. D., *Mat. Sci. Eng.*, Vol. 10, p. 33, 1972.

Beck, P. A., *J. Appl. Phys.*, Vol. 20, p. 637, 1949.

Bengough, G. D., *J. Inst. Metals*, Vol. 7, p. 123, 1912.

Bird, J. E., Mukherjee, A. K., and Dorh, J. E., Quantitative Relations Between Properties and Microstructure, pp. 255-342, *Israel Univ. Press*, Jerusalem, 1969.

Bochvar, A. A., and Sviderskaya, Z. A., *Izvest. Akad, Nauk SSSR, Ordel Tekhn. Nauk*, Vol. 9, p. 821, 1945.

P-i-knell, R. H., and Edington, J. W., *Met. Trans.*, Vol. 10A, pp. 1257-1263, 1979.

Cahn, R. W., *Proc. Phys. Soc.*, Vol. 60A, p. 323, 1950.

Cahoon, J. R., *Met. Sci.*, Vol. 9, p. 346, 1975.

Csnnon, W. R., and Sherby, O. D., *Metall. Trans. I*, p. 1030, 1970.

Clark, M. A., and Alden, T. H., *Acta. Met.*, Vol. 21, p. 1195, 1973.

Cline, H. E., and Alden, T. H., *Trans. A.I.M.E.*, Vol. 239, p. 710, 1967.

Cotner, J. R., and Tegart, W. J., *J. Inst. Metals*, Vol. 97, pp. 73-79, 1969.

Cottrell, A. H., and Jaswon, M. A., *Proc. R. Soc.*, Vol. A199, p. 104, 1949.

Darekar, Y. S., and Chaudhari, R. D., *Trans. Indian Inst. Met.*, Vol. 23, p. 56, 1970.

Darken, L. S., *Trans. A.I.M.E.*, Vol. 175, p. 184, 1949.

Davies, G. J., Edington, J. W., Cutler, C. P., and Padmanabhan, K. A., *J. Mat. Sci.*, Vol. 5, pp. 1091-1092, 1970.

Doherty, R. D., "Nucleation", Recrystallization of Metallic Materials, 2nd Edition, F. Haessner (ed.), pp. 23-61, *Riederer-Verlag*, Stuttgart, 1978.

Edington, J. W., *Metals Technol.*, Vol. 3, p. 138, 1976.

156

Edington, J. W., Melton, K. N., and Cutler, C. P., *Prog. Mat. Sci.*, Vol. 21, p. 61, 1976.

Exell, S. E., and Warrington, D. H., *Philos. Mag.*, Vol. 26, p. 1121, 1972.

Friedel, J., <u>Dislocations</u>, *Pergamon Press*, 1964.

Fujita, H., *J. Phys. Soc.*, Vol. 16, p. 397, Japan, 1961.

Fulop and McQueen, H. J., <u>Super Alloys Processing</u>, pp. H1-H21, *Metals-Ceramics Information Center*, Columbus, 1972.

Gardner, K. J., and Grime, R., *Met. Sci.*, Vol. 13, p. 216, 1979.

Garofalo, F., *Trans. Met. Sci. A.I.M.E.*, Vol. 227, pp. 351- 356, 1963.

Giami, A. F., Anton, D. I., and Dairon, R. E., <u>Superplastic Forming of Structural Alloys</u>, edited by N. E. Paton and C. F. Hamilton, *AINE*, Warrendale, PA, 1982.

Gifkins, R. C., *Met. Trans. A.*, Vol. 7A, p. 1225, 1976.

Gittus, J., <u>Creep Viscoelasticity and Creep Fracture in Solids</u>, p. 509, *Applied Science Publishers, Ltd.*, London, 1975.

Griffith, P., and Hammond, C., *Acta. Met.*, Vol. 20, p. 935, 1972.

Grimes, R., Baker, C., Stowell, M. J., and Watts, B. M., *Aluminum*, Vol. 51, pp. 720-723, 1975.

Grimes, R., Stowell, M. J., and Watts, B. M., *Metals Technol.*, Vol. 3, pp. 154-160, 1976.

Haessner, F. (ed.), <u>Recrystallization of Metallic Materials</u>, 2nd Edition, p. 1, *Riederer-Verlag*, Stuttgart, 1978.

Hales, S. J., and McNelley, T. R., *Acta. Metall.*, in press.

Hamilton, C. H., Bampton, C. C., and Paton, N. E., <u>Superplastic Forming of Structural Alloys</u>, edited by N. E. Paton and C. H. Hamilton, p. 173, *The Metallurgical Society of AIME*, 1982.

Hammond, C. H., <u>Superplastic Forming of Structural Alloys</u>, edited by N. E. Paton and C. H. Hamilton, *AIME*, Warrendale, PA, 1982.

Harper, J. G., and Dorn, J. E., *Acta. Met.*, Vol. 5, p. 654, 1957.

Hart, E., *Acta. Met.*, Vol. 5, p. 597, 1957.

Hartmann, T. S., "Mechanical Characteristics of a Superplastic Aluminum-10.2% Mg-0.1% Zr Alloy", Master's Thesis, Naval Postgraduate School, Monterey, CA, June 1985.

Hillert, M., *Acta. Met.*, Vol. 9, p. 825, 1965.

Holm, K., Embury, J. D., and Purdy, G. R., *Acta. Met.*, Vol. 25, p. 1191, 1977.

Holt, D. L., and Backofen, W. A., *Trans. A.S.M.*, Vol. 59, pp. 755-768, 1966.

Holt, D. L., *Trans. A.I.M.E.*, Vol. 242, p. 25, 1968.

Hornbogen, E., and Koster, U., Recrystallization of Metallic Materials, 2nd Edition, p. 159, F. Haessner (ed.), *Riederer-Verlag*, Stuttgart, 1978.

Hu, H., Recovery and Recrystallization of Metals, p. 311, L. Himmel (ed.), *John Wiley and Sons*, New York, 1963.

Ishikaw, H., Mohamed, F. A., and Langdon, T. G., *Phil. Mag.*, p. 1269, 1975.

Johnson, R. H., *Metall. Rev.*, Vol. 15, p. 115, 1970.

Johnson, W., Al-Naib, T. Y. M., and Duncan, J. L., *J. Inst. Metals*, Vol. 100, p. 45, 1972.

Jonas, J. J., "Superplastic Forming of Structural Alloys", edited by N. E. Paton and C. H. Hamilton, *Conf. Proc. A.I.M.E.*, p. 57, 1982.

Jonas, J. J., Sellars, C. M., and Tegart, W. J., *Met. Rev.*, Vol. 14, pp. 1-24, 1969.

Kaibyshev, O. A., Rodionov, B. V., and Valiev, R. Z., *Acta. Metall.*, Vol. 26, pp. 1877-1886, 1978.

Kashyap, B. P., and Mukherjee, A. K., Superplasticity, edited by B. Baudelet and M. Suery, p. 4.1, 1985.

Kayali, E. S., Sunada, H., Oyama, T., Wadsworth, J., Sherby, O. D., *J. Mat. Sci.*, Vol. 14, pp. 2688-2692, 1979.

King, H. W., *J. Mater. Sci.*, Vol 1, p. 79, 1966.

Köster, W., *Z. Metallk.*, Vol. 39, p. 1, 1948.

Lee, D., *Acta. Met.*, Vol. 17, p. 1057, 1969.

Lee, E. W., and McNelley, T. R., *Mat. Sci. Eng.*, Vol. 93, pp. 45-55, 1987.

Lee, E. W., McNelley, T. R., and Stengel, A. F., *Metall. Trans. A.*, Vol. 17A, p. 1043, 1986.

Li, J. C. M., Recrystallization, Grain Growth and Textures, H. Margolin (ed.), p. 45, *ASM*, Merals Park, OH, 1966.

Li, J. C. M., *Appl. Phys.*, Vol. 33C, p. 2958, 1962.

Lloyd, D. J., and Moore, D. M., Superplastic Forming of Structural Alloys, edited by N. E. Paton and C. H. Hamilton, *AINE*, Warrendale, PA, 1982.

Lozinsky, M. G., and Simeonova, I. S., *Acta. Met.*, Vol. 7, p. 709, 1959.

Lundy, T. S., and Murdock, J. F., *J. Appl. Phys.*, Vol. 33, p. 1671, 1962.

Luthy, H., Miller, A. K., and Sherby, O. D., *Acta. Met.*, Vol. 28, pp. 169-178, 1980.

Luton, M. J., and Jonas, J. J., *Can. Met. Quart.*, Vol. 11, pp. 79-90, 1972.

Mahidhara, K. R., and Mukherjee, A. K., *Mat. Sci. Eng.*, Vol. 80, pp. 181-193, 1986.

Marder, A. R., *Trans. Met. Soc. A.I.M.E.*, Vol. 245, p. 1337, 1969.

Martin, J. W., and Doherty, R. D., The Stability of Microstructure in Metals, *Cambridge University Press*, Cambridge, 1976.

Marya, S. K., and Wyon, G., *Proc. Fourth Int. Conf. Strength of Metals and Alloys*, Vol. 1, pp. 438-442, Nancy, France, 1976.

Matsuki, K., Morita, H., Yamada, M., and Murakami, Y., *Metal Sci.*, Vol. II, pp. 156-163, 1977.

Matsuki, K., Yeno, Y., Yamada, M., *J. Japan Inst. Metals*, Vol. 38, pp. 219-226, 1977.

Matsuki, K., Uetani, Y., Yamada, M., and Murakami, Y., *Met. Sci.*, Vol. 10, p. 235, 1976.

Matsuki, K., and Yamada, M., *J. Japan Inst. Metals*, Vol. 37, pp. 448-454, 1973.

McElroy, R. J., and Szkopiak, Z. C., *Int'l. Met. Rev.*, Vol. 17, pp. 175- 202, 1972.

McNelley, T. R., unpublished research, 1987

McNelley, T. R., Lee, E. W., and Mills, M. E., *Metall. Trans.*, Vol. 17A, p. 1035, 1986.

McNelley, T. R., and Garg, A., *Scripta Met.*, Vol. 18, p. 917, 1984.

McQueen, H. J., *Met. Trans. A.*, Vol. 8A, pp. 807-824, 1977.

McQueen, H. J., and Jonas, J. J., Treatise on Materials Science and Technology, Vol. 6, Plastic Deformation of Materials, pp. 393-493, *Academic Press*, New York, 1975.

McQueen, H. J., and J .. s, J. J., *Manufacturing Eng. Trans. (SME)*, Vol. 2, pp. 209-233, 1973.

McQueen, J. M., *Trans. Japan Inst. Metals*, Vol. 9, Supp. 1, pp. 170-177, 1968.

McQueen, H. J., Wong, W. A., and Jonas, J. J., *Can. J. Phys.*, Vol. 45, pp. 1225-1235, 1967.

Merrick, H. F., Superplastic Forming of Structural Alloys, edited by N. E. Paton and C. F. Hamilton, *A.I.M.E.*, Warrendale, PA, 1982.

Mohamed, F. A., and Ginter, T. J., *Acta. Met.*, Vol. 30, pp. 1869-1881, 1982.

Mohamed, F. A., and Langdon, T. G., *Acta. Metall.*, Vol. 22, p. 779, 1974.

Mohamed, F. A., Murty, K. L., and Morris, J. W., Jr., *Met. Trans. A.*, Vol. 4, p. 935, 1973.

Morris, J. G., *Mat. Sci. Eng.*, Vol. 13, pp. 101-108, 1974.

Morris, J. G., and Roopchand, B. J., *Proc. 4th Int. Conf. Strength Metals and Alloys*, Vol. 2, pp. 617-623, 1976.

Motohashi, Y., and Shibata, T., *Aluminum*, Vol. 58, p. 546, 1982.

Mukherjee, A. K., *Ann. Rev. Mater. Sci.*, Vol. 9, p. 191, 1979.

Mukherjee, A. K., Grain Boundaries in Engineering Materials, J. L. Walter, et al. (ed.), pp. 93-105, *Claitor Publishing*, Baton Rouge, LA, 1975.

Mukherjee, A. K., Treatise on Materials Science and Technology, Vol. 6, R. J. Arsenault (ed.), p. 163, *Academic Press*, New York, 1975.

Mukherjee, A. K., *Mater. Sci. Eng.*, Vol. 8, p. 83, 1971.

Mukherjee, A. K., *Mater. Sci. Eng.*, Vol. 8, pp. 83-89, 1971.

Murty, L. K., *Phil. Mag.*, Vol. 29, p. 429, 1974.

Murty, K., Mohamed, F. A., and Dorn, J. E., *Acta. Metall.*, Vol. 20, p. 1009, 1972.

Naziri, H., Pearce, R., Brown, M., and Hale, K. F., *Acta. Metall.*, Vol. 23, p. 489, 1975.

Nes, E., Superplasticity, edited by B. Baudlet ar d. (. Suery, Paris, 1985.

Nes, E., *Meturgia I, adl. Wunictwo*, Vol. 5, pp. 209-224, 1979.

Nes, E., Ryun, N., and Hunderi, O., *Acta. Metall.*, Vol. 33, pp. 11-22, 1985.

Nix, W. D., Superplastic Forming, S. P. Agrawai (ed.), *ASM*, p. 3, 1984.

Northwood, D. O., and Smith, I. O., *Mat. Sci. Eng.*, Vol. 66, pp. 205-212, 1984.

Nuttall, K., *J. Inst. Metals*, Vol. 100, p. 114, 1972.

Oliver, W. C., and Nix, W. D., *Act. Metall.*, Vol. 30, pp. 1335-1347, 1982.

Otsuka, M., Miura, Y., and Horiuchi, R., *Scripta Metall.*, Vol. 8, pp. 1405-1408, 1974.

Paton, N. E., Hamilton, C. H., Wert, J. A., and Mahoney, M. W., *J. Metals*, Vol. 34, pp. 21-27, 1982.

Pearson, C. E., *J. Inst. Metals*, Vol. 54, p. 111, 1934.

Piatti, G., Pellegrini, G., and Trippodo, R., *J. Mater. Sci.*, Vol. II, pp. 186-190, 1976.

Pollard, G., and Nutting, J., *J. Inst. Metals*, Vol. 93, p. 464, 1964.

Portnoy, V. K., Novikov, I. I., and Levchenko, V. S., *Phys. Met. Metall.*, Vol. 51, No. 4, pp. 164-169, 1981.

Presnyakov, A. A., and Chervyakova, V. V., *Akad., Nank SSSR, Otdel. Tekh.*, No. 3, p. 92, 1960.

Presnyakov, A. A., and Chervyakov, V. V., *Kaz, SSSr Rylym Akad. Khabarshysy, Vest. Akad. Nank Kaz. SSSR*, No. 10, pp. 76-80, 1958.

Reed-Hill, R. E., Physical Metallurgy Principles, 2nd Edition, *PWS Engineering*, Boston, MA, 1973.

Rhines, F. N., and Craig, K. R., *Met. Trans.*, Vol. 5, p. 413, 1974.

Rosenhain, W., and Ewen, W., *J. Inst. Metals*, Vol. 8, p. 149, 1912.

Rosenhan, W., Haughton, J. L., and Bingham, K. E., *J. Inst. Metals*, Vol. 25, p. 261, 1920.

Ruano, O. A., and Sherby, O. D., *Mater. Sci. Eng.*, Vol. 56, p. 167, 1982.

Ruano, O. A., Miller, A. K., and Sherby, O. D., *Mater. Sci. Eng.*, Vol. 51, pp. 9-16, 1981.

Ruano, O. A., Wadsworth, J., and Sherby, O. D., *J. Mat. Sci.*, Vol. 20, pp. 3735-3744, 1985.

Sauveur, A., *Iron Age*, Vol. 113, p. 581, 1924.

Sellars, C. M., and Tegart, W. J., *Int. Met. Rev.*, Vol. 17, pp. 1-24, 1972.

Senkov, O. N., and Myshiyav, M. M., *Acta. Metall.*, Vol. 34, No. 1, pp. 97-106, 1986.

Servi, C. S., and Grant, N. J., *Trans. A.I.M.E.*, Vol. 191, p. 909, 1951.

Sheppard, T., Zaidi, M. A., Hollinshead, P. A., and Raghunathan, N., Microstructural Control in Aluminum Alloys, edited by E. H. Chia and H. J. McQueen, *A.I.M.E.*, p. 19, 1985.

Sherby, O. D., and Wadsworth, Deformation Processing and Structure, G. Krauss (ed.), Chap. 8, *American Society for Metals*, Metals Park, OH, 1982

Sherby, O. D., Caligiuri, R. D., Dayali, E. S., and White, R. A., Advances in Metal Processing, edited by J. J. Burke, R. Mehrahian and V. Weiss, p. 133, *Plenum Press*, 1981.

Sherby, O. D., and Miller, A. K., *J. Eng. Mat. Technology*, Vol. 101, p. 387, 1979.

Sherby, O. D., Klundt, R. H., and Miller, A. K., *Met. Trans. A.*, Vol. 8A, pp. 843-850, 1977.

Sherby, O. D., Walser, B., Young, C. M., and Cady, E. M., *Scripta Met.*, Vol. 9, p. 569, 1975.

Sherby, O. D., and Burke, P. M., *Prog. Mater. Sci.*, Vol. 13, p. 325, 1967.

Shin, D. H., Selby, D., Belzunce, J., Roberts, S., and Sherby, O. D., unpublished work, 1987.

Smith, C. S., *J. Inst. Metals*, Vol. 74, p. 747, 1948.

Stowell, M. J., Robertson, J. L., and Watts, B. M., *Met. Sci. J.*, Vol. 3, p. 41, 1969.

Suery, M., and Baudlet, B., *Revue de Physique Appliquee*, Vol. 13, p. 53, 1978.

Taplin, D. M. R., Dunlop, G. L., and Langdon, T. G., *Ann. Rev. Mater. Sci.*, Vol. 9, p. 151, 1979.

Tweed, C. J., Ralph, B., and Hansen, N., *Acta. Met.*, Vol. 32, pp. 1407-1414, 1984.

Ujiiye, N., *Mater. Sci. J. Japan*, Vol. 6, p. 182, 1969.

Underwood, E. E., *J. Metals*, Vol. 14, p. 914, 1962.

Valiyev, R. Z., Kaybyshev, O. A., Rabinovich, M. Kh., Timoshenko, Yu. P., and Chistova, O. L., *Fiz. Metal. Metalloved*, Vol. 51, No. 3, pp. 615-624, 1981.

Vaidia, M. L., Murty, K. L., Dorn, J. E., *Acta. Metall.*, Vol. 21, p. 1615, 1973.

Voort, G. F. V., Metallography - Principles and Practice, Editor, p. 449, *McGraw-Hill Book Co.*, 1984.

Wadsworth, J., Superplastic Forming, S. P. Agrawal (ed.), p. 43, *ASM*, Metals Park, OH, 1984.

Wadsworth, J., Palmer, I. G., Crooks, D. D., and Lewis, R. E., Aluminum-Lithium Alloys, *Proc. Second Int. Aluminum- Lithium Conf.*, edited by T. H. Sanders, Jr., E. A. Starke, Jr., *A.I.M.E.*, Warrendale, PA, 1984.

Wadsworth, J., Palmer, I. G., and Crooks, D. D., *Scripta Metall.*, Vol. 17, pp. 347-352, 1983.

163

Wadsworth, J., Oyama, T., and Sherby, O. D., *6th Inter- American Conf. on Materials Technology, San Francisco, August 1980*, Vol. II, I. LeMay(ed.), p. 29, *ASME*, New York, 1980.

Watts, B. M., Stowell, M. J., Baikie, B. L., and Owen, D. G. E., *Metal Sci.*, Vol. 10, pp. 189-206, 1976.

Weertman, J., *Trans. Am. Inst. Min. Engrs.*, Vol. 218, p. 207, 1960.

Weertmann, J., *J. Appl. Phys.*, Vol. 28, p. 1185, 1957.

Weill, F., and Wyon, G., *Proc. Fifth Int. Conf. Strength of Metals and Alloys*, pp. 387-392, Aachen, W. Germany, 1979.

Weisert, E. D., and Stacker, G. W.,Superplastic Forming of Structural Alloys, edited by N. E. Paton and C. H. Hamilton, *A.I.M.E.*, p 2~3, 1982.

Wert, J. A., Microstructural Control in Aluminum Alloys, edited by E. H. Chia and H. J. McQueen, *A.I.M.E.*, p. 67, 1985.

Wert, J. A., and Paton, N. E., *Met. Trans.*, Vol. 14A, pp. 2535-2544, 1983.

Wert, J. A., Superplastic Forming of Structural Alloys, edited by N. E. Paton, and C. H. Hamilton, *A.I.M.E.*, pp. 69-84, Warrendale, PA, 1982.

Wert, J. A., Paton, N. E., Hamilton, C. H., and Mahoney, M. W., *Metall. Trans. A.*, Vol. 12A, pp. 1267-1276, 1981.

Williamson, J. R., Superplastic Forming of Structural Alloys, edited by N. E. Paton and C. H. Hamilton, *A.I.M.E.*, p. 291, 1982.

Wu, M. Y., and Sherby, O. D., *Acta. Metall.*, Vol. 32, p. 1561, 1984.

Yarovchuk, A. V., Aubakivova, R. K., and Presnyakov, A. A., *Zavodskaya Laboratonya*, No. 5, pp.594-596, May 1976.

Yoder, G. R., and Weiss, V., *Metall. Trans.*, Vol. 3, p. 675, 1972.

Zehr, S. W., and Backofen, W. A., *Trans. Quart. A.S.M.*, Vol. 61, p. 300, 1968.

Zhang, Y., and Grant, N. J., *Mat. Sci. Eng.*, Vol. 68, pp. 119-124, 1984.

INITIAL DISTRIBUTION LIST

No. Copies

1. Defense Technical Information Center 2
   Cameron Station
   Alexandria, VA 22304-6145

2. Library, Code 0142 2
   Naval Postgraduate School
   Monterey, CA 93943-5002

3. Department Chairman, Code 69Mx 1
   102 Department of Mechanical Engineering
   Naval Postgraduate School
   Monterey, CA 93943-5000

4. Professor T. R. McNelley, Code 69Mc 10
   Department of Mechanical Engineering
   Naval Postgraduate School
   Monterey, CA 93943-5000

5. Dr. L. E. Sloter, Code AIR 931 1
   Naval Air Systems Command
   Naval Air Systems Command Headquarters
   Washington, D. C. 20361-9310

6. Dr. S. J. Hales, Code 69He 1
   Department of Mechanical Engineering
   Naval Postgraduate School
   Monterey, CA 93943-5000

7. Dr. Eui-Whee Lee, Code 6063 1
   Naval Air Development Center
   Warminster, PA 18974

8. Professor Oleg D. Sherby 1
   Department of Materials Science and Engineering
   Stanford University
   Stanford, CA 94305

9. Professor John R. Neighbours, Code 61Nb   1
   Department of Physics
   Naval Postgraduate School
   Monterey, CA 93943-5000

10. Professor A. Jeffrey Perkins, Code 69Ps   1
    Department of Mechanical Engineering
    Naval Postgraduate School
    Monterey, CA 93943-5000

11. Professor David A. Salinas, Code 69Sa   1
    Department of Mechanical Engineering
    Naval Postgraduate School
    Monterey, CA 93943-5000

12. BGEN Ahmed Abou-Salama   10
    1 Nasr Soliman St., # 13
    Dokki-Giza, Egypt

13. Dr. Saad El-Raghy   1
    Faculty of Engineering
    Cairo University
    Giza, Egypt

14. Training Authority   1
    Armed Forces
    Giza, Egypt

15. Eqyptian Military Attache   1
    2308 Tracy Place, N.W.
    Washington, D.C. 20008

END

DATE

FILMED

DTIC

6-88